Scientific and Technological Alliance for Guaranteeing the European Excellence in Concentrating Solar Thermal Energy

FP7 Grant Agreement number:	**609837**
Start date of project:	**01/02/2014**
Duration of project:	**48 months**

STAGE-STE Deliverable 9.4

D9.4: Final report on "Technology Roadmap for Solar Fuels"

WP9 – Tasks 9.4	Deliverable 9.4
Submitted:	**December 5, 2017**
Work Package Leader:	**PSI**
Task leader:	**DLR**
Author(s):	**Christian Sattler (DLR), Nathalie Monnerie (DLR), Anis Houaijia (DLR), Manuel Romero (IMDEA), José González-Aguilar (IMDEA), Miguel A. Reyes (IMDEA), Luca Turchetti (ENEA), Alberto Giaconia (ENEA), Domenico Mazzei (ENEA), Giampaolo Caputo (ENEA), Antonio Ienna (UNIPA), Benedetto Schiavo (UNIPA), Onofrio Scialdone (UNIPA), Alessandro Galia (UNIPA), Gilles Flamant (CNRS), Alfonso Vidal (CIEMAT), Aleix Jové Llovera (ABENGOA), Christian Wieckert (PSI)**
Revised by:	**All involved partners**
Document version:	**6**
Reviewed/supervised by:	**Christian Sattler (DLR), Christian Wieckert (PSI)**
Dissemination level:	**PU**

Table of contents

1. Executive Summary

In the framework of the European project STAGE-STE the aim of Task 9.4 is to carry out a technology assessment of solar fuel production, to describe the essential R&D requirements needed in the future and to define a technology roadmap for the development up to large scale solar fuels production. The WP9 STAGE-STE consortium is composed of the following partners:

- DLR, Germany (Task 9.4 Leader)*
- PSI, Switzerland (WP Leader)*
- ETHZ, Switzerland
- ENEA, Italy*
- UNIPA, Italy
- CNRS, France*
- IMDEA, Spain*
- CIEMAT, Spain*
- ASNT, Spain
- LNEG, Portugal
- UEVORA, Portugal*

The institutions marked with a star are formal partners of Task 9.4, within which this document has been worked out.

The development of an energy economy based on hydrogen produced by renewable energy will have a positive impact on the reduction of CO_2 emissions [1]. High temperature processes driven by concentrated solar radiation can be operated in large scale industrial plants. Therefore, they can provide large amounts of hydrogen to achieve the goal of an economical and sustainable energy economy.

Within WP9 of STAGE-STE the whole spectrum of high temperature solar processes shown in Table 1 were evaluated. Thermochemical cycles to split water into hydrogen and oxygen have the potential to avoid any CO_2 emissions. However, based on their development level and local or regional prioritization also solar processes based on carbonaceous feedstocks were investigated. A roadmap was drawn and tailor-made paths can be found how to implement the technologies under different circumstances. The technologies are listed in the table below regarding their technology readiness level (TRL).

Table 1: Solar high temperature processes selected.

Process	TRL
Non-volatile metaloxide cycle	5-6
Hybrid sulphur cycle	5
Solar steam reforming of natural gas (at high temperature and at low temperature molten salt heated)	5-6
Solar gasification of carbonaceous materials and wastes	5
ZnO/Zn cycle	4-5
ZnO/Zn carbothermal cycle	4
Solar driven solid oxide electrolysis	4
Molten carbonate electrolysis	3
Solar molten salt heated hydrothermal liquefaction of wet biomass	2-3

The proposed R&D actions for these selected processes are summarized in the roadmap presented in Figure 1. Figure 2 shows the scale-up strategy roadmap.

These roadmaps are describing the way to be followed by the upcoming EERA program and the European CSP Research Agenda in order to facilitate scaling up the solar fuels technologies in a fast and efficient way.

TRL	Processes	2018	2020	2025	2030	2035	2040
≥ 5	Non-volatile metal oxide cycle	On-going projects expected outcomes	Research on reactor/receiver and on materials	Optimization of the coupling of the available energy heat to the thermochemical process to operate the plant as continuously as possible	Optimization of demo plant and its production		
	ZnO/Zn cycle		Research on effective separation of O_2 and inert gas / Fundamental research for alternative $Zn(g)$-O_2 separation processes / Research on quenching options using reduced amount of gas / Research on nanoparticles handling	In case of break-through results of R&D activities latest till about 2028: Optimization of the small MW scale plant realised in this case			
	Hybrid sulphur cycle		Research on high temperature storage (i.e. 900°C) for continuous operation and on heat recovery system and gas separation / Material development and optimisation of sulphuric dioxide electrolyser	Pressurization of sulphuric acid splitting reactor and of sulphuric dioxide electrolyser			
	Solar steam reforming 1- high temperature 2- low temperature molten salt heated		Find industrial partner to built MW demo plant in sunbelt country / Research on catalysts and reactor design / Prototype testing and evaluation	Optimization of the demo-unit	Completion and qualification of the system		
	Solar gasification of carbonaceous materials and wastes		Research on more continuous process (e.g. pushing furnace) / Windowless design for 100 kW scale	In depth study for specific feedstock of interest, e.g. regarding residues and gas cleaning / Windowless design for MW scale	Optimization of demo-plant	Completion and qualification of the system	
	ZnO/Zn carbothermal cycle		Identification of industrial partner(s) / Optimization of interfaces between solar reactor and hydrolysis reactor / Basic study of more direct path to solar H_2 via this process by integrating the hydrolysis reactor	Windowless design for MW scale	Optimization of demo-plant	Completion and qualification of the system	
4	Solar driven SOE		Closer cooperation needed between CSP and SOE research teams / Research on SOE and optimization of the coupling of solar part and SOE part	Improving efficiency	Further optimization		
≤ 3	Molten carbonate electrolysis		Development of electrolyser	System analysis and integration / Analysis of other CO_2 separation processes / Selection of optimal CSP plant size	Optimization of reactor concept and design		
	Solar molten salt heated hydrothermal liquefaction of wet biomass		Link with liquid fuels programm to maximize chances to go further / Investigation of the process in lab-scale continuous systems heated by molten salts	Investigation of the design of the solar plant to adapt it to the chemical plant	Improvement and optimization of the technology		

Figure 1: Summary of the R&D Strategy Roadmap.
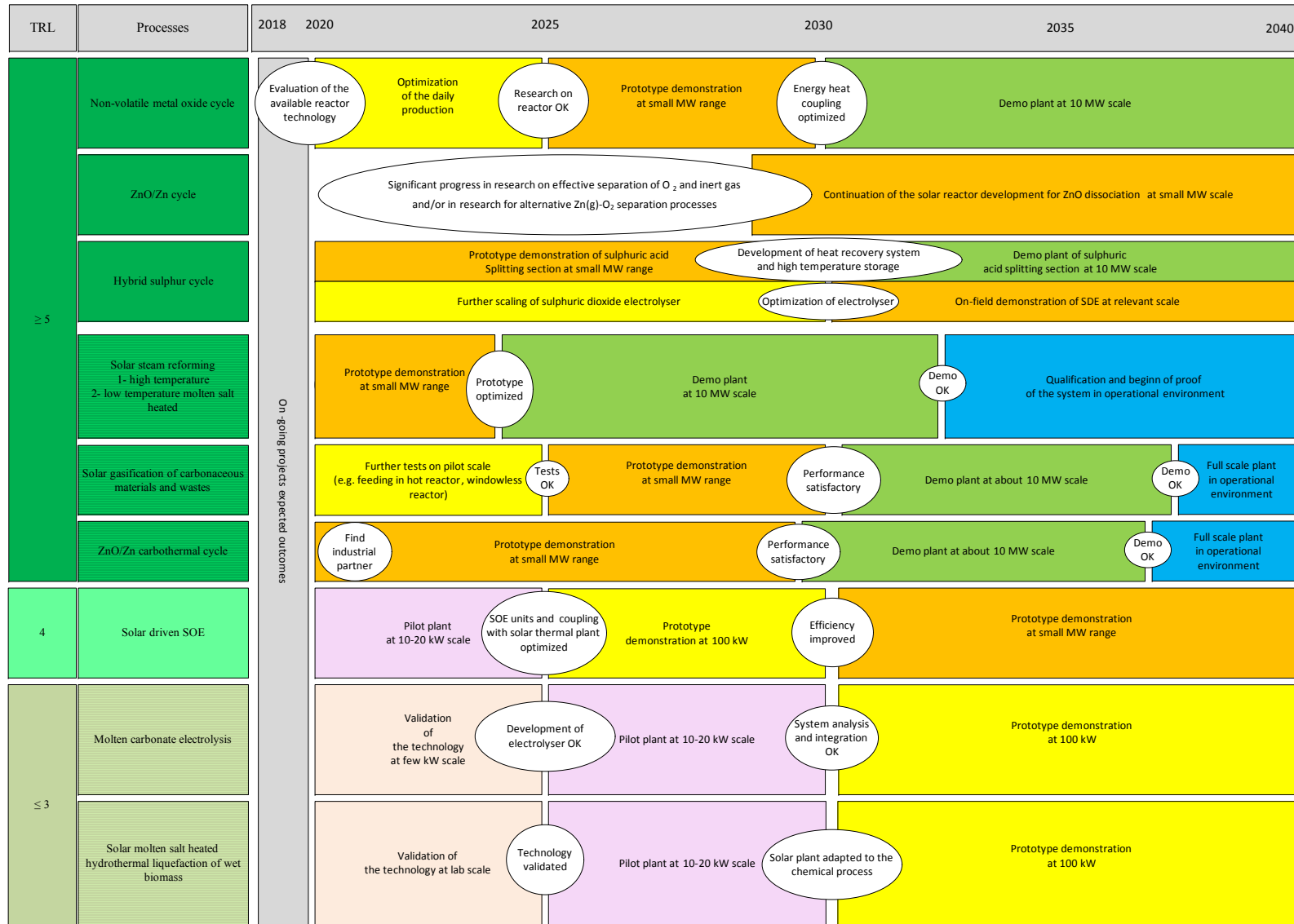
Figure 2: Summary of the Scale-up Strategy Roadmap.

2. Abbreviations

AWP	Annual Work Plan
BMC	Bare Module Cost
BoP	Balance of Plant
CAPEX	Capital Expenses
CPC	Compound Parabolic Collector
CS	Concentrating Solar
CSP	Concentrating Solar Power
CST	Concentrated Solar Thermal
DNI	Direct Normal Irradiance
DoW	Description of Work
JU-FCH	Fuel Cells and Hydrogen Joint Undertaking
FP	Framework Programme
HHV	Higher Heating Value
HT	High Temperature
HTE	High Temperature Electrolysis
HTF	Heat Transfer Fluid
HTL	Hydrothermal Liquefaction
HTS	High Temperature water-gas Shift
HX	Heat Exchanger
ITSE	Intermediate Temperature Steam Electrolysis
LFR	Linear Fresnel Reflector
LHV	Lower Heating Value
LTS	Low Temperature water-gas Shift
MAWP	Multi Annual Work Plan
MCE	Molten Carbonate Electrolysis
MCEC	Molten Carbonate Electrolysis Cell
MCFC	Molten Carbonate Fuel Cell
MCSE	Molten Carbonate Steam Electrolysis
MDEA	Methyldiethanolamine
MFSP	Minimum Fuel Selling Price

MS	Molten Salt
MS n	Milestone n
MT	Medium Temperature
NG	Natural Gas
NPV	Net Present Value
OPEX	Operation Expenses
P2G	Power-to-Gas
PEC	Purchased Equipment Costs
PEM	Proton Exchange Membrane
PSA	Pressure Swing Adsorption
SA	Sulphuric Acid
SDE	Sulphur Dioxide Depolarized Electrolyser
SF	Solar Field
SMR	Steam Methane Reforming
SOE	Solid Oxide Electrolysis
SOEC	Solid Oxide Electrolyser Cell
SOFC	Solid Oxide Fuel Cell
TC	Thermochemical Cycle
TCI	Total Capital Investment
TCS	Thermochemical storage
TES	Thermal Energy Storage
TRL	Technology Readiness Level
VHTR	Very High Temperature Reactor
WC	Working Capital
WGS	Water Gas Shift
WP	Work Package
WS-TR	Water splitting-thermal reduction

3. Introduction

Hydrogen produced from renewable resources has a great potential as energy vector. Concentrated solar technologies have the potential to produce hydrogen from renewable energy efficiently. The conversion of solar radiation into chemical energy carriers, e.g. hydrogen, represents an interesting pathway to its long-term storage. It opens up the possibility to transport it from the earth's sun-belts to highly populated regions. Figure 3 shows the different pathways for converting solar energy into hydrogen.
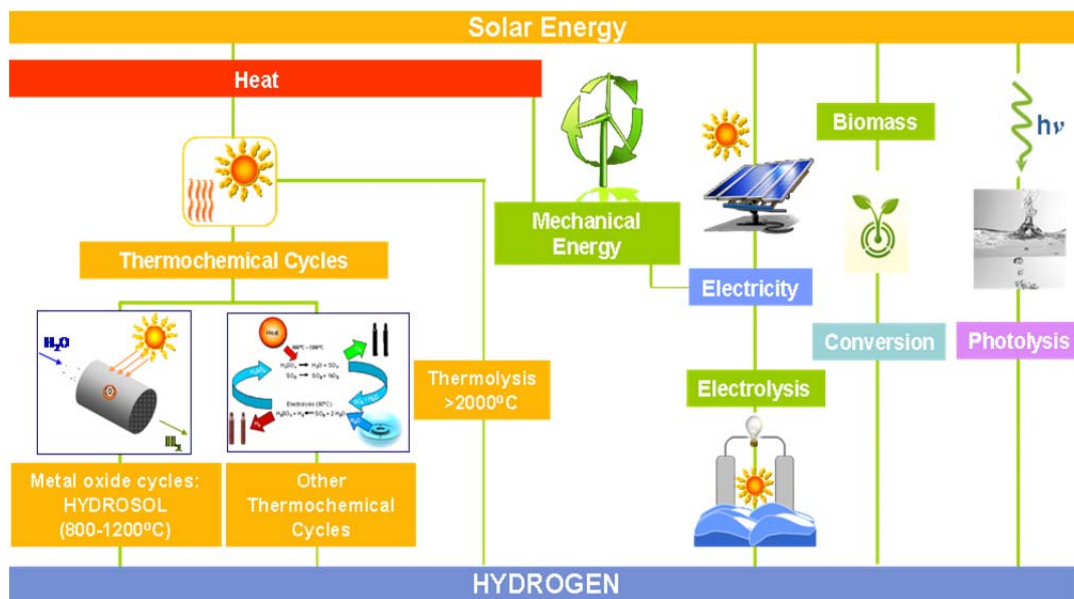

Figure 3: Pathways of solar hydrogen production processes [2].

The first idea mentioned in the DoW of the STAGE-STE project was to consider only solar thermochemical water splitting cycles for hydrogen production. However, being given the importance of some other processes, it has been decided by the WP9 partners to investigate also other technologies like high temperature electrolysis and carbon based processes namely solar steam reforming of methane and solar gasification of carbonaceous materials especially wastes. The analysis also includes new processes such as the molten carbonate electrolysis and the solar molten salt heated hydrothermal liquefaction of wet biomass.

A methodology was defined for the evaluation of the processes. This is necessary for developing the roadmap in order to compare the different solar processes selected on the same level. Following the assessment of the different solar fuels production processes, the technology roadmap was prepared and is presented in this document to foster further development of solar fuels production processes and to facilitate scaling up the solar fuels technologies in a fast and efficient way.

4. Methodology of the technology assessment

Assessing technical and economic viability, the overall techno-economic analysis involves the three major steps shown in Figure 4. The overall system analysis consists of the flowsheet elaboration, the simulation of the process and the economic analysis. This methodology is applied to the hydrogen production processes in the framework of WP 9.4.
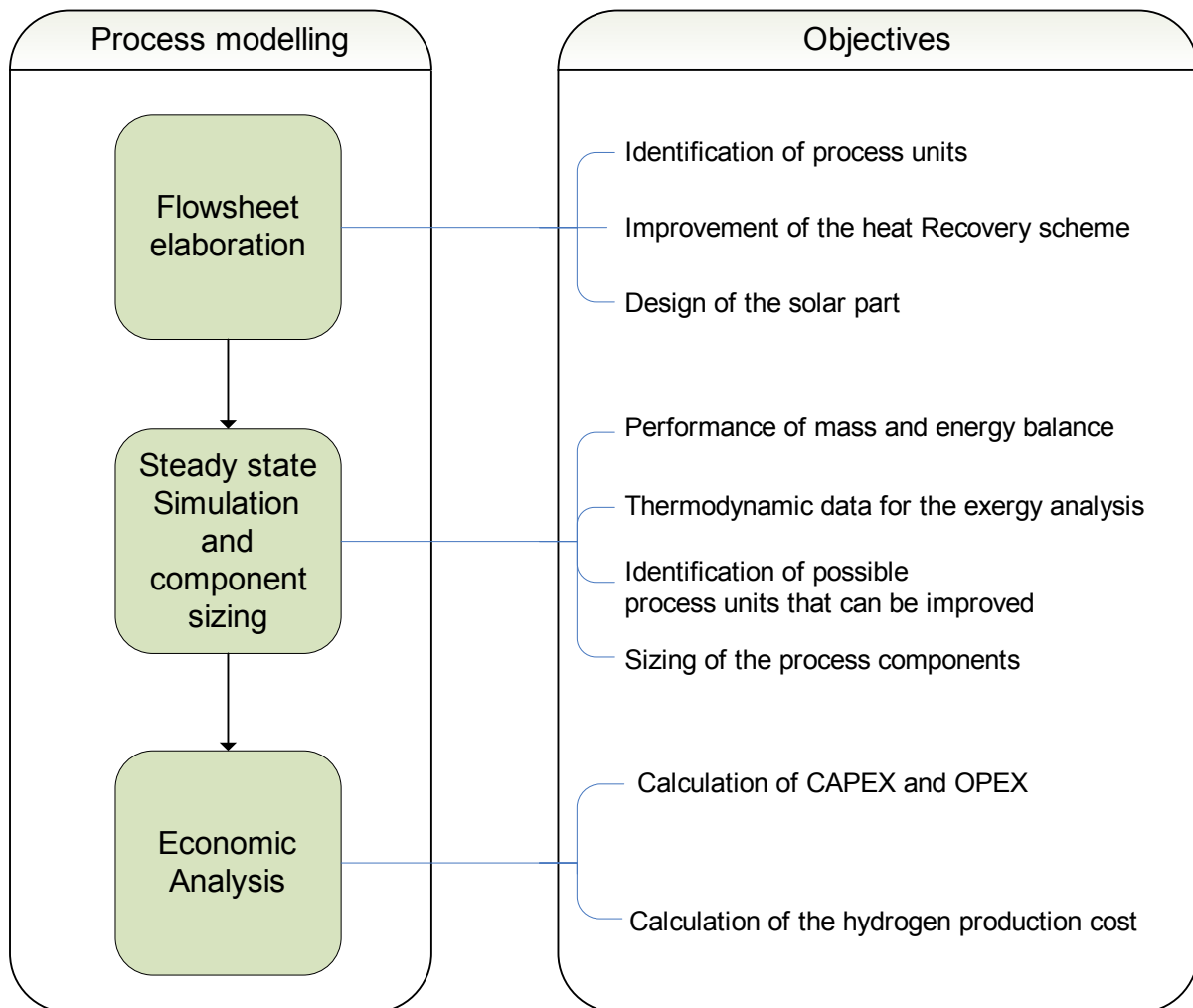
Figure 4: Methodology of the overall system analysis.

The overall system analysis begins with the elaboration of the flowsheet in order to indicate the general flow of plant process streams and equipment. The flowsheet displays the relationship between the major equipment items of a plant facility. Solar energy concentrating technologies able to deliver heat and electricity were identified and investigated in the report on MS 37 in order to assess their compatibility with the processes defined. Once the flowsheet is elaborated, the simulation of the process can be performed by using commercial tools Aspen Plus and Ebsilon Professional as well as Matlab and Excel.

The last step of the analysis consists of calculating the hydrogen production cost by taking into consideration the plant output and costs along its full lifetime. Calculations take into account the CAPEX as well as the OPEX [3]. At project stage, a plant cost estimate also includes provisions for contingencies that are meant to cover all cost sources not yet identified. The boundary conditions of the economic analysis, in terms of interest rate, plant lifetime etc., have been defined by the WP9 partners. Input data have been collected from the WP9 partners and literature.

The CAPEX as well as the OPEX will be calculated for each process. For this economic analysis, the total capital investment (TCI) of the different plants will be calculated by using the factor method [3]. The various shares are taken into account by percentages of the purchased equipment costs (PEC) calculated before. The shares include direct and indirect costs:

- Direct costs include the costs for installation, measurement, electrical equipment and materials, civil and architectural works.
- Indirect costs include the costs of engineering, supervision, and insurance.

In order to carry out the economic analysis, some assumptions have to be made and initial conditions have to be defined:

- Lifetime of the plant: 25 years
- Annual effective interest rate: 8%

Different scenarios have been considered depending on the advantages and boundary conditions of each process. In line with the standard cases defined by FCH-JU mostly a plant producing about 4000 kg H_2/day ("industrial scale") and in some cases also a smaller plant for production of about 400 kg H_2/day ("mobility scale") are considered.

This study evaluates also the technologies maturity and the current state of the art is assessed for each solar fuel production technology as well as the Technology Readiness Level (TRL) according to the TRL definition described in Table 2.

After the assessment of the different processes, a technology roadmap is proposed with recommendation for future R&D priority work including a list of development areas.

Table 2: Technology Readiness Level (TRL) [source: FCH JU 2014].

TRL	Description
1	Basic principles observed
2	Technology concept formulated
3	Experimental proof of concept
4	Technology validated in lab
5	Technology validated in relevant environment (industrially relevant environment in the case of key enabling technologies
6	Technology demonstrated in relevant environment (industrially relevant environment in the case of key enabling technologies)
7	System prototype demonstration in operational environment
8	System complete and qualified
9	Actual system proven in operational environment (competitive manufacturing in the case of key enabling technologies)

5. Screening of thermochemical cycles

The ideal thermal reaction for hydrogen production from water is the thermal dissociation.

$$H_2O \leftrightarrow H_2 + \tfrac{1}{2} O_2 \qquad \textbf{Equation 1}$$
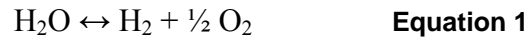
But even at temperatures far beyond 2000 K it needs reduced pressure to move the equilibrium of the reaction to the hydrogen side [4].
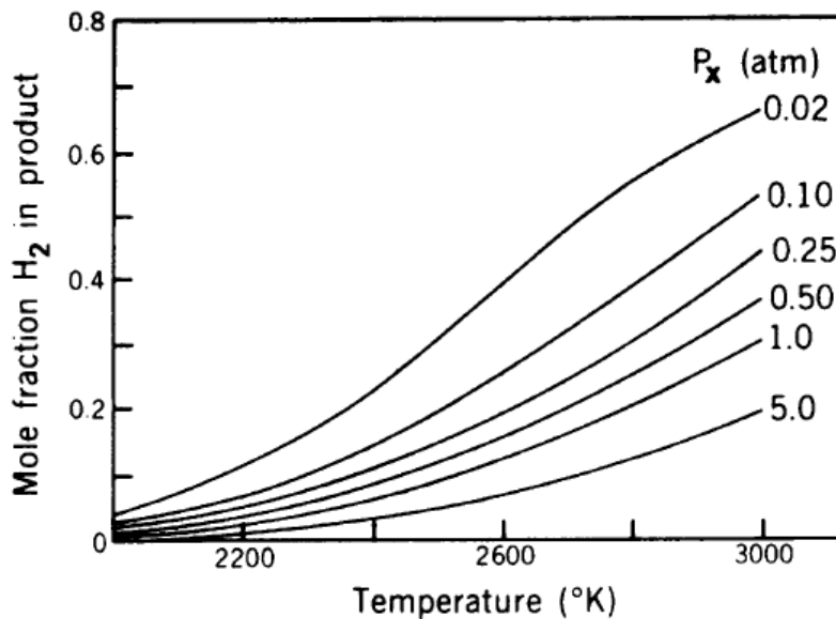
Figure 5: Variation of mole fraction of hydrogen in product with reactor temperature at various reactor pressures in an idealized effusional separation [4].

To lower the temperature thermochemical cycles were proposed. They are consecutive oxidation and reduction processes that divide the thermal water dissociation in two or more steps. The main steps are the attraction of oxygen from water by a reduced chemical (X) and the simultaneous production of hydrogen

$$X + H_2O \rightarrow XO + H_2 \qquad \textbf{Equation 2}$$
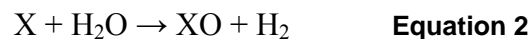
followed by the release of oxygen from the oxidized chemical (XO) at a higher temperature

$$XO \rightarrow X + \tfrac{1}{2}O_2 \qquad \textbf{Equation 3}$$

The more steps are used the lower the temperature can be but also the lower the possible efficiency is. In general, the highest temperature is needed to release the oxygen from the redox-material. Table 3 shows the classification of the different thermochemical water splitting processes.

Table 3: Well researched thermochemical cycles for water splitting.

	Steps	Maximum Temperature (°C)	LHV Efficiency (%)
Sulphur Cycles			
Hybrid Sulphur (Westinghouse, ISPRA Mark 11)	2	900	43
Sulphur Iodine (General Atomics, ISPRA Mark 16)	3	900	38
Volatile Metal Oxide Cycles			
Zinc/Zinc Oxide	2	1800	45
Hybrid Cadmium	2	1600	42
Non-volatile Metal Oxide Cycles			
Iron Oxide	2	2200	42
Ceria	2	2000	68
Ferrites	2	1100 – 1800	43
Low-Temperature Cycles			
Hybrid Copper Chlorine	4	530	39

The cycles can be characterized by the state of matter of the reaction partners (gaseous, liquid, solid), by the material used (metal, metal oxide, non-metal) or by the number of steps. To further improve the efficiency also electrochemical steps can be used. Then the cycles are named hybrid thermo-electrochemical. A prominent example is the hybrid sulphur or Westinghouse cycle.

To operate such thermochemical cycles a matching heat source is necessary. Originally, they were developed to couple them to nuclear reactors. This excludes metal and metal-oxide cycles as even the very high temperature reactors (VHTR) are only able to provide temperatures up to 950°C. By using concentrated solar radiation, even higher temperatures can be reached. However, because the heat is reradiation with T^4 and because of material issues also solar plants will not be able to be operated at temperatures substantially above 1500°C even if the theoretical limit is at about 5000°C.

The cycles are not only carried out at very high temperatures but also using toxic or corrosive substances. Therefore, safety issues have to be taken into account seriously in the selection process. Economically the availability and cost of raw materials are decisive. To lower the operation temperature carbothermal cycles have been proposed, e.g. the carbothermal ZnO/Zn cycle.

Perovskites cycles have been also explored for the production of solar H_2. In perovskites structures elements are structured as depicted in Figure 6: an A cation, represented by the big green spheres, B, another cation, by the blue ones and, finally, O, the red Oxygen circles, represents the anion.
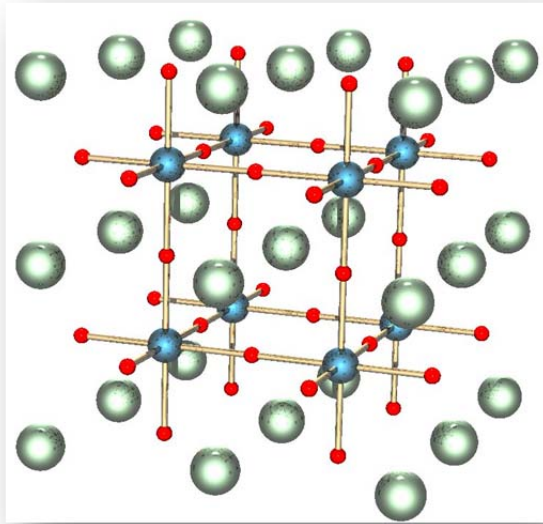

Figure 6: Structure of perovskites.

Cations are easily replaced by similar elements thus the compound presents a wide array of possible chemical behaviours while keeping a similar structure. While keeping this structure as well, perovskite is mostly immune to some problems that catalysts and other TCE materials exposed to such high temperatures fall to: sintering, crushing,… Apart from the unaffected perovskite structure, the porosity for oxygen transport eases the chemical reaction for the solar production of H_2. Furthermore, since these proposed structures are made of common and available materials that can be obtained at reduced costs, perovskite cycles constitute an interesting route to be further explored.

Table 4 lists some compositions which have been studied [5]. This process has a TRL 3.

Table 4: Summary of perovskites cycles.

Structure	Tr [ºC]
$La_{1-x}Sr_xMn_{1-y}Al_yO_3$	800-1320
$La_{1-x}Sr_xMnO_{3-\partial}$	800-1000
$La_{1-x}Sr_xCo_{1-y}Fe_yO_{3-\partial}$	300-1000
$CaTi_{1-x}Fe_xO_3$	1000-1360
$NaMgF_3$	778

Another reaction, which allows water splitting at lower temperatures than 1000ºC, is the one based on aluminium spinel structures. Table 5 shows the proposed reaction [6]:

Table 5: Summary of hercynite cycle.

Structure	Tr(ºC)
$CoAl_2O_4 + 2FeAl_2O_4 + H_2O <-->CoFe_2O_4 + 3Al_2O_3 + H_2 (g)$	940-1360

$CoFe_2O_4/Al_2O_3$ was capable of being cycled producing significant amounts of hydrogen [7]. The process has a TRL of 3 [8].

6. Technology assessment of the solar fuels processes

6.1 Non-volatile metal oxide cycle

6.1.1 Process description

In this process, the metal oxide is reduced at high temperature in a first step, releasing oxygen. In a second step, the material is oxidized with water at reduced temperature, producing hydrogen and returning to its initial state. The cycles based on ferrites and most recently ceria have received most attention [9].

The last reactors developed for this process in the frame of the European project "HYDROSOL Plant" applies nickel-ferrite as reactive species which works at 1000°C for the water splitting step and at 1400°C for the regeneration step [10]. The principle is illustrated in Figure 7.
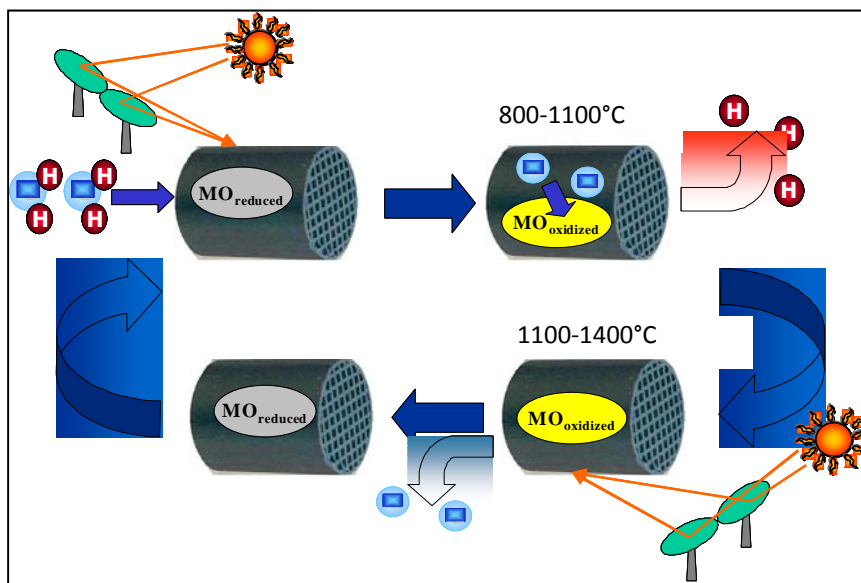
Figure 7: Principle of hydrogen production by thermochemical water splitting process.

The first examples of honeycomb reactors for solar-aided chemistry applications can be traced back to 1989 when researchers at WIS have deposited Rh first on alumina and then on cordierite honeycombs and irradiated it in their solar furnace to catalyse the reaction of CO_2 methane reforming. However such honeycomb reactors have first been used for thermochemical water splitting when the HYDROSOL research group has introduced the concept of monolithic, honeycomb solar reactors for performing redox pair cycles [11]. The reactor is inspired on the one hand from solar-radiation-absorbing honeycomb volumetric receivers made of silicon carbide (SiC) employed in solar tower power plants using air as the heat transfer medium [12, 13] and on the other hand from the well-known automobile catalytic converters [14]. It has no moving parts and is based on the incorporation of active

redox pair powders as coatings on multi-channelled monolithic honeycomb structures capable of achieving and sustaining high temperatures when irradiated with concentrated solar radiation. When steam passes through the solar reactor, the coating material splits water vapour by "trapping" its oxygen and leaving in the effluent gas stream pure hydrogen. In a subsequent step the oxygen-"trapping" coating is thermally reduced by increasing the amount of solar heat absorbed by the reactor. Such redox-material-coated-honeycombs have achieved continuous solar-operated WS-TR cycles. The issue of continuous production has been resolved with a modular dual-chamber, illustrated in Figure 8, fixed honeycomb absorber design and implementation [15].
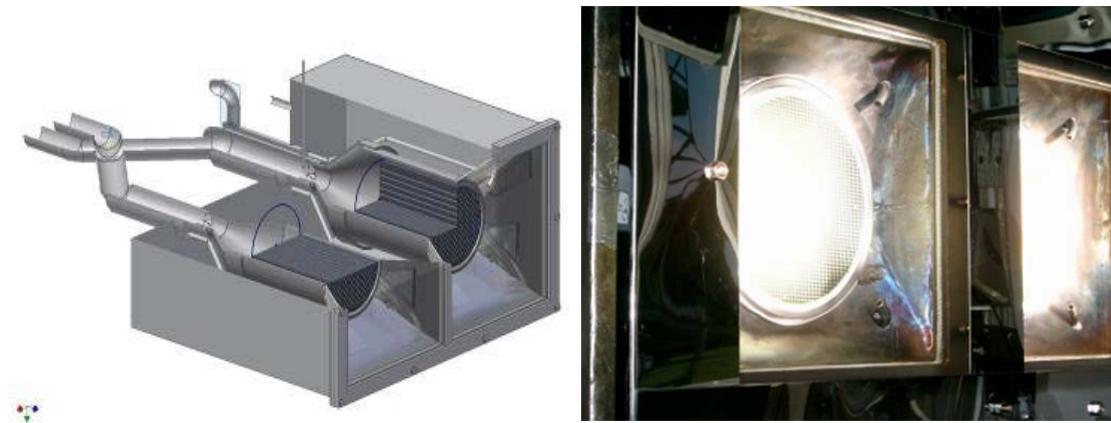

Figure 8: Continuous solar hydrogen production concept and the first dual-chamber reactor in operation.

One part of modules splits water while the other is being regenerated; after completion of the reactions, the regenerated modules are switched to the splitting process and vice versa by switching the feed gas [16]. Due to its modularity and the lack of movable parts, this design is amenable to straightforward scale-up and can be effectively coupled with a solar platform facility placed on a solar tower for continuous mass production of hydrogen. Indeed, such a modular, dual-chamber, ferrite-coated-honeycomb HYDROSOL reactor has been scaled up to the $100kW_{th}$ level, coupled on a solar tower facility (Plataforma Solar de Almería, Spain) and achieved continuous solar-operated WS-TR cycles demonstrating the "proof-of-concept'' of the proposed design [17]. In such a facility, the different heat demands for the two process stages were realized not by moving the reactors, but by adjusting the flux density on each module when the status of the cycle is switched from regeneration to splitting and vice versa, via partitioning the heliostat field and providing two "switchable" focal spots with independent power modulation [18].

An optimization of the reactor shape has been carried out to reduce the quite high re-radiation losses due to the high temperatures and the large exposed absorber surface area revealed by experiments and simulations [19]. A new reactor design has been proposed [20] where the overall shape of the absorber is close to a hemisphere and a suitable secondary reflector is included as well. The reactor-receiver consists of two parts: a receiver "flat" part made of non-redox, square-shaped honeycombs at the front plate of the reactor (just behind the quartz window) and a "domed" part at the rear which is the reactor part consisting of the redox-

coated modules. The introduction of a spherical shape of the absorber and a suitable secondary reflector ensures a more homogeneously distributed solar flux and therefore a more homogeneous temperature distribution than that of the previous, "flat design" version. The cavity design ensures also that the thermal radiation is more efficiently absorbed inside the reactor since different parts of the absorber face each other instead of facing the environment like in the previous flat design. Furthermore, the whole reactor set-up and all components were designed in a way allowing easy maintenance and replacement of parts, in particular of the individual absorber monoliths.

A prototype of 750 kW_{th} has been designed, studied and constructed at DLR for solar thermochemical water splitting cycle to produce hydrogen [10]. Hydrogen will be produced by thermochemical water splitting. The goal is to produce 3 kg H_2 in one week of operation. Figure 9 illustrates the development of this process during the last decade.
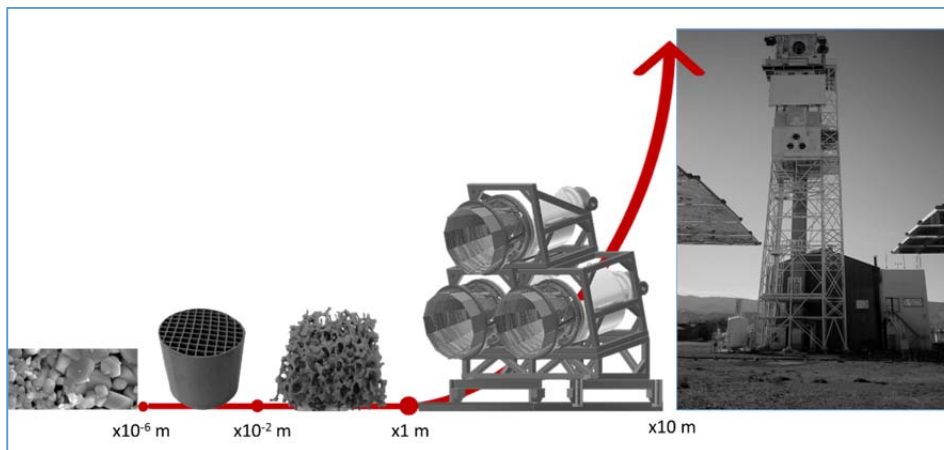
Figure 9: Illustration of the different development scales of the HYDROSOL-PLANT.

Recently, a metal oxide redox cycle was proposed based on ceria (CeO_2) [21, 22]. The ceria-based oxides have namely appeared as attractive non-volatile redox candidates because they present faster kinetics and better stability and selectivity in comparison to the ferrite-based oxides [9, 23-25]. Ceria has been used in both stoichiometric and nonstoichiometric cycles, where the former has shown difficulties due to vaporization of CeO_2 at the required elevated temperatures of about 2300 K [26]. The nonstoichiometric ceria cycle has received more attention in recent years. The reaction scheme is:

$$1/(\delta red-\delta ox)\ CeO_{2-\delta ox} \rightarrow 1/(\delta red-\delta ox)\ CeO_{2-\delta red} + \tfrac{1}{2}\ O_2(g) \qquad \textbf{Equation 4}$$

$$H_2O(g) + 1/(\delta red-\delta ox)\ CeO_{2-\delta red} \rightarrow 1/(\delta red-\delta ox)\ CeO_{2-\delta ox} + H_2\,(g) \qquad \textbf{Equation 5}$$

Pure CeO_2 was used by Cheh et al. for their experiments and doping of the material with other elements such as Gd, Y, Sm, Ca, Sr, Fe, Ni, Mn, ZrO_2, or CrO_2 has been also analyzed theoretically and experimentally to lower the reduction temperature and to increase the oxygen nonstoichiometry [24, 25, 27-29].

Different reactor concepts have been proposed in the literature, including a simple cavity design [30], counter-rotating rings inside a cavity [31-35], moving particle beds [36], and an aerosol reactor [37].

This cycle has been demonstrated at laboratory scale in a 4 kW setup using a solar reactor containing a ceria-based reticulated porous structure undergoing the redox cyclic process [38] and the promising potential of this solar thermochemical cycle has been demonstrated. Within the on-going project Sun-to-Liquid, a 50 kW pre-commercial plant is designed, built and tested [39]. The goal is to convert not only H_2O to H_2, but a mixture of H_2O and CO_2 to syngas, and to perform the subsequent processing to Fischer-Tropsch liquid hydrocarbon fuels.

The non-volatile redox cycle has a TRL of 5-6.

6.1.2   Technology assessment

The Hydrosol Process has been simulated using the software tool Aspen Plus. Figure 10 shows the simplified flow sheet of the plant. Demineralized water is fed at ambient conditions (25°C and 1 bar) to the preheater PREHX, where it is heated up to 85°C by the product gas PRODUCT2. After the preheating, the water stream WATER3 is divided in the splitter SPLITT1 into the two substreams WATER4 and WATER6. The first substream is evaporated in the heat exchanger EVAPORA1 by the product gas PRODUCT1, while the second one is evaporated in the heat exchanger EVAPORA2/EVAPORA3 by the stream O2N2-1, which leaves the solar reactor REGNE-R at 1344°C. After evaporation, the streams WATER6 and WATER7 are mixed in the mixer MIX1. Then, the stream WATER8 is overheated in the superheater SUPERHX1/SUPERHX2 up to 545°C by the stream O2N2-2, which contains N_2 and O_2. The redox material is normally fixed in the reactor, but due to the fact that ASPEN PLUS does not contain a reactor model, where solids can be implemented, the reduced material has been simulated as a stream, which will be reintroduced to the water-splitting reactor REAC-RE. After regeneration, the FeO stream 13 is removed in a cyclone and the stream 12 is used for water evaporation of the substream WATER4 and the overheating of the stream WATER8. The overheated steam WATER9 is introduced to the water splitting reactor REAC-RE with the redox material stream FEO, which has been already heated up to 992°C by the stream INT6. The water stream WATER9 flows into the reactor REAC-RE at a temperature of 545°C. According to ASPEN calculation, the water splitting reaction takes place at 934°C. A H_2O to H_2 conversion of 35% has been assumed according to the dynamic model of the solar reactor.

Oxygen released during the metal oxide regeneration is considered as a plant product and does have to be separated from the sweeping nitrogen for valorisation. The incoming O_2/N_2 mixture GAS3 is pressurized by the compressor COMP6 up to 6 bar. In order to reach the required distillation conditions, the air is first cooled down by the heat exchanging between the O_2/N_2 mixture and the pure nitrogen stream N2-7. Further cooling is achieved by the pure oxygen stream O2-1. The distillation process is the main operation of the cryogenic air

separation and occurs in two distillation columns in order to achieve higher purity of the by-product oxygen:

- A high pressure column COLUMN1 operated at 3 bar
- An ambient pressure column COLMUN2.

It is important that the mixture entering in the column must contain a liquid phase, otherwise there will only be one phase (gas phase) in the column, which means that distillation would not be possible. Therefore, an expansion valve has been implemented before the high pressure column where the O_2/N_2 mixture expands down to 3 bar allowing the partial condensation of oxygen. The distillation column enables efficient contact of the descending liquid and the rising gas. Two main operations take place in the distillation column: a) cooling and partial condensation of the rising gas and b) heating and partial vaporization of the descending liquid. In the distillation column, liquid oxygen and nitrogen is produced at the bottom and pure nitrogen at the top. The storage of the hydrogen has been defined for this case at 350 bar. Therefore, the compressions of the hydrogen after the PSA takes place in 3 multi-stage compressors with inter cooling. Each compression stage has a compression ratio of 3.08 with an isentropic efficiency of 0.69.

Table 6 and Table 7 show the simulation results of the heat exchangers, compressors and pumps of the process.
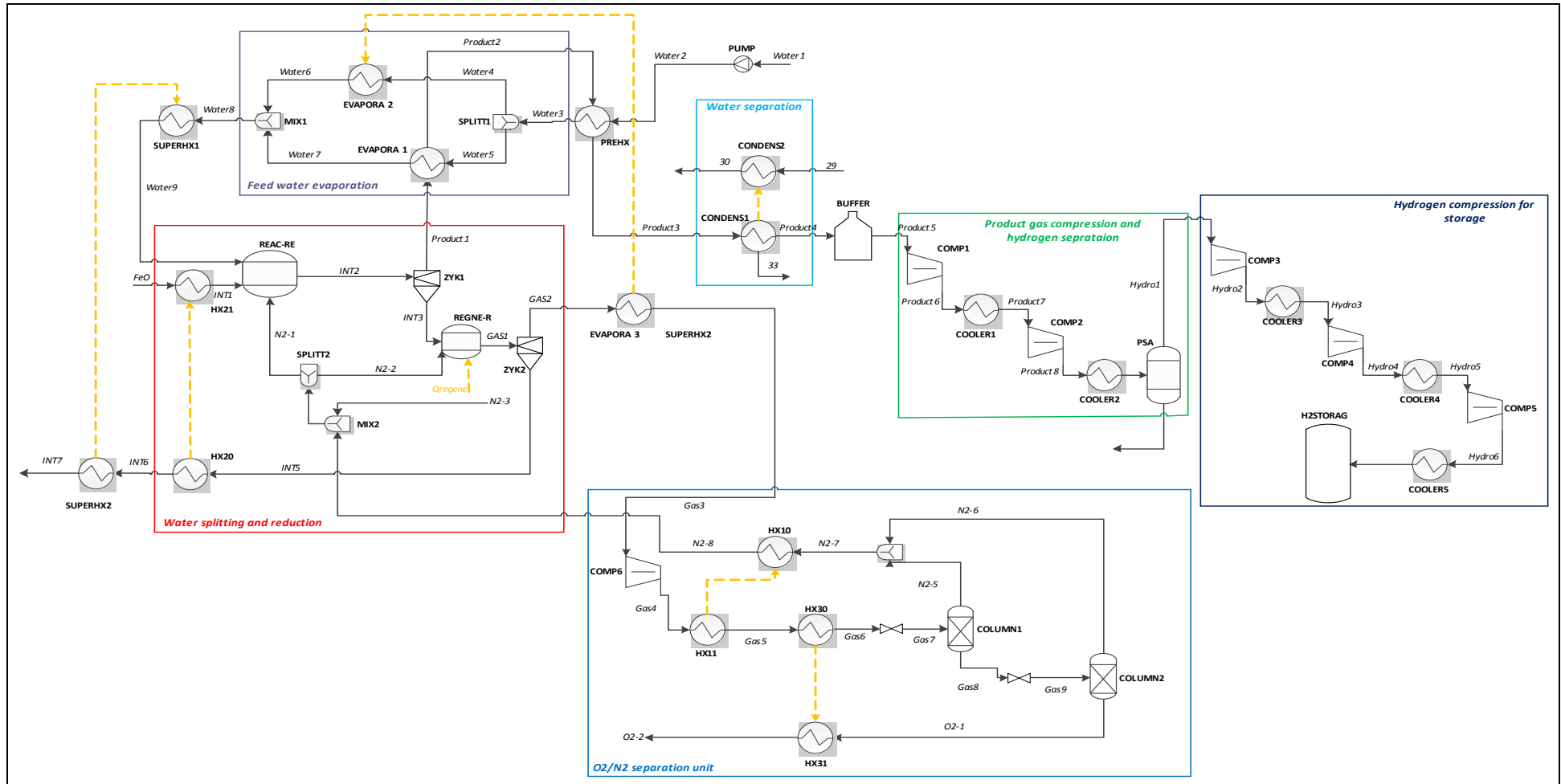
Figure 10: Flow sheet of the Hydrosol plant.

Table 6: Results for heat exchangers of the process.

	Hot side					Cold side					
	T_{in} [°C]	T_{out} [°C]	P_{in} [bar]	P_{out} [bar]	Mass flow [kg/hr]	T_{in} [°C]	T_{out} [°C]	P_{in} [bar]	P_{out} [bar]	Mass flow [kg/hr]	Heat duty [MW]
PREHX	231	144	1	1	7494	50	85	1.066	1.066	10809	0.81
EVAPORA1	896	231	1	1	7494	85	103	1.066	1.066	3242	2.17
EVAPORA2/EVAPORA3	1149	150	1	1	33000	85	103	1.066	1.066	7566	5.08
CONDENS	298	40	1	1	476	25	75	1	1	431487	6.1
HX10/HX11	453	243	6	6	5584	-196	300	1	1	1700	0.33
HX30/HX31	243	-94	6	6	5584	-184	100	1	1	3884	0.51

Table 7: Results for compressors and pumps of the process.

	Mass flow [kg/hr]	P_in [bar]	P_out [bar]	P_{el} [kW]
PSA compression				
COMP1	476.7	1	4	369
COMP2	476.7	4	15	374
Hydrogen compression				
COMP3	431	15	36.9	297.3
COMP4	431	36.9	113.8	320
COMP5	431	113.8	350	339
Air separation				
COMP6	5584.5	1	6	425.88
Water Pump	10809	1	1.066	0.022

After the component sizing, an economic evaluation has been done. Almeria, Spain, has been chosen as plant location. The results are summarized in Table 8 and Table 9:

Table 8: Costs of the solar part.

Equipment / Item	Cost (M€)
Heliostats	10.29
Tower	3.02
Solar reactors including honeycombs and redox material	4.87
Total	18.17

Table 9: Total cost of the equipments of the plant.

Summary of the equipment cost of the plant	Cost (M€)
Compressors and pumps	5.3
Heat exchangers	2.7
Air separation unit (ASU)	3.0
Hydrogen separation unit (PSA)	1.9
Solar part	18.2
Total PEC	31.1

After having calculated the direct and indirect costs and considering a plant life time of 25 years and discount rate of 8%, the hydrogen production costs have been estimated to 8.9 - 10.9 €/kg depending on the percentage factors used for the economic analysis in the factor method (optimistic percentage factors vs. conservative percentage factors).

6.2 Zn-ZnO cycle

6.2.1 Process description

The Zn-ZnO redox cycle has been identified as a promising route due to its potential of reaching high solar-to-fuel energy conversion efficiency [40, 41]. For this thermochemical cycle, concentrated solar light is used to heat ZnO to a temperature above which thermal dissociation of ZnO to Zn (g) and O_2 occurs, that is to more than 1700°C. In a second step the produced Zn - potentially after storage and/or transport – is reacted at a much lower temperature with H_2O to ZnO and H_2, as sketched in Figure 11.
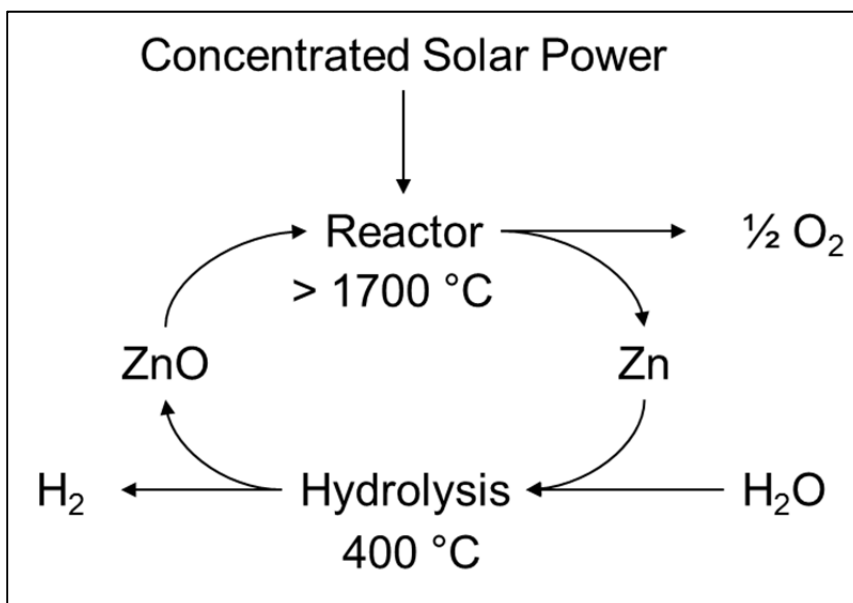

Figure 11: Scheme of ZnO/Zn thermochemical cycle for splitting of H_2O [42].

The following equations describe the chemical reactions. ZnO, the reoxidation product of Equation 7, can be returned to the solar reactor to close the cycle.

1st step: solar-driven endothermic reduction of ZnO:

$$ZnO(s) \rightarrow Zn(g) + \tfrac{1}{2} O_2, \quad \Delta H = 456 \text{ kJ/mol} \qquad \textbf{Equation 6}$$

2nd step: exothermic oxidation of Zn into ZnO and hydrogen:

$$Zn + H_2O \rightarrow ZnO(s) + H_2, \quad \Delta H = -104 \text{ kJ/mol} \qquad \textbf{Equation 7}$$

Remark: The solar produced Zn can also be reacted with CO_2 in the second step according to

$$Zn + CO_2 \rightarrow ZnO(s) + CO, \quad \Delta H = -67 \text{ kJ/mol} \qquad \textbf{Equation 8}$$

By choosing a specific mixture of H_2O and CO_2 for the reaction, a tailor made syngas (H_2, CO) can be produced, suitable for further processing to liquid fuels.

In this study, we concentrate on hydrogen production rather than the production of syngas that is we focus on the combination of Equations 6 and 7.

Many solar reactor concepts were considered by researchers worldwide for the reduction of ZnO using solar energy, from packed beds to entrained and aerosolized flows, to quasi-batch arrangements [43]. The largest scale development so far has been conducted by PSI and ETHZ based on a solar rotary reactor design. Starting with a design initially proposed and investigated at the fundamental and laboratory scale since 1998 it culminated in the demonstration of the process at the 100 kW pilot scale in 2014 [44]. The pilot scale solar reactor is shown in Figure 12.
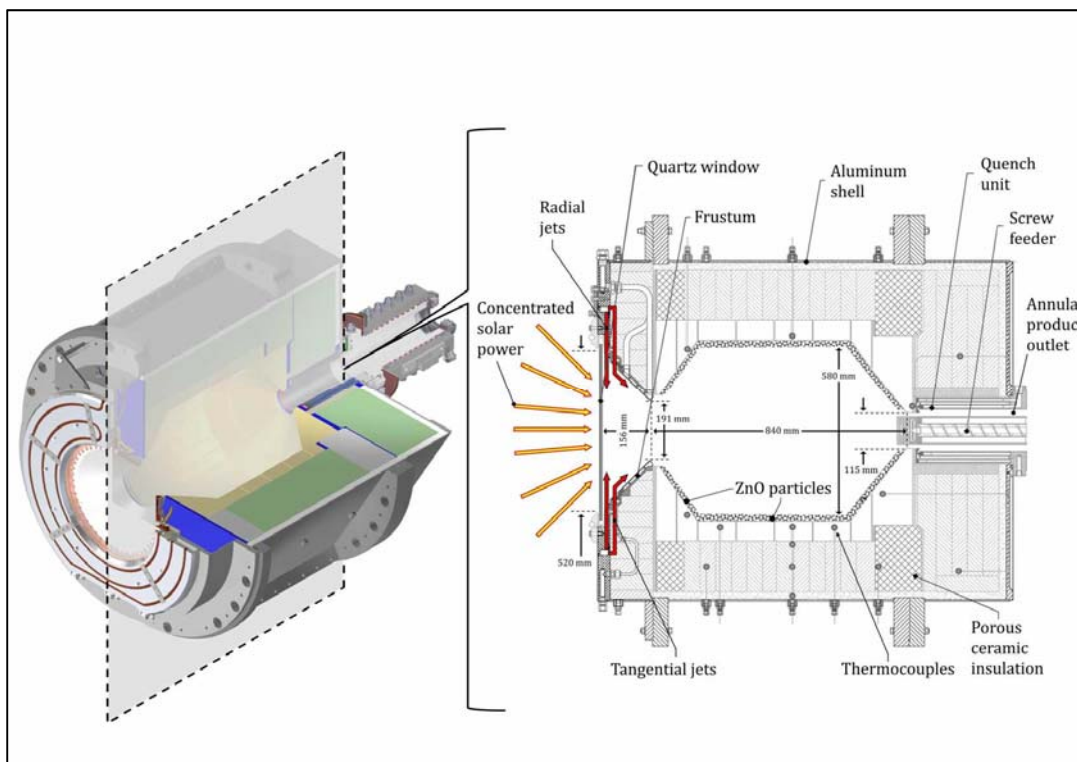

Figure 12: Schematic of the 100 kW solar reactor for ZnO dissociation [44].

In contrast to "non-volatile" cycles like the ones based on ferrites and ceria where the reduced cycling material remains in solid form in the solar reactor and just O_2 and inert carrier gas leaves, in the "volatile" ZnO/Zn cycle a gas-mixture of Zn(g) and O_2 is produced, from which the Zn has to be condensed. This is a challenging step due to the strong tendency for recombination of these gases, once they cool down. Very fast quenching with inert gas is the state of the art approach to recover Zn from this gas mixture. However, as has been shown by modelling [45, 46], an acceptable recovery rate of more than about 50% as Zn (the rest being reoxidized ZnO) can only be expected for a very low partial pressure of Zn (below about 100 Pa). This is in line with experimental findings [47]. Consequently, a very strong dilution of the product gas leaving the solar reactor by a large flow of inert quench gas is required and therefore there is a need to recycle this inert gas by separating it from the product gas O_2 after

filtering off the condensed Zn/ZnO particles. Figure 13 shows these major components in a simplified flow sheet.

Once the Zn is recovered in liquid or solid form, it allows for a flexible storage and transport prior to the performance of the second (oxidizing) step for H_2 production. Hence here H_2-production *on demand* is possible.
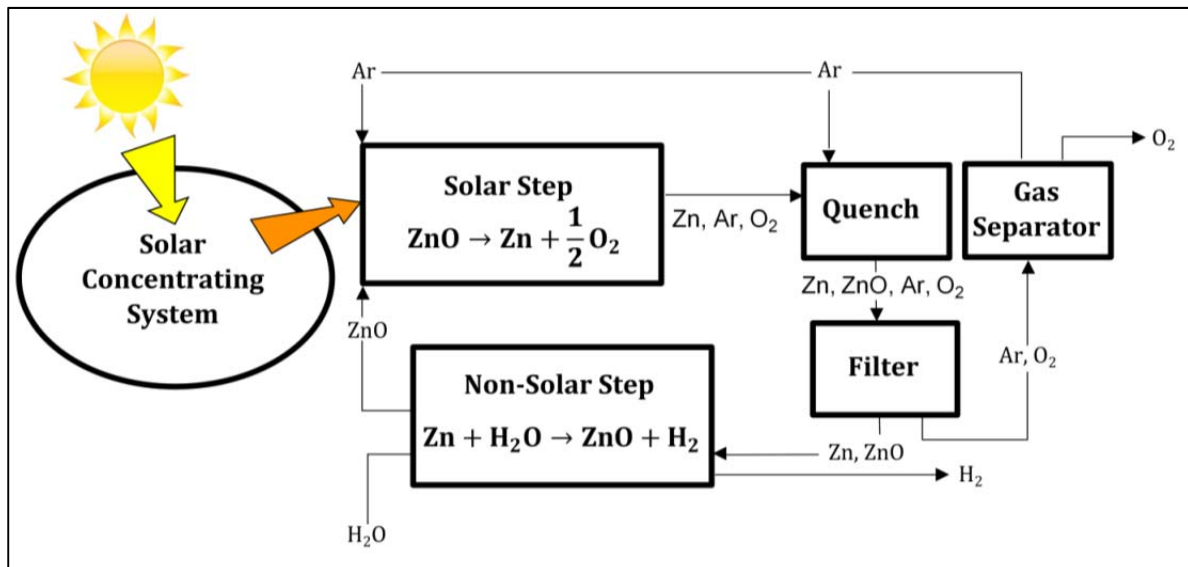

Figure 13: Major steps/components relevant for technology assessment [48].

It should be noted here, that the inevitable occurrence of ZnO in the Zn-particles has been shown to be advantageous for the second process step, the production of H_2 from the Zn/ZnO particles and H_2O [49] (or CO from CO_2 [50]), this in case a solid-gas process operating below the melting point of Zn (420°C) is used. For Zn/ZnO particle mixtures such a process appears to be advantageous compared to hydrolysis reactor concepts operating a higher temperatures with molten or gaseous Zn [51]. A "mixer reactor" concept has been selected and was tested on laboratory scale with respective Zn/ZnO mixtures [51].

A concise more detailed information about the status of the PSI/ETHZ approach for the ZnO/Zn thermochemical cycle can be found in [43].

The Zn/ZnO cycle was long considered as the most promising candidate for thermochemical fuel production, as it possesses a high theoretical process efficiency due to a high operating temperature (that is at the same time achievable) and the fact that the specific fuel capacity of ZnO is very high compared to non-volatile metal oxides because the entire mass participates in the redox cycle [43]. However, meanwhile it is clear that the mentioned issues related to

separation of the Zn and O_2 produced and kinetic limitations make it challenging to reach the full potential of this redox cycle. [1]

The rotary solar ZnO dissociation technology has been demonstrated at TRL 4-5 (Pilot scale tests at PROMES-CNRS/Odeillo with 100 kW solar radiative power input [44] (see Figure 14)). The second (hydrolysis) step is currently TRL 3-4 (lab scale tests [51]). This step is however expected to be the much less challenging one compared to the solar dissociation step.
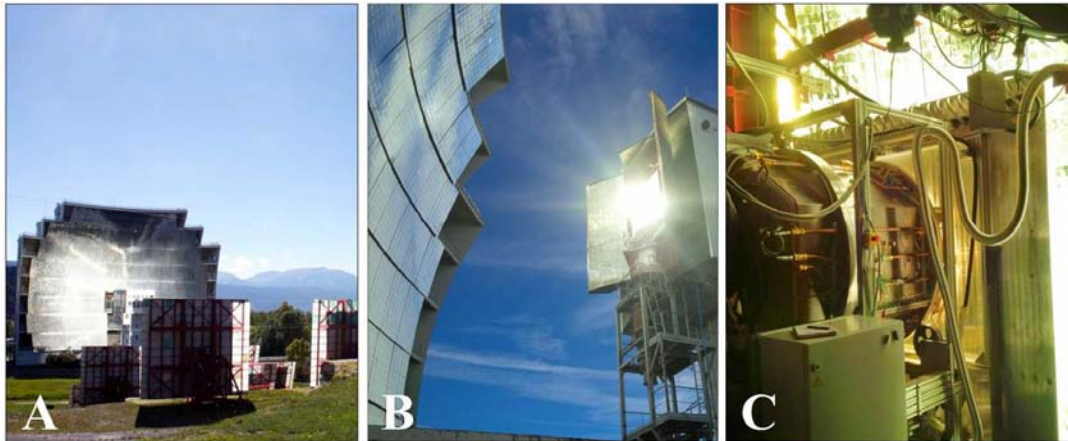

Figure 14: Solar concentrating research facility and pilot plant installation. (A) – Large solar furnace in Odeillo, France. (B) – View of parabolic dish and reactor mounted in experimental tower. (C) – Solar reactor in operation, parabolic dish seen in background.

6.2.2 Technology assessment

The following technology assessment considerations are mostly based on the rotary cavity design for the solar ZnO dissociation reactor followed by a gas quench. Respective technology assessment work has been conducted by [52-58], with [58] basing on [52] and [55]. The most recent work is [48]. Figure 13 shows the main components that have to be considered in the analyses. An important role is played by the inert gas, which is required to some extend in the solar reactor and to a large extend for the quenching process. As explained above it has to be recycled in the process, which requires a gas separation between the produced O_2 and the inert gas ("gas separator").

Table 10 provides an overview over key assumptions and results regarding the expected H_2 cost. Based on the current understanding of the separation process for the Zn-O_2-inert gas mixture a recycling of the inert gas is absolutely necessary, since due to the high amount of

---

[1] These issues can be avoided, if instead of a thermal ZnO-dissociation a carbothermal reduction of ZnO is performed. For this a carbonaceous material acting as reductant is mixed with the ZnO. The product gas is basically a mixture of Zn(g) and CO, a composition whose handling is well known in conventional Zn-pyrometallury. The use of a reductant furthermore lowers the operation temperature from around 1700-1800°C to 1100-1200°C (see Chapter 6.3).

inert gas the related costs would otherwise be even higher. As can be seen in the last lines of Table 10 most analyses did not account for this (or were assuming much lower inert gas rates, which are insufficient based on current knowledge). If one includes this even under quite optimistic further assumptions [48] hydrogen costs of more than 20-30 $/kg have to be expected.

Table 10: overview of cost predictions for H$_2$ production via the ZnO/Zn solar thermochemical cycle.

	Steinfeld [52]	Felder Meier [42, 53, 54]	Charvin et al [55]		Weimer et al [56, 57][1]		Jakober/Koepf [48]	
			Small	Large	2015	2025	Base case	"Realistic improved case"
Reactor rating [MW$_{th}$]	90	50	11	55	112	112	110	110
# of reactors	1	1	1	1	1	1	3	3
Tower height m		100	50	80	250	250	160	160
Total heliostat Area [1000 m^2]	155.2	75.5	21	54.8	167.5	167.5	205.2	205.2
Specific heliostat cost $/m^2	150	140	150	150	126.5	90	151	108
Solar concentration [kW/m^2]	5000	5000	5000	5000	7414	7414	4941	4941
T$_{reactor}$ [K]	2300	2000	2000	2000	2073	2073	2100	2100
Zn - conversion [%]	100	95	61	61	70	85	80	80
H$_2$ -production rate [kg/h]	796	300	50	250	278	297.6		
H$_2$ -production rate [tpd]					6.7	7.1	4.1	4.1
H$_2$ pressure [bar]		30			*20*	20	1	1
H$_2$-Price [$/kg]	5.02	10.0	14.75	7.98	6.07	4.18	8.36	6.2
H$_2$-price accounting for inert gas recycling [$/kg]	> 9						>31.2	>21.9

[1] This work considers another solar reactor concept (indirectly heated falling particles), with costs that are roughly similar with the concept considered in the other investigations.

6.3 Carbothermal ZnO/Zn cycle

6.3.1 Process description

Compared to the ZnO-dissociation process introduced in section 6.2 the addition of carbon as a reducing agent allows to operate at a strongly reduced temperature and to avoid the major issues with the separation of solid Zn from the product gases. In the carbothermal Zn/ZnO thermochemical cycle, carboreduction of ZnO into metallic Zn occurs above about 1000°C and is followed by the exothermic reaction between Zn and H_2O and/or CO_2 to H_2 and/or CO, which is – after optional storage and/or transport - performed in a separate step and at lower temperature, as shown in Figure 15.
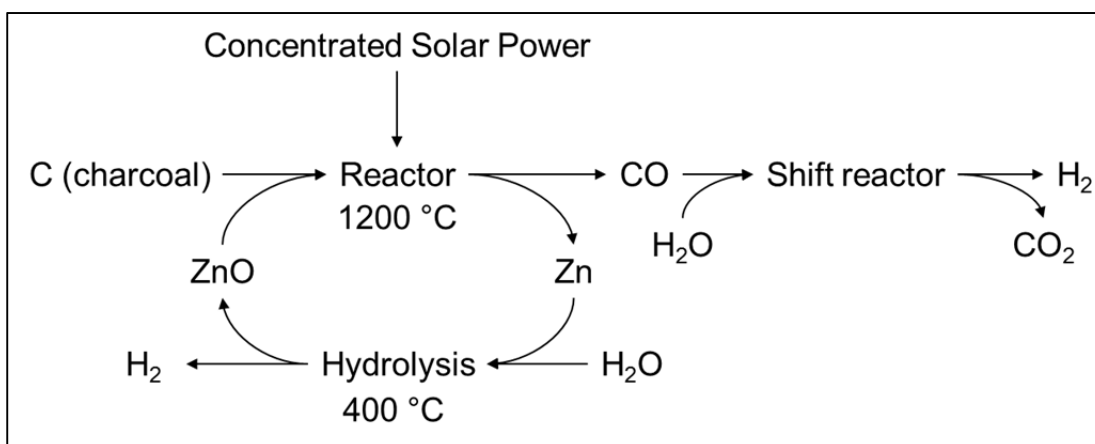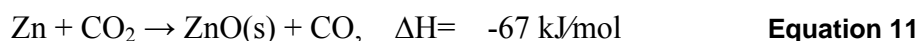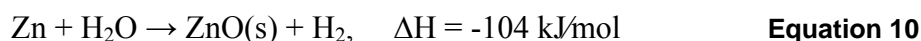

Figure 15: Scheme of ZnO/Zn thermochemical cycle for splitting of H_2O [42].

The following equations describe the chemical reactions.

1st step: solar-driven endothermic reduction of ZnO:

$$ZnO(s) + C(s) \rightarrow Zn(g) + CO, \quad \Delta H_{1500\,K} = 350 \text{ kJ/mol} \qquad \textbf{Equation 9}$$

2nd step: exothermic oxidation of Zn into ZnO and product gases:

$$Zn + H_2O \rightarrow ZnO(s) + H_2, \quad \Delta H = -104 \text{ kJ/mol} \qquad \textbf{Equation 10}$$

$$Zn + CO_2 \rightarrow ZnO(s) + CO, \quad \Delta H = -67 \text{ kJ/mol} \qquad \textbf{Equation 11}$$

In this study, we concentrate on hydrogen production rather than the production of syngas, that is the combination of Equations 9 and 10.

For the first step several solar reactor concepts have been considered for carbothermal reduction of ZnO using solar energy [43]. The largest scale development so far has been conducted by PSI and is based on an indirectly heated packed bed design requiring a vertical concentrated irradiation (beam-down optical concentration system). The process has been developed first on 5kW$_{th}$ laboratory scale [59, 60] and then within the EU-FP5 project

SOLZINC on a pilot scale of 300 kW$_{th}$ concentrated power entering the solar reactor [61], realized at the Weizmann Institute of Science in Rehovot/Israel. Figure 16 shows schematics of the respective solar reactors used on both scales. The gas leaving the reactor is quenched with cold gas. In the pilot plant product gas is used for this (inner recycling loop schematically shown in Figure 17). This results in the formation of μm-size Zn-dust [61]. Depending on specific project requirements larger Zn-particles (Zn-powder) or bulk Zn might be produced, as well, this by using a modified offgas handling system.

In standard pilot tests, a batch of 116 kg pre-mixed ZnO and beech charcoal is placed in the reactor prior to a test day. A slightly understochiometric mixture of carbon and ZnO is used, since this leads - compared to a stoichiometric mixture - to an increased fraction of the energy in the targeted product zinc and a reduced fraction in the (by-)product gas CO [62]. In this case the effective overall reaction reads:

$$ZnO + \alpha C \rightarrow Zn + (2\alpha - 1)\ CO + (1 - \alpha)\ CO_2 \qquad \textbf{Equation 12}$$
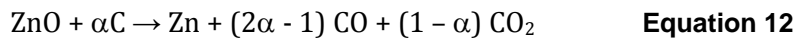
with a stoichiometry factor α typically between 0.8 and 0.9, leading to an uniform reaction of the packed bed from the top without remaining residual ZnO or C, this in contrast to even lower stoichiometries. For the current technology assessment investigation $\alpha = 0.8$ is used for which the gas exiting the solar reactor approximately consists of a mixture of 1 mol Zn, 0.2 mol CO_2, 0.6 mol CO (and a small amount of hydrogen originating from the volatiles in the carbon material).
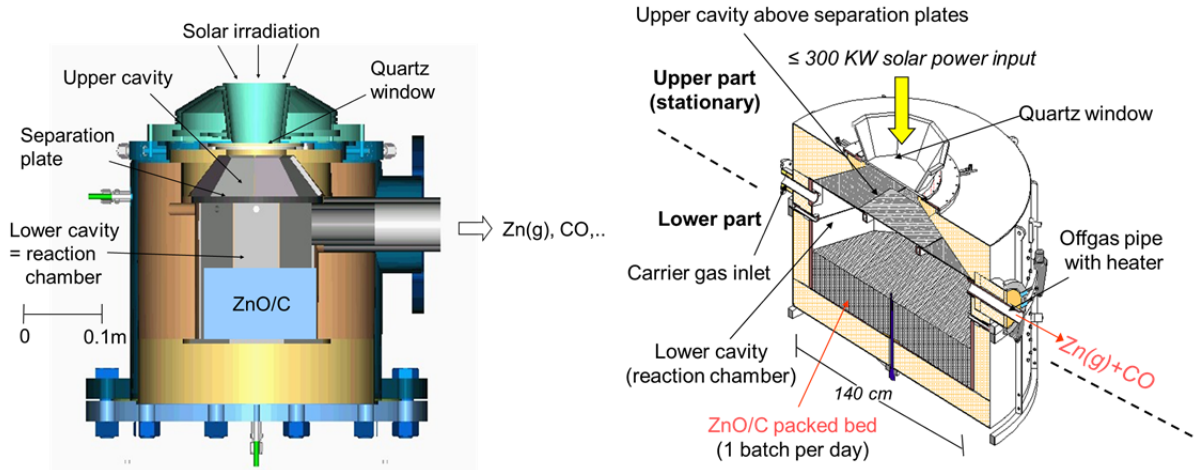

Figure 16: Schematics of lab-scale (left) and pilot scale (right) two-cavity solar reactors for carbothermal reduction of ZnO.

After the promising performance of the pilot plant - by using about 300 kW concentrated solar irradiation up to 50 kg/h Zn dust composed of about 95% Zn and 5% ZnO were produced at a thermal efficiency of about 30% [61] - conceptual design studies for a 5 MW$_{th}$ plant for 1.7 t/h Zn dust production and, less detailed, for a full scale 30 MW$_{th}$ plant for about 10 t/h Zn dust production were worked out [63].

This work formed the basis for the technology assessment activities [42, 64]. A more detailed overview of this development is to be found in [43].
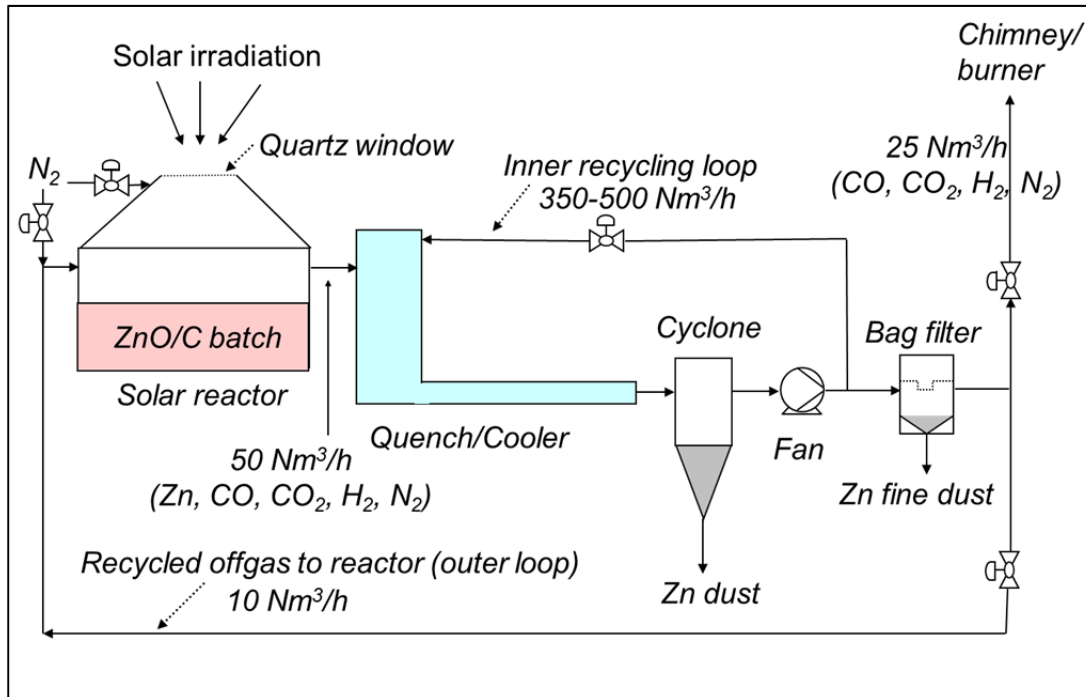
Figure 17: Schematics of the complete SOLZINC pilot plant for carbothermal reduction of ZnO with typical gas volume flows.

For the second step, the Zn-hydrolysis, process studies have been performed on laboratory scale based on the solid Zn - steam reaction (temperature below 420°C, the melting point of Zn), on liquid Zn - steam reaction [65] and on the gaseous Zn - steam reaction [66, 67]. These studies are relevant for the ZnO dissociation cycle (section 6.2) as well as for the carbothermal ZnO/Zn cycle. Low temperature solid gas reactors (e.g. a "mixer reactor" tested on laboratory scale [51]) seem to be specifically suited, especially in case the Zn-particles contain ZnO [50, 51]. Typical solar Zn dust produced via solar carbothermal reduction contains 5-10% ZnO, the rest being Zn. Hydrolysis of original Zn-dust produced in the Solzinc pilot plant [61] at temperatures of up to about 600 °C has been investigated by Vishnevetsky and Epstein [68, 69].

The first step, the two-cavity packed-bed reactor technology including the production of Zn-dust from the offgas, has been demonstrated at TRL 5 (Pilot scale tests at Weizmann Institute of Science with 300 kW solar radiative power input within the SOLZINC project [61]). The second step (Zn hydrolysis [e.g. [51]) is currently TRL 3. However, this step is expected to be the less challenging one compared to the solar reduction step.

6.3.2 Technology assessment

Figure 18 shows the main components of a solar hydrogen production based on the carbothermal ZnO/Zn solar cycle. Figure 19 provides estimated values for a mass and energy balance of a carbothermal ZnO reduction plant suited to produce about 4000 kg H_2 per day, if supplemented by a shift and a hydrolysis reactor. From the offgas about 200 kg H_2/h can be

produced in the shift reactor and about 340 kg/h H_2 can be produced by hydrolysis of the Zn dust, adding up to about 540 kg H_2 per operation hour (or about 4000 kg H_2/day).

Figure 18: Major steps/components relevant for technology assessment.

Figure 19: Process scheme including approximate mass and energy flows of a 32 MW solar carbothermal ZnO reduction plant.

Anticipated costs of upscaled plants based on this solar reactor concept have been estimated [42, 64]. The following table provides some key data from these publications. Only Ref. [42] calculates hydrogen costs, while Ref. [64] is about the cost of the first step only. The last column in Table 11 gives new best guess estimates for a plant as shown in Figure 19.

Table 11: Key inputs and outputs of technology assessments for carbothermal ZnO reduction.

	Felder [42]	Kräupl et al [64] medium	long term	new estimate (based on reactor design)
Annual DNI [kWh/m^2/a]	2000	2100	2100	2138
Nominal irradiation [W/m^2]	860	900	900	742
Reactor rating [MW$_{th}$]	40.5[1]	30	30	32
Total heliostat area [1000 m^2]	75.5[2]	64.1	55.6	82.0[3]
Specific heliostat cost [\$/m^2]	140	150	100	140
Cost heliostat field [M\$]	10.6	9.6	5.6	11.5
Cost land [M\$]	1.0	0.65	0.56	1.0
Cost tower [M\$]	2.2	1.8	1.8	1.59
Cost secondary reflector [M\$]	1.36	1.3	0.7	2.2
Cost CPCs [M\$]	0.91	0.77	0.56	1.9
Cost reactor with offgas system [M\$]	8.2	2.7	2.04	7.2
H$_2$-production hydrolyser [kg/h]	441			339
Cost hydrolyser [M\$]	2.6			2.6
H$_2$-production rate total [kg/h]	624			543
BoP/indirect/contingency [M\$]	4.4			5.1
Invest cost cycle [M\$]	31.3			32.9
Cost shift reactor [M\$]	1.8			1.9
Cost compressor 30 bar [M\$]	7.7			7.1
H$_2$ pressure [bar]	30			30
Invest total [M\$]	42.7			41.9
Carbon cost [\$/t]	20	120	70	100
Annual costs total [M\$/a]	8.75			5.59
H$_2$-Price [\$/kg] at plant	7.3[4]			3.57[5]

[1] 40.5 MW in reactor relates to 50 MW on the tower (prior to hyperbolic mirror and CPC).

[2] based an annual mean efficiency to tower of 0.64.

[3] assuming an optical efficiency to quartz window of 0.52.

[4] assuming capital recovery factor of 0.166.

[5] assuming capital recovery factor of 0.094.

6.4 Hybrid sulphur cycle

6.4.1 Process description

The two-step hybrid sulphur cycle producing hydrogen and oxygen out of water using solar energy is depicted in Figure 20. In the first reaction, sulphuric acid is decomposed at high temperature forming sulphur dioxide and oxygen; the latter being separated from the product gas as a by-product.

The sulphuric acid decomposition is divided into two steps: an evaporation step and a splitting of sulphur trioxide.
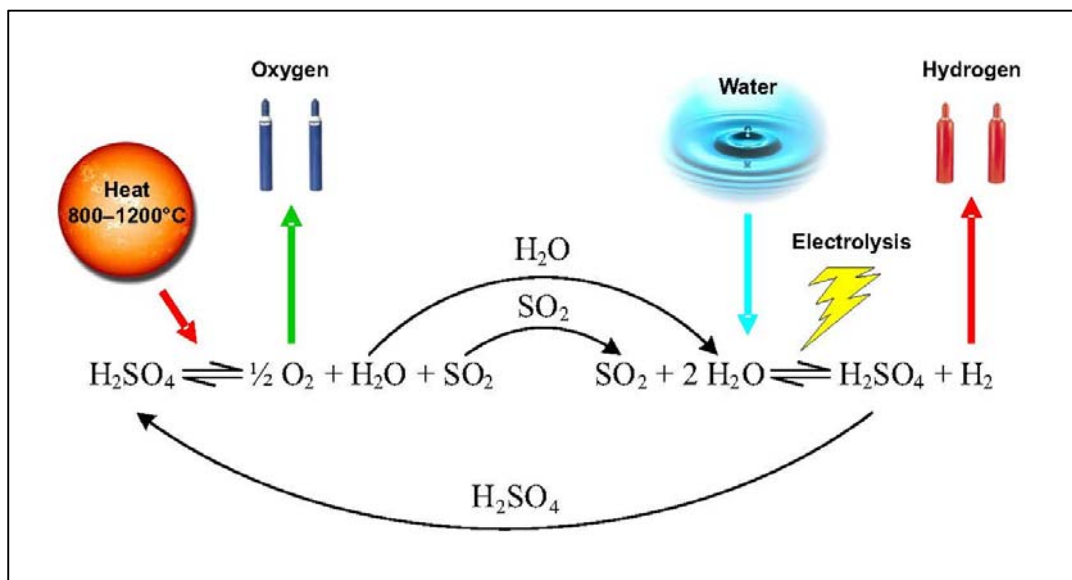
$$H_2SO_{4(l)} \rightarrow SO_{3(g)} + H_2O_{(g)} \qquad (400°C) \qquad \textbf{Equation 13}$$

$$SO_{3(g)} \rightarrow SO_{2(g)} + ½ O_{2(g)} \qquad (800\text{-}1200°C) \quad \textbf{Equation 14}$$

Figure 20: The hybrid sulphur cycle [70].

Sulphur dioxide is electrolysed at about 80 °C together with water in the second reaction generating hydrogen and fresh sulphuric acid, which is recycled back to the first reaction. The standard potential required for this electrolysis is only about a seventh of that needed for conventional water electrolysis, so that the power demand for hydrogen production can be significantly reduced.

The solar sulphuric decomposition step has been studied at DLR since the beginning of the 1990s originally examining solar regeneration of spent sulphuric acid [71]. From 2004 to 2016 DLR has investigated the hybrid sulphur cycle in several European projects developing a directly irradiated receiver/reactor concept for sulphuric acid splitting.

Figure 21 illustrates the development of this process during the last decade including labscale catalyst testing [72], solar furnace experiments of a two chamber solar receiver/reactor for vaporisation of liquid sulphuric acid and subsequent decomposition of sulphur trioxide (compare equations 11 and 12) and, most recently, a demonstration at the Juelich Solar Tower of DLR in Germany at the pilot plant scale (total thermal power of 100 kW, Figure 22) as part of the European project SOL2HY2 [73]. Also, ENEA has widely studied the sulphuric acid decomposition step of the sulphur-family cycles for more than a decade in national (TEPSI) and European (HYCYCLES, SOL2HY2) projects.
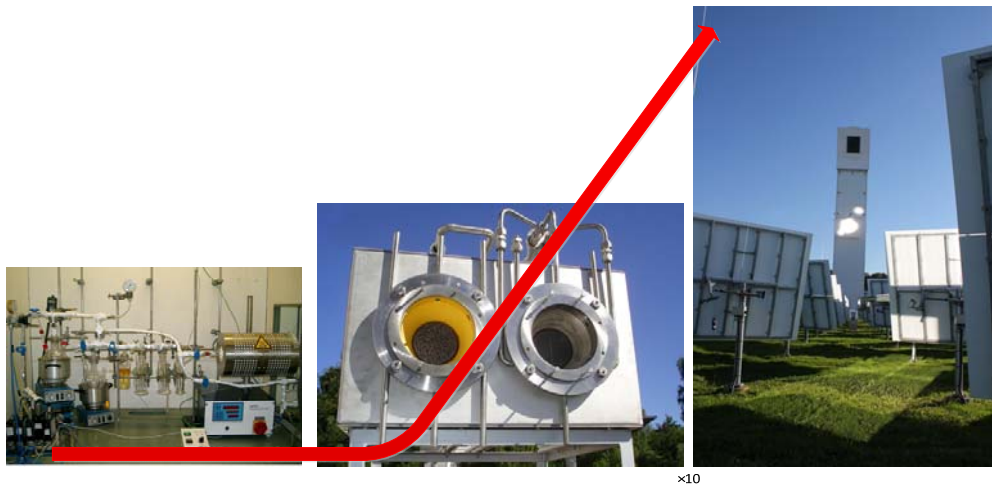

×10

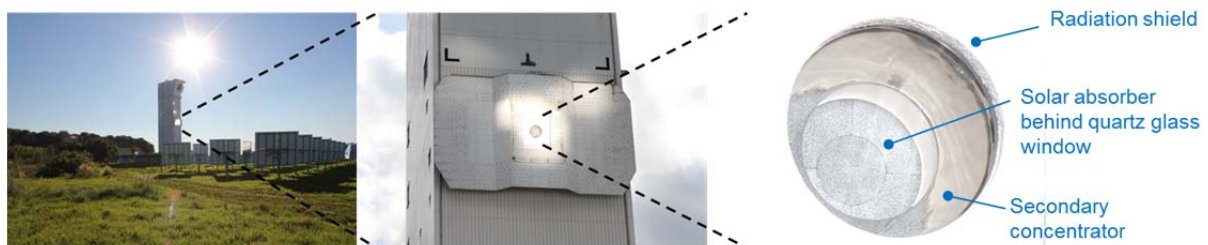**Figure 21: Illustration of the different development scales of the solar hybrid sulphur cycle.**

Figure 22: Pilot plant for sulphuric acid cracking during operation at Juelich Solar Tower (DLR).

Of the sulphur dioxide depolarised electrolyser (SDE) a prototype was developed by Savannah River National Laboratory (SRNL) and installed at the SRNL test facility [74]. Based on experimental results obtained at SRNL, a potential of 0.6 V is attainable at current density of 500 mA/cm^2, under operating temperatures of the order of 100 °C, pressures of greater than 10 bar and with an anode feed stream consisting of SO_2 dissolved in a 50 wt% H_2SO_4–H_2O solution. During the above mentioned project SOL2HY2, the Finnish university AALTO developed and operated a SDE lab system (see Figure 23) designed to operate at room temperature and near ambient pressure while eliminating platinum group metals catalysts completely allowing substantial costs reduction by nearly 70 % compared to analogue PEM designs.
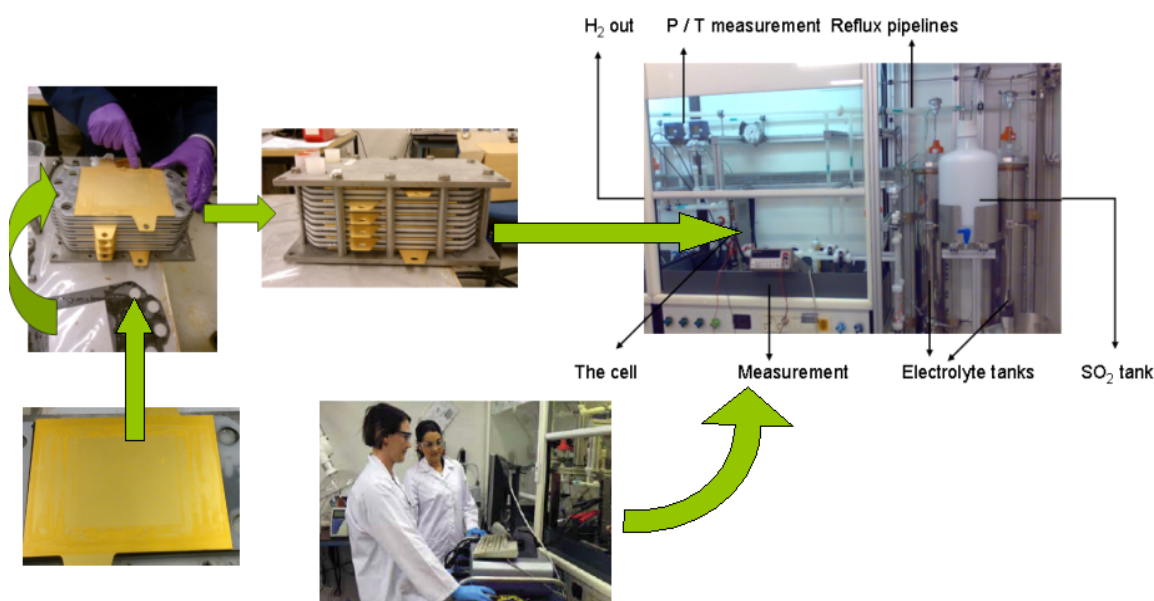
Figure 23: Sulphur dioxide depolarised electrolyser (SDE) lab system of AALTO University, Finland.

6.4.2   Technology assessment

Considering the concept of a directly irradiated sulphuric acid decomposer, Guerra et al. 2015 [75] developed a flowsheet of the hybrid sulphur cycle stressing the importance of heat recovery between high temperature step (sulphuric acid splitting) and low temperature step (sulphur dioxide depolarised electrolysis) and predicting a process efficiency close to 30 %. Corgnale et al. 2011 [76] come to a similar value of 33 % for an indirectly heated sulphuric acid decomposer unit with integrated heat recovery. In this study an economic analysis was carried out projecting hydrogen production costs of 4.80 $/kg (2005 US $) with a strong reduction potential down to 3.19 $/kg due to future development of process components. As part of the SOL2HY2 project (see above), Liberatore et al. 2016 [77] performed a techno-economic study of a process scheme illustrated in Figure 24 and detailed below.

The process considered assumes that the Sulphur Depolarized Electrolyzer (SDE) operates at close to ambient conditions. The effluent anolyte Sulphuric Acid (SA) solution from the SDE is concentrated before being evaporated and heated at 1000 °C; here, concentration from 20% to 75% (weight basis) is assumed. The gas stream at 1000 °C, which is composed almost only of SO_3 and H_2O, is fed to an adiabatic reactor where SO_3 is decomposed in SO_2 and O_2. The conversion of such reaction is thermodynamically limited so that separation and recycling of unreacted SO_3 to the reactor's feed is required. Finally, the produced SO_2 is separated from O_2 by refrigerated compression and recycled to SDE.
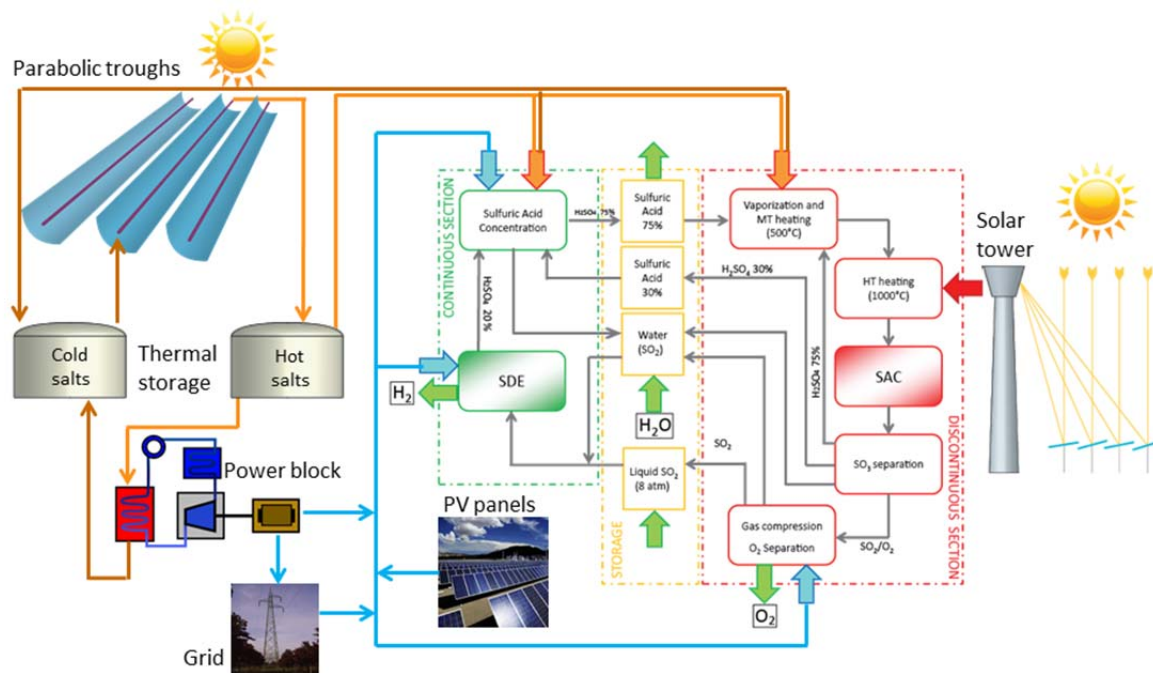
Figure 24: Plant concept scheme of an open hybrid sulphur cycle process.

For the supply of medium temperature (MT) heat, a parabolic trough CSP plant using solar salt as heat transfer and storage medium was considered; 8 h of daily operation were assumed with 16 h of heat storage in order to allow for continuous operation (in nominal conditions) for the process units that rely on this type of energy input. A set of trough loops connected in parallel with 6 collectors per loop was considered for the MT solar field. A central receiver CSP plant was considered to provide high temperature (HT) heat, which is only needed for SA decomposition; 8 h of daily operation and no heat storage were considered in this case, so that SA decomposition and, consequently, SA vaporization and unreacted SO_3 separation are assumed to operate discontinuously, only at daytime.

The CSP plant was sized by fixing the solar power collected at the mirror's surface under specified conditions and accounting for the heat requirements of the chemical plant. A solar-to-heat collection efficiency of 52% and 40% was assumed for the MT and HT CSP plant, respectively.

As for the operating regime and heat input fed to each process block, the following choices were made:

- SA decomposition requires high temperatures, which can be obtained with a CSP system such as a Solar Central Receiver. Since currently consolidated technologies ensure just a few hours of heat storage at this temperature level, this process block was assumed to operate discontinuously (8 h per day).

- SA vaporization is also operated only at daytime, but requires MT heat, which can be provided by the solar trough plant.

- SA concentration is operated continuously, due to the cost of equipment, amortization optimization and, most of all, to avoid daily start-up and shutdown operations, which this type of plant can hardly afford.
- Also in consideration of the temperature level required (< 200°C), this block is powered with MT heat production by the Solar Troughs CSP plants supplied with proper thermal storage and backup systems, in order to ensure the continuity of operation.
- SDE and gas separation units require an electric energy supply and are assumed to work continuously.

Therefore, the CSP plant provides the chemical plant with 3 types of thermal energy input: continuous MT heat, discontinuous MT heat and discontinuous HT heat.

As for electric energy source, multiple options were considered (alone or in combination): electric grid, PV and inclusion of a power block in the parabolic trough plant.

Partially open cycle configurations were also considered: in this case, an external source of SO_2 is required and co-production of H_2 and SA is obtained. The SO_2 required to open the cycle may be produced by burning sulphur if available. In this case, sulphur oxidation also provides a part of the required process heat. The multiple scenarios considered were analysed by multi-objective optimization, finding the lowest specific hydrogen costs of 8.02 €/kg for a plant located in the Atacama desert of Chile with a share of renewable energy of 56 %. In the case of 100 % renewable energy (no consumption of fossil fuels or sulphur), the hydrogen costs increase to 13 €/kg.

6.5 Solar high temperature steam reforming

6.5.1 Process description

Steam reforming of natural gas is the most common method of producing commercial hydrogen. It combines steam and hydrocarbons, which are reacting in a reformer at temperatures above 600°C to produce syngas. The syngas is mainly composed of CO and H_2. The syngas is then treated in order to improve the production yield and to achieve the required specifications and purity of the hydrogen for sale.

Solar heated pressurized volumetric air receivers are used for the steam reforming of carbonaceous feedstocks like natural gas or LPG. Hydrogen production by methane steam reforming wherein concentrated solar radiation is the energy source of process heat contributes to produce energy from a renewable source and reduce CO_2 emissions due to the decrease in fossil fuel burning. Figure 25 shows a simplified flow chart of the solar reforming process.
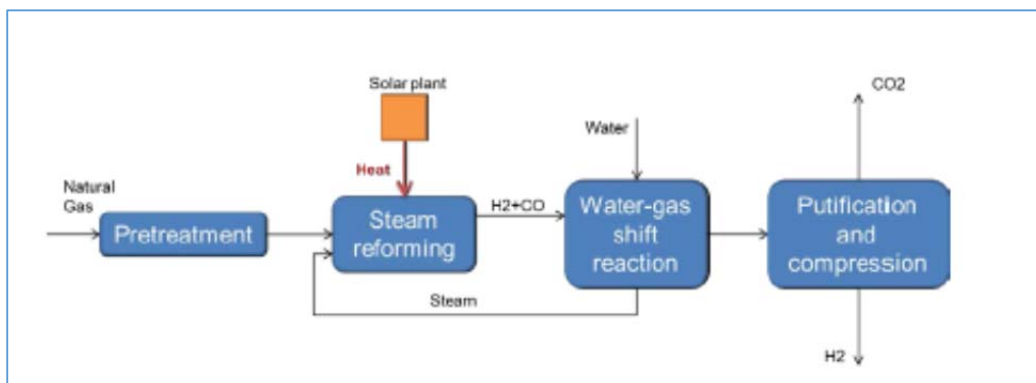

Figure 25: Flowsheet of the solar steam reforming.

A first solar reactor SOLASYS was developed and successfully tested in 2001 for the solar steam reforming (see Figure 26) [78].

Figure 26: SOLASYS Installation on the solar tower of the Weizmann Institute of Science, Rehovot, Israel (2001).

This technology was improved and a cost reduction of 5% [79] could be achieved with the advanced volumetric receiver 400 kW$_{th}$ SOLREF. It was able to be operated at high pressure of up to 15 bar and temperatures of up to 950°C to reach higher conversion rates of methane to hydrogen and higher efficiency [80]. The receiver was more compact than the SOLASYS and the redesign prevented the deposition of carbon in the reactor. The reactor was purged with either CO_2 or hydrogen to avoid steam condensation in the cold parts of the reformer. The system was successfully tested in 2010 on top of the solar tower at the Weizmann Institute of Sciences in Rehovot, Israel (see Figure 27) with a CH_4 conversion of 94,6% and hydrogen was produced.
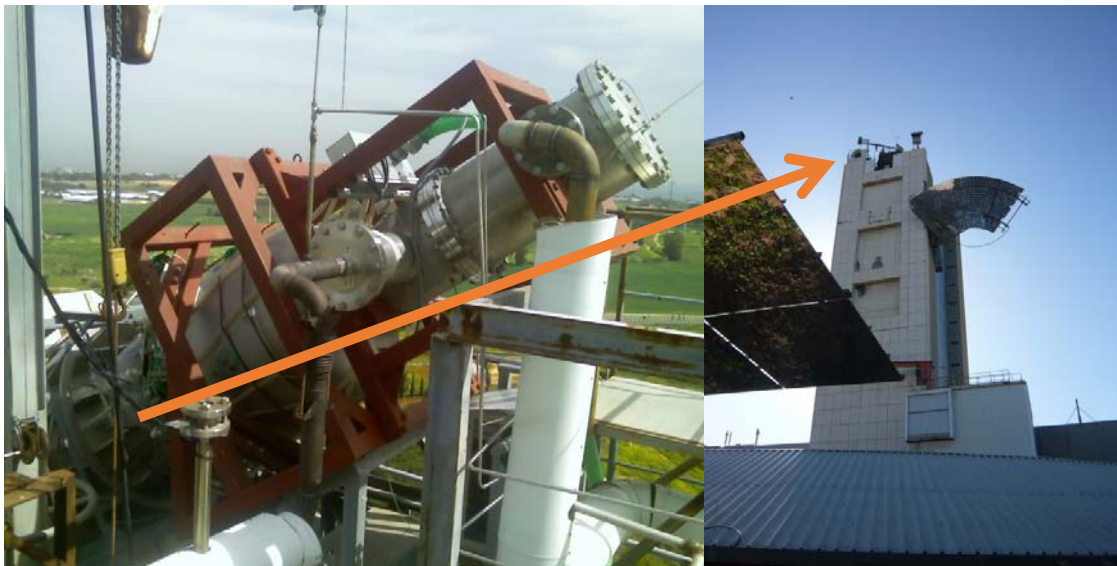

Figure 27: SOLREF Installation on the solar tower of the Weizmann Institute of science, Rehovot, Israel (2010).

This technology is a near-term process and has a TRL of 5-6.

6.5.2 Technology assessment

Flowsheets and simulations of the solar steam reforming process have been carried out for a hydrogen production rate of 400 kg/h. The hydrogen is compressed at 21 bar. The corresponding Aspen flow sheet is shown in Figure 28.
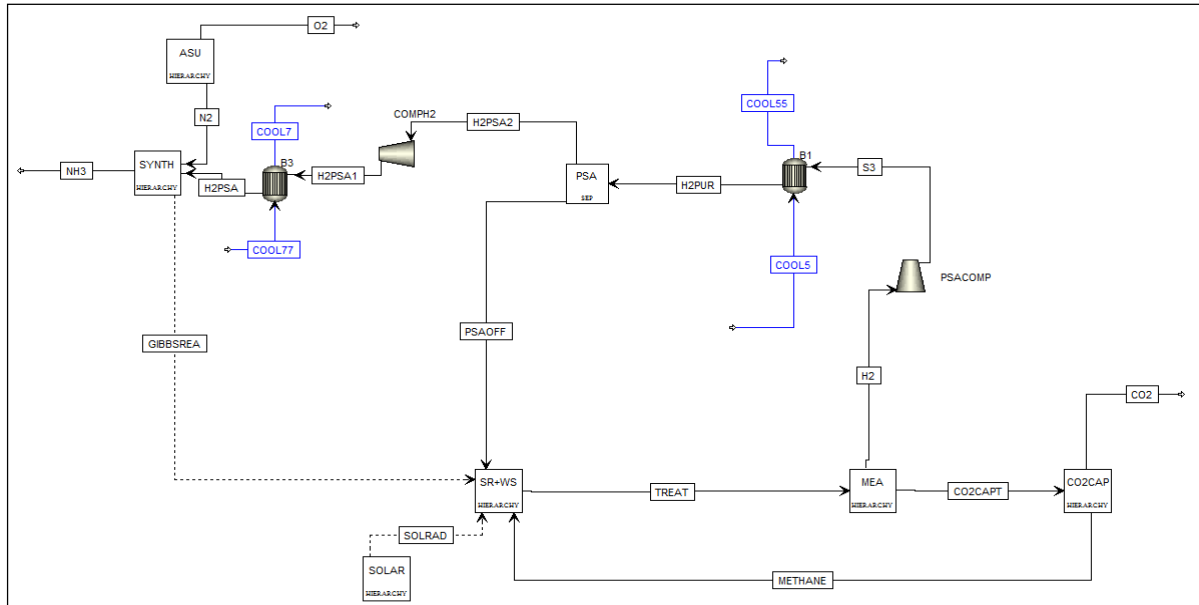
Figure 28: Flowsheet of the solar steam reforming process (DLR).

The Aspen Plus main flowsheet of the solar SMR process shows several hierarchy blocks describing different process operating Units of the process. Five units are considered:

- SR+WS: Steam reforming and water gas shift Unit
- CO2CAP: CO_2 Capture Unit
- CO2COMP: CO_2 Compression Unit
- PSA: Pressure Swing Adsorption Unit
- SOLAR: Solar loop Unit

This process model unit of the steam reforming and WGS reactions contains 4 equilibrium reactors (REquil):

- Pre-reformer
- Steam-Methane Reformer (SMR)
- High-Temperature water-gas Shift (HTS)
- Low-Temperature water-gas-Shift (LTS)

The process hat two main feed streams the natural gas (NG) and the water (WATERIN). The natural gas is, mixed with the two obviously mentioned recycling streams (PSAOFF and METHANE) before been further associated with preheated steam. The pressure of reactants is fixed at 27 bar. The steam is generated by using heat recovery system. The feed water is pumped into the process. A pressure of 31 bars is calculated after considering the pressure drop in each heat exchanger. The feed water is preheated then evaporated by using the heat of the exothermic shift reaction and the syngas leaving the low temperature shift reactor. The produced steam at 210°C is fed later to the top of the high temperature water-gas shift reactor and reaches a temperature of 232°C. The last heating step occurs in the top of the main reformer where the syngas is cooled from 900°C to 350°C. The steam is superheated till 800°C and flows with the gas mixture in the pre-reformer. Under those conditions, no heat is

required for the activation of the highly endothermic cracking reaction in the pre-reformer. This heat recovery strategy allows saving almost 2496 kW, which is supposed to be externally supplied. The pre-preforming is assured at a range of 400-550°C [81]. For the Aspen Simulation the reactor temperature is chosen as 550°C in order to assure optimal preheating conditions for the main reformer.

Two CO_2 purification technologies have been investigated within the analysis of the solar steam reforming, namely the physical and the chemical separation. In order to compare which process is exergetically and energetically more suitable and more effective, a CO_2 recovery of 94% was fixed for both processes. Figure 29 shows the results of the exergy analysis of the steam reforming process for the two CO_2 separation technologies. The exergy efficiency of the solar steam methane reforming is defined as the ratio of the product exergy flow recovered in the hydrogen stream to the total exergy delivered into the system. The exergy efficiency is given by the next equation:

$$\eta_{exergy} = \frac{\dot{E}_{H2}}{\dot{E}_{NG} + \dot{E}_{elec} + \dot{E}_{Heat} + \dot{E}_{Cooling}} \qquad \textbf{Equation 15}$$
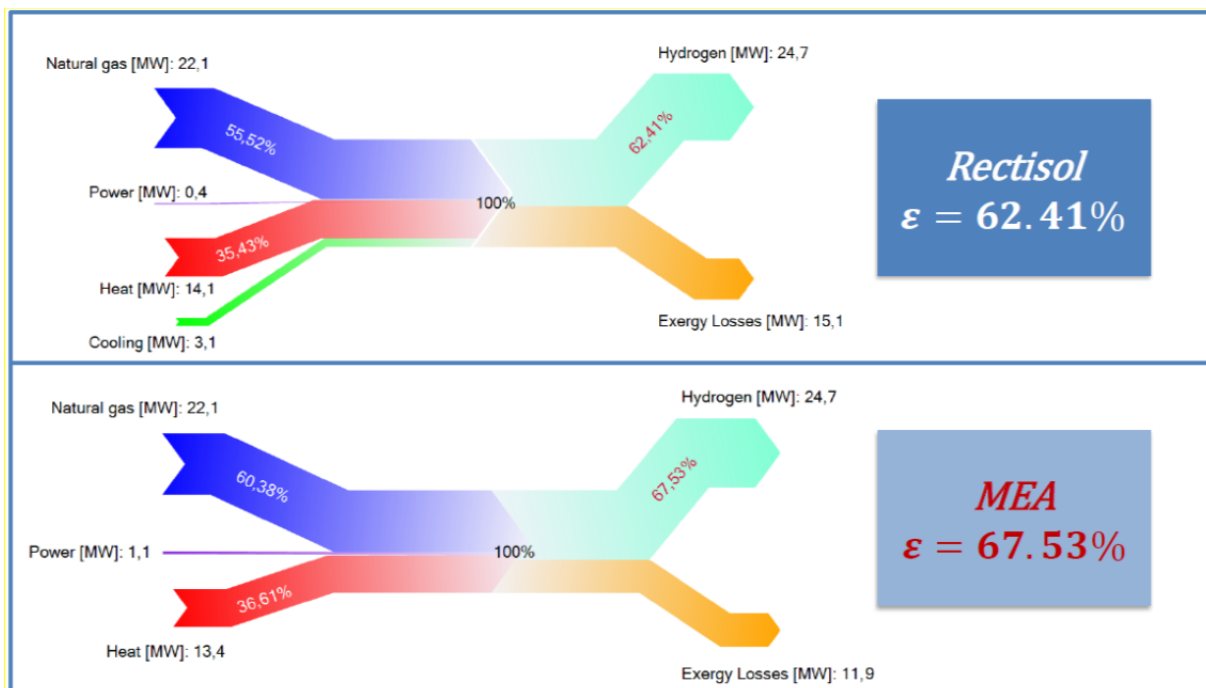

Figure 29: Exergy analysis of the solar steam reforming for both separation technologies.

The analysis shows that the chemical separation of CO_2 is the most efficient process based on the exergy efficiency. This was calculated to be at 67.53%.

The design of the CSP solar tower has then been generated by the DLR internally developed software HFLCAL. According to the latitude and the elevation of the site as well as the operating conditions of the receiver and the plant thermal duty, the layout of the concentrating

solar tower and the heliostats field is generated. Table 12 shows the results of the design of the solar part of the plant.

Table 12: Results of the solar part of the plant.

Parameter	Value
Receiver inlet temperature [m²]	309
Receiver outlet temperature [°C]	920
Thermal duty of the receiver [°C]	25
Tower height [m]	60
Tower diameter [m]	16
Heliostat area [m²]	122
Number of heliostat	365

The process efficiency was calculated to be 40%. The economic study of the solar steam reforming process has been carried out. The results are shown on Figure 30.
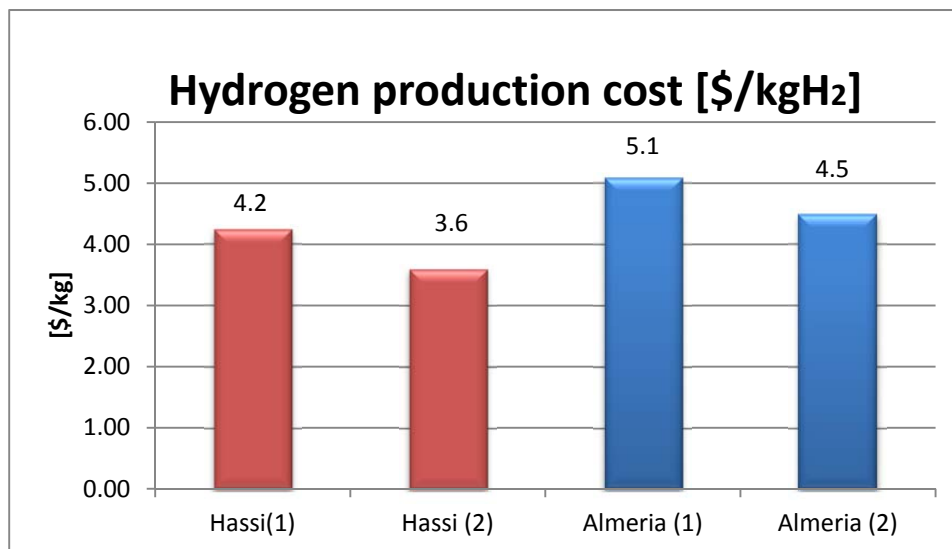

Figure 30: Hydrogen production costs for the solar steam reforming process (DLR).

6.6 Solar low temperature MS-heated reforming

6.6.1 Process description

Conventional steam reforming processes are carried out at temperatures above 800 °C in externally heated tubular reactors and the reaction heat duty is provided by placing the reactor tubes inside fossil fuel furnaces. Several economic and environmental advantages could be obtained by lowering the operating temperature below 565 °C; among these are: the use of lower grade materials, reduced overall process heat requirements and the possibility to provide the heat of reaction with concentrated solar thermal (CST) plants using the so-called solar salt, i.e. a binary molten salt (MS) mixture of $NaNO_3$ and KNO_3 (60%/40% w/w), as heat transfer fluid. Such type of installations can rely on the only commercial heat storage solution available to date for CST plants; this is a very important feature, especially when the CST plant must provide process heat. Indeed, heat storage ensures a smoother and extended heat supply to the chemical plant, potentially attaining round-the-clock solar operation with the appropriate design and insolation conditions. Therefore, the operation of the chemical plant is more stable and its capacity factor dramatically improved.

An innovative steam reforming reactor was recently developed and tested at the laboratory and pilot scale within the CoMETHy project [82]. Such reactor was designed for the low-temperature (450-550°C) steam reforming of several carbonaceous feedstocks like methane, biogas and (bio)ethanol using a MS stream at 550-565°C as heat transfer fluid to provide the process heat.

The reactor has a shell-and-tube configuration (see Figure 31), where the MS stream flows in the shell-side.
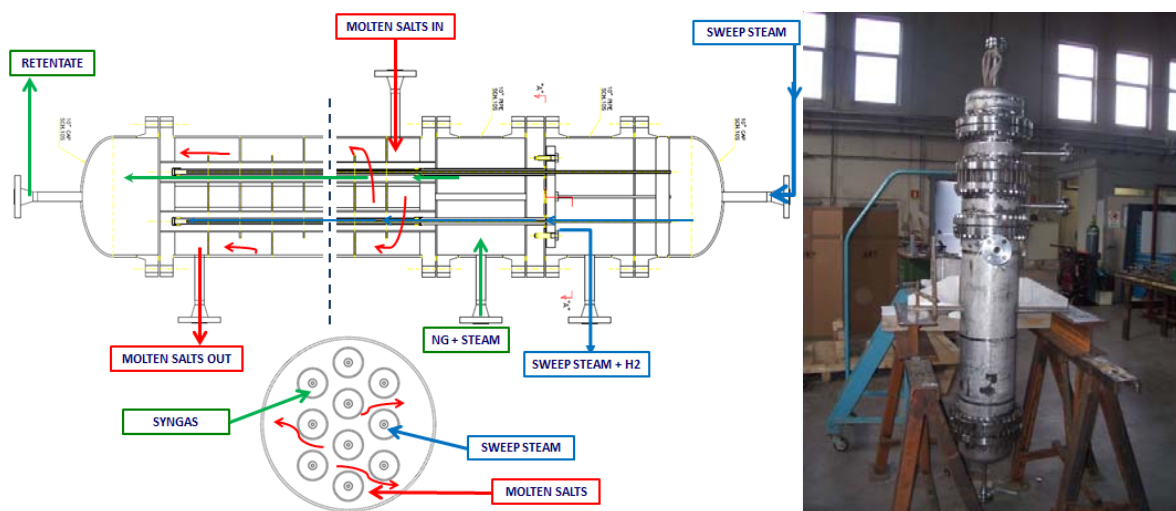

Figure 31: Integrated membrane reactor. Left: Reactor scheme. Right: Lab-scale reactor.

Reaction tubes are immersed in the molten salt flow and are composed by two coaxial elements: an external steel tube, which is in direct contact with molten salts, and an internal cylindrical hydrogen-permeable membrane (see Figure 32).
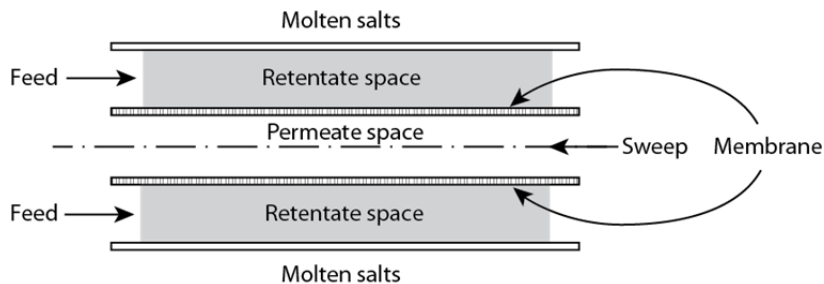

Figure 32: Details of the reaction tube as part of the membrane reactor.

A sweep gas such as steam is fed inside the membrane (permeate space) in counter current flow to enhance hydrogen permeation.

By continuously removing hydrogen from the reaction space, the integrated membranes allow to push the conversion of the feedstock beyond the low values that could be obtained with conventional reformers at such low temperatures.

6.6.2 Technology assessment

The system analysis for low-temperature MS-heated reforming is based on a membrane reactor and considers CH_4 as reformable feedstock. In the process analysis, the plant is assumed to operate continuously using heat from the hot MS stream coming from the solar plant: when solar energy is not available and the heat storage of the CST plant is depleted a backup fuel fired heater to heat the MS [83].

Two main process configurations were analyzed:
- Retentate recirculation: in this configuration, the retentate at the outlet of the reactor is compressed and recycled to the reactor's feed after CO_2 removal; the heat duty of the reactor is entirely provided by the Molten Salt (MS) stream, which is heated either by the CST plant or by a backup burner.
- Retentate burning: in this configuration, the retentate, which contains CH_4 and H_2, is burnt to provide a part of the heat duty of the reactor, while the remaining part is provided by the hot MS stream.

Only solutions with retentate recycling will be considered here. For such solutions, two further cases were studied:
- Power export: MS provide heat only for the chemical process (reactor heat duty and generation of process steam) and for the generation of superheated steam to be used in a power cycle. The excess power produced is exported to the grid.
- No power export: MS provide heat only for the chemical process.

Finally, for the moment 2 different plant capacities were considered: 1,500 Nm^3/h (3.2 t/d) and 5,000 Nm^3/h (10.8 t/d). Different reactor architectures were assumed for the different plant capacity (see Figure 33): an integrated membrane reformer (such as the one previously described) for the 1,500 Nm^3/h and a multi-stage reformer with inter-stage membrane separation of hydrogen for the 5,000 Nm^3/h plant. The reason for this choice is that the non-integrated configuration appears as more suitable for larger capacity reactors.
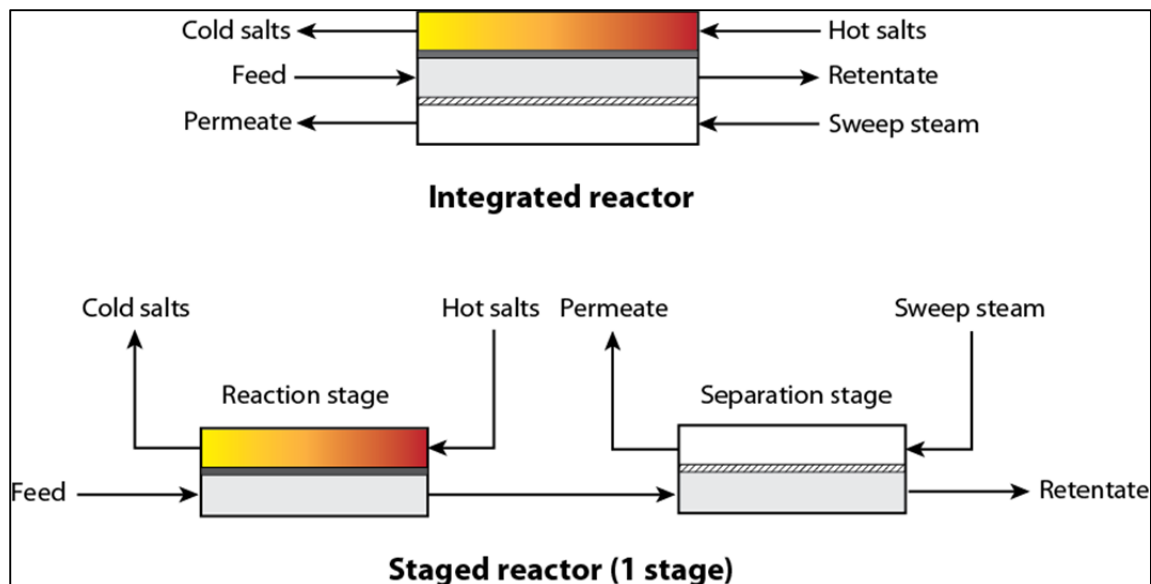

Figure 33: Conceptual schemes of the integrated (top) and staged (bottom) membrane reformer (only one stage is represented for the staged configuration).

Figure 34 shows the reference process flow chart for the retentate recirculation scenario with power export. The solar plant, which includes the solar field and thermal energy storage system, is designed to heat and store MS up to a temperature of 550°C. MS are fed to the SR section (blue shaded circle in Figure 34). The MS temperature at the outlet of the reaction section is around 490°C. Since cold salts are stored at 290°C the residual MS heat is used to produce the process steam required for the SR reaction and the sweeping steam for membrane separation stages; additional steam is produced and used to generate power in a steam turbine. Excess electrical power is exported to the grid.

The NG is mixed with steam and sent to the reaction section, which operates at about 540°C and 10 bar. Hydrogen recovered by the membrane units is compressed up to 20 bar. The retentate, which contains unreacted CH_4 and H_2O, CO_2 and CO (a few mole percent) produced by the reaction and H_2 not separated by the membranes, is firstly cooled down and the heat recovered is used to generate steam. Subsequently, CO_2 is removed by a conventional amine absorption process and the remaining stream is compressed and recirculated to the feed of the SR section.

When the cost of electricity is low, a second option can be considered which excludes power export. In this case the steam generator/superheater placed downstream of the reforming

section is substituted with a lower duty steam generator, which produces only low pressure and process steam. As a result, the temperature of the molten salts stream returned to the cold storage tank is about 400°C and the thermal duty of the solar plant is about 40% lower compared to the scenario including power export. In general, compared to conventional steam reforming processes, the solar processes developed in CoMETHy require higher initial CAPEX due to the rather relevant investment for the CST plant and ancillary items: the CAPEX impact on the hydrogen cost is, in most cases, > 45%, while the CAPEX impact in conventional steam reforming routes is usually < 25%. This larger CAPEX is however balanced by savings in operative costs for the feedstock and the fuel in the solar process. As a result, the overall hydrogen production cost obtained by CoMETHy solar steam reforming technology does not significantly differ from conventional routes.

- In the 5,000 Nm^3/h solar steam reforming schemes, hydrogen COP is within the range of 1.09-1.22 €/kg, considering a 5,000 hours/year full-solar operation. These values are rather close (< ±10% difference) to the value of 1.19 €/kg estimated for a conventional steam reforming process (i.e. without solar input) under similar assumptions (including CO_2 recovery).
- In the process scheme with 1,500 Nm^3/h hydrogen production capacity, with 2,000 – 4,500 solar hrs/year (the balance is non-solar reforming using retentate combustion as back-up to heat molten salts) considering the results from the sensitivity study (economic parameters: depreciation factor, cost of NG, catalysts, membranes, CST plant, by-products, etc.) the hydrogen production costs obtained were always within the range of 2.02-3.36 €/kg, a cost that is rather close to the one obtained in conventional steam reforming of 1.74 €/kg.

Further information can be found in the final summary report of the CoMETHy project [84].

Figure 34: Process flow chart for low temperature MS-heated reforming ("retentate recirculation" scenario with power export).

6.7 Solar driven solid oxide electrolysis

6.7.1 Process description

Since 1990, more than 41 international power-to-gas (P2G) pilot plants have been installed and run producing hydrogen for Grid balancing [85]. With P2G, excess electricity is converted into hydrogen by water electrolysis. This hydrogen can be stored in pressurized tanks and, when needed, it can be reconverted into electricity with fuel cells or hydrogen combustion engines. Besides its use as an energy vector for electricity, hydrogen can be used as fuel for transport applications, as a raw material for the chemical industry, or for the synthesis of various hydrocarbon fuels such as methane. Additionally, a certain percentage of hydrogen could be directly fed into the gas distribution system; furthermore, there should be no limitations, whereas hydrogen is previously converted to methane [85, 86].

Current P2G projects commonly integrate alkaline or proton exchange membrane (PEM) electrolyser for hydrogen generation due to the maturity of this technology. However, the power consumption of water electrolysis is still above 4.5 kWh_{el}/Nm^3 of hydrogen, and also these plants required a second system to convert the hydrogen back to electricity [86, 87]. These hydrogen-to-electricity systems use to be PEM Fuel cell or internal engines [85]. High temperature steam electrolysis with Solid-Oxide cells shows great advantages conventional alkaline and PEM electrolyser [87]. These advantages stay on its high operational temperature, among 600 to 1000 ºC. From a thermodynamic point of view, hydrogen split reaction can be described by the Gibbs function:

$$\Delta G = \Delta H - T \cdot \Delta S \qquad \textbf{Equation 16}$$

where ΔH is the overall energy needed, ΔG is the electrical energy and $T \cdot \Delta S$ is direct heat. As can be seen in Figure 35, electrical requirement decreases and heat energy demand increases with increasing temperature. Even though total energy demand increases, the decrease in electrical energy demand is more noticeable. Operation at high temperature can therefore decrease the electricity consumption and projects less generation cost. Cost reduction can be greater if the heat energy demand can be fulfilled by industrial waste heat source [87, 88].
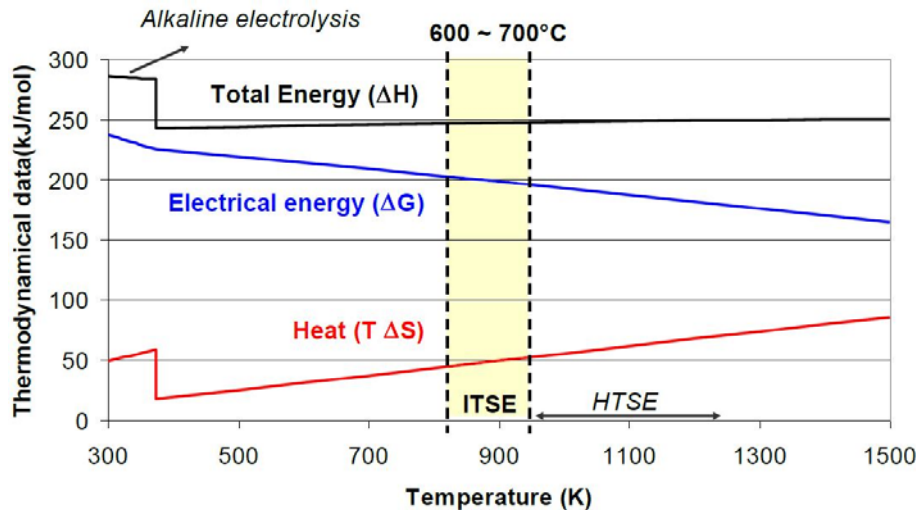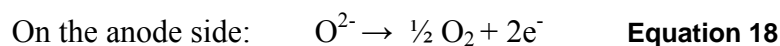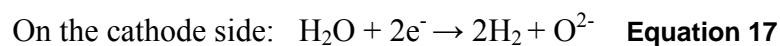
Figure 35: Free energy water split diagram. Temperature interval 600-700ºC would apply to Intermediate Temperature Steam Electrolysers (ITSE). Temperatures above 700ºC are used by High Temperature Steam Electrolysers (HTSE).

From the kinetic point of view, high temperature helps to promote electrode activity and reduce cell overvoltage. It means that power density can be increased, reducing the size of the electrolyser for a given production. On the other hand, lower cell overvoltage can be translated to lower energy losses, thus more electric efficient process [89]. Additionally, Solid-Oxide systems are able to work either as electrolyser (SOEC) or as fuel cell (SOFC), reducing the number of units and its auxiliary elements.

In the literature several studies about hydrogen production by hybrid plants where SOEC systems are integrated into solar, biomass or nuclear power plants can be found [90-93].

The total energy demand of the electrolyser unit consists of electricity and heat, which can be both generated by solar concentrating energy systems. The feed water of the electrolysis process is introduced as superheated steam at a temperature about 750°C. The splitting of water can be achieved through the high temperature electrolysis, which uses a combination of electrical energy and high temperature heat [94]. The chemical reactions, which take place in the electrolyser, are given as follows:

On the cathode side: $H_2O + 2e^- \rightarrow 2H_2 + O^{2-}$ **Equation 17**

On the anode side: $O^{2-} \rightarrow \frac{1}{2} O_2 + 2e^-$ **Equation 18**

Both reactions give the overall water splitting reaction:

$H_2O \rightarrow H_2 + \frac{1}{2} O_2$ **Equation 19**

The SOEC technology is still at applied research stage or lab-scale and has a TRL of 4. Moving from lab-scale to large scale prototype (TRL 5) tested in intended environment will be crucial for technology deployment. This design should be based in a modular stack. Crucial is to demonstrate lifetime.

6.7.2 Technology assessment of the coupling of a solid oxide cell unit and a solar power tower

A 3 kWe high temperature electrolyser has been recently developed and built to be coupled with a concentrated solar energy source [95]. The coupling was successfully done with a solar receiver delivering superheated steam (Figure 36) at the solar simulator from DLR, Cologne.

Figure 36: Solar receiver operating in the solar simulator at DLR, Cologne.

Different possibilities of the solar energy source integration to HTE system have been studied including the different CSP technologies. Being given the importance of a good storage for the fully solar-driven HTE system, it has been focused in this study on the coupling of pressurized high temperature (co-) electrolyser with the molten salt solar tower technology due to its higher storage capacity. This coupling has been thus studied in details including a thermal storage [96]. The analysis has shown that this technology is able to provide the electrolyzer with the required energy in order to run the electrolysis process. The system consists of the molten salt tower, the HTE unit and the heat recovery system. The molten salt tower system includes the tower, the solar receiver and the heliostat field, which reflects the incident solar radiation onto the receiver, as well as the thermal storage and the engine, which converts heat into mechanical work. An electrical generator, attached to the heat engine, generates electricity. The Solid Oxide electrolyzer operates at 750°C and 15 bars. In this study, a steam-to-hydrogen conversion of 50% is assumed. The main specifications of the HTE unit are provided in Table 13.

Table 13: Main specifications of the HTE unit.

Parameter	Value
Operation Mode	Thermoneutral
Sweep gas/cathode stream ratio	1:1
Steam conversion	50%
Operating pressure	15 bar
Inlet/outlet cathode temperature	750°C
Inlet/outlet anode temperature	750°C
H_2 concentration at cathode inlet	10%

Process flow sheets have been developed for corresponding MW-scale plants with the simulation software Aspen Plus 8.4 with regards to the optimal integration of the pressurized high temperature electrolyser with the solar energy source for a large-scale system. In Figure 37 the process for production of hydrogen is represented. The flowsheet does not include the solar part (heliostat field, receiver and storage) of the plant. The heat exchanger named HX-Receiver represents the heat supply from the receiver or energy storage. The solar electricity is generated by a Rankine cycle, where water is preheated, evaporated and superheated by the heat transfer fluid (molten salt) already heated in the solar receiver.
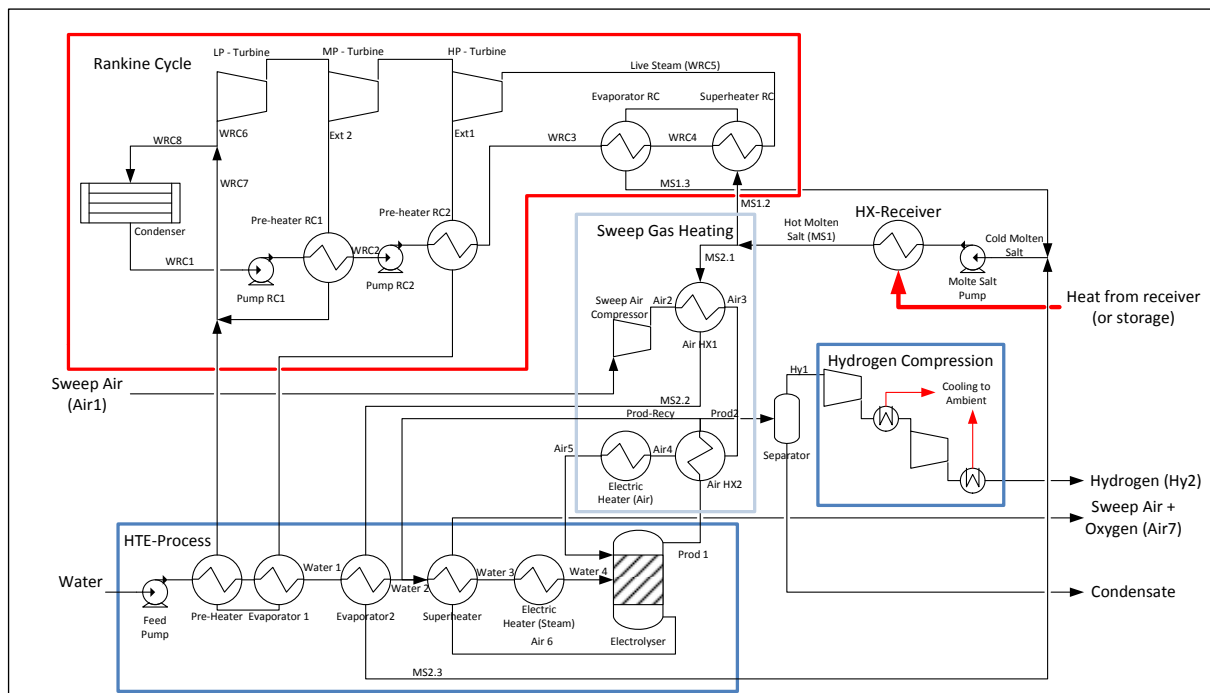
Figure 37: Flow sheet of the HTE process coupled to a molten salt solar tower.

In order to enhance the economics of the process, thermal energy storage is considered in order to increase the electrolysers operating time beyond the hours of sunlight. By doing this, the size of the process can be reduced for a given output, because the operating hours are increased. Furthermore, the daily operating time will strongly depend on the size of the heliostat field, solar receiver and thermal storage, as well as of the size of the process itself. Therefore, two scales of 400 kg/d for mobility and 4000 kg/d for industrial use are considered as guidance value, rather than a fixed parameter. For the design of the process, an average optimized operating time of 12 h per day is assumed, resulting in an hourly production of hydrogen of 33.33 kg/h for mobility and 333.33 kg/h for industrial use. This always refers to the hydrogen output. In the case of syngas production, the total mass output is accordingly higher. Furthermore, because it can be expected, that for the larger scale the turbines of the Rankine cycle will have higher efficiency, the industrial scale will consider an improved Rankine cycle efficiency.

In the process, the molten salt is heated to a temperature of 565 °C. A part of the molten salt is used to generate steam for the Rankine Cycle, which then generates electricity to supply the parasitic loads as well as the electrolysis unit. Another part of the molten salt is used to preheat the air that is used for sweeping the oxygen from the electrolysis unit and afterwards to partially evaporate the feed water. The feed water is pumped to the required pressure level and pre-heated and partially evaporated (approx. one third) by the first extraction from the turbine. Subsequently molten salt evaporates the remaining water. The steam is mixed with a recycle stream and they are superheated by the hot sweep air and oxygen flow from the electrolyser. In order to achieve the required inlet temperature, an electric heater further heats the steam flow. The water is partially split in the electrolyser to hydrogen and oxygen. The hydrogen leaves the electrolyser with the remaining water on the anode side of the cell. The water/hydrogen mix heats the incoming air and is further cooled in a separator in order to condensate the water. The hydrogen is then compressed to the required pressure in an intercooled multi stage compressor. The oxygen is transported through the membrane to the cathode side and swept with hot air. The oxygen enriched air leaves the cathode side and is cooled by heating the steam. In the Rankine cycle, two turbine extractions are used for preheating the feed water.

In Table 14 the results for significant streams for the process for mobility scale (400 kg/d H_2) are given. In industrial scale (4000 kg/d H_2), the general process layout is identical but the efficiency of the turbines is increased to 85%, compared to the reference value of 69%. The results for the relevant streams in the industrial scale flow charts are given in Table 15.

Table 14: Data for process with H_2 as end-product mobility scale (400 kg/d).

Stream	H_2O kg/hr	H_2 kg/hr	O_2 kg/hr	N_2 kg/hr	Mass Flow kg/hr	Mole Flow kmol/hr	Temperature ° C	Pressure bar	Vapor Fraction
Water	546.3	0	0	0	546.3	30.3	25	1	0
Water1	546.3	0	0	0	546.3	30.3	198	15	0.335
Water2	595.7	6.6	0	0	602.4	36.4	256	15	1
Water3	595.7	6.6	0	0	602.4	36.4	720	15	1
Water4	595.7	6.6	0	0	602.4	36.4	750	15	1
Prod1	297.9	40	0	0	337.8	36.4	750	15	1
Prod2	248.4	33.3	0	0	281.7	30.3	586	15	1
Prod-Recy	49.5	6.6	0	0	56.1	6,0	586	15	1
Hy1	0.7	33.3	0	0	34.0	16.6	25	15	1
Hy2	0.7	33.3	0	0	34.0	16.6	80	30	1
Air1	0	0	244.3	804.6	1049.0	36.4	25	1	1
Air3	0	0	244.3	804.6	1049.0	36.4	545	17	1
Air4	0	0	244.3	804.6	1049.0	36.4	720	17	1
Air5	0	0	244.3	804.6	1049.0	36.4	750	15	1
WRC3	8082.3	0	0	0	8082.3	448.6	190	123	0
WRC5	8082.3	0	0	0	8082.3	448.6	545	121	1
MS1	-	-	-	-	54579.7	596.9	565	20	0
MS1-3	-	-	-	-	52670.8	576.0	220	18	0
MS2-2	-	-	-	-	1908.9	20.9	220	20	0

Table 15: Data for process with H$_2$ as end product industrial scale (4000 kg/d).

Stream	H$_2$O kg/hr	H$_2$ kg/hr	O$_2$ kg/hr	N$_2$ kg/hr	Mass Flow kg/hr	Mole Flow kmol/hr	Temperature ° C	Pressure bar	Vapor Fraction
Water	5463.2	0	0	0	5463,2	303,3	25	1	0
Water1	5463.2	0	0	0	5463,2	303,3	198	15	1
Water2	5957.7	66.3	0	0	6024,1	363.6	256	15	1
Water3	5957.7	66.3	0	0	6024.1	363.6	720	15	1
Water4	5957.7	66.3	0	0	6024.1	363.6	750	15	1
Prod1	2978.9	399.7	0	0	3378.5	363.6	750	15	1
Prod2	2484.4	333.3	0	0	2817.7	303.3	586	15	1
Prod-Recy	494.5	66.3	0	0	560.8	60.4	586	15	1
Hy1	6.5	333.3	0	0	339.9	165.7	25	15	1
Hy2	6.5	333.3	0	0	339.9	165.7	80	30	1
Air1	0	0	2443.4	8047.1	10490.5	363.6	25	1	1
Air3	0	0	2443.4	8047.1	10490.5	363.6	545	17	1
Air4	0	0	2443.4	8047.1	10490.5	363.6	720	17	1
Air5	0	0	2443.4	8047.1	10490.5	363.6	750	15	1
WRC3	64812.4	0	0	0	64812.4	3597.6	190	123	0
WRC5	64812.4	0	0	0	64812.4	3597.6	545	121	1
MS1	-	-	-	-	441647.0	4830.0	565	20	0
MS1-3	-	-	-	-	422610.0	4621.8	220	18	0
MS2-2	-	-	-	-	19036.4	208.2	540	20	0

The thermal-to-fuel efficiency of the process is defined as the higher heating value (HHV) flow of the product in relation to the thermal energy input. The central data for energetic evaluation of process for hydrogen production and the two scales is given in Table 16.

Table 16: Data on process with end-product hydrogen.

	Mobility Scale	**Industrial Scale**
Thermal Energy Input (kW)	6053	48981
Thermal Energy to RC (kW)	5882	47006
Efficiency Rankine Cycle	27.1 %	33.8 %
Electricity Consumption Electrolyser (kW)	1391	13919
Hydrogen Production (kg/h)	33.33	333.33
Hydrogen Production, HHV (kW)	1312.5	13127
Thermal-to-Fuel Efficiency	21.7 %	26.8 %

The simulations showed that thermal energy demand is very low in the mobility case (6 MW$_{th}$). It is expected that for a process at this scale the efficiency of components such as the turbines is much lower than at larger scales. The thermal energy demand for the industrial scale is in the range of 50 MW$_{th}$, hence closer to the state of the art solar power plants. The results indicate that the larger scale industrial HTE-process will achieve significantly higher efficiencies than the small-scale application.

The efficiency of the solar part is defined as the ratio of the solar heat supplied to the solar reactor to the available solar resource. The final solar-to-fuel efficiency, taking into account the thermal-to-fuel efficiency and the efficiency of the solar part has been calculated to be 15.1% considering the specifications described in Table 16.

The economy study of the solar driven high temperature electrolysis process has been carried out for the case of the production of hydrogen in Huelva, southern Spain by coupling the high temperature electrolyser with the molten salt solar tower technology. The CSP installation was considered in this case as the single source of heat and electricity to feed the whole process. A production of 4,000 kg hydrogen per day was estimated for the year 2025. The annual DNI in Huelva is about 2,054 kWh/m². To simulate a whole year, real data from Meteonorm were used. The values were given in hourly intervals for a typical year for the chosen location. The solar part of the plant consisting of the heliostat field, the tower and the solar receiver was simulated and dimensioned with HFLCAL software. The component costs for all main components of the overall plant have been estimated and finally, CAPEX and OPEX have been calculated. An operation time of 12 hours per day of the electrolyser was considered with a thermal storage capacity of 6 hours as well as hydrogen storage. Considering an economic life time of 25 years, the estimated costs of solar hydrogen are 10.9 €/kg.

The composition of all major equipment costs as well as indirect costs is shown in Figure 38.
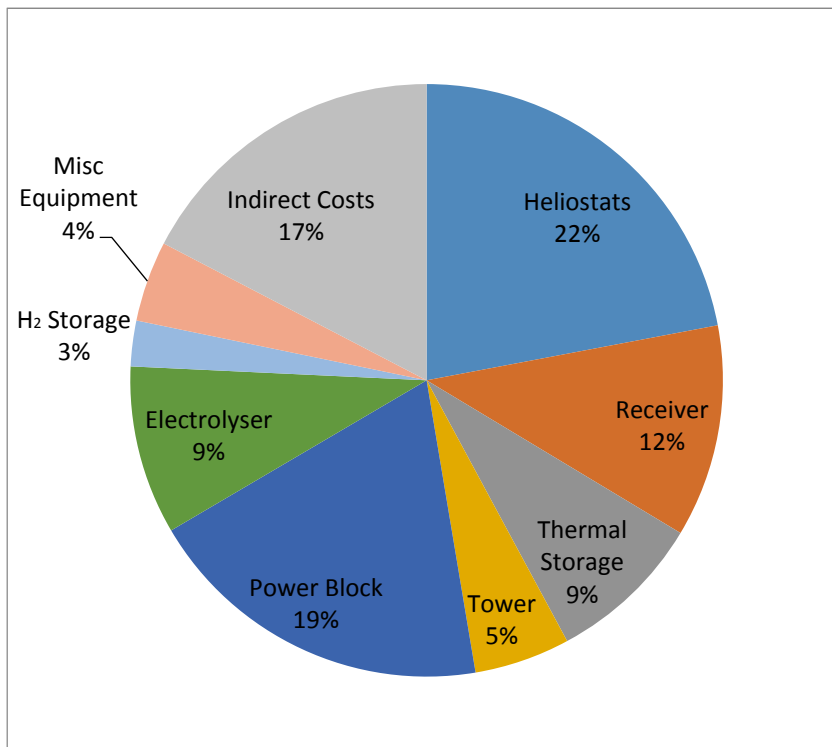

Figure 38: Cost distribution, 4000 kg/d H$_2$, Spain.

With 22 %, the heliostat field is the most expensive part of the overall plant. Together with the tower, the solar receiver, the power block and the thermal storage, the solar part represents 67 % of the overall costs. With additional on green grid production of 17.5% on cloudy days the cost will decrease to 9.6 €/kg. Neither extra revenues (as extra heat or oxygen valorization) nor typical subsidies for solar generated electricity were considered here, which will result in a reduction of the hydrogen production costs. Results are shown on Figure 39. Considering an optimistic development of solar components costs and an additional grid production up to 20% as well as subsidies, the hydrogen production costs could decrease to 3 €/kg.

Moreover, a sensitivity analysis was carried out taking into account the variability of the component costs (Figure 40). The indirect costs, the heliostat field and the power block cause a change of the production costs of hydrogen of more than 8% by a 50% component discount. The solar receiver and the electrolyser have an impact of 4 % to 6 %. The thermal storage, the tower and the hydrogen storage only have an impact of less than 4 %. Reducing all costs about 20 % and estimating the same values for yearly production, recovery period and O&M as above means an overall discount of almost 40 % on the production costs of hydrogen.
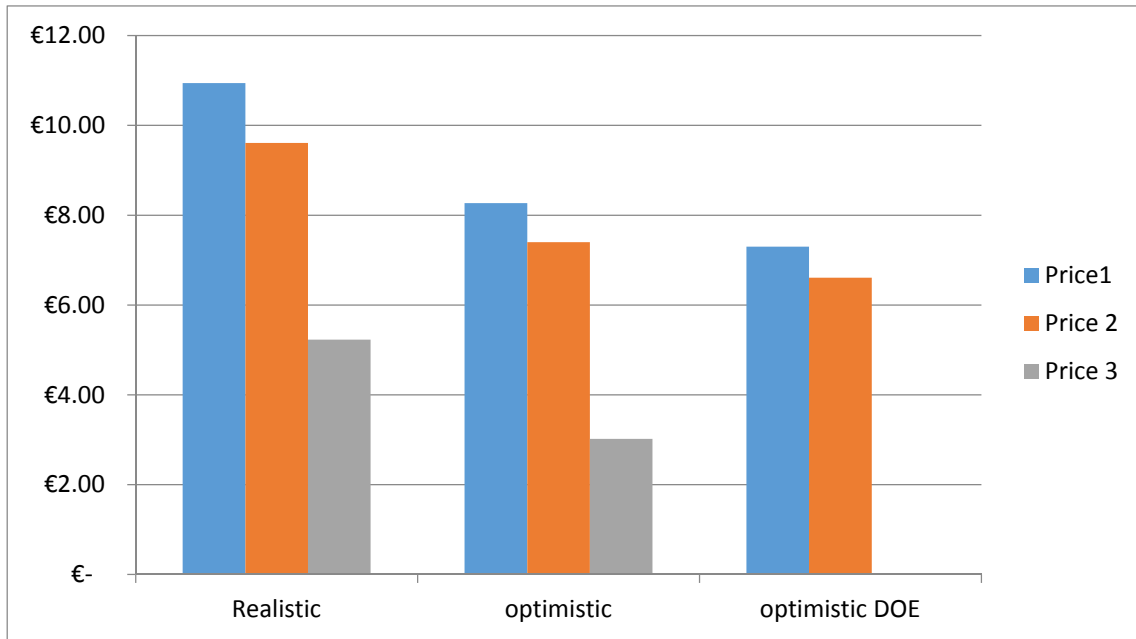
Figure 39: Hydrogen production costs for the solar driven high temperature electrolysis and sensitivity analysis- Price 1: Basic costs of hydrogen production - Price 2: Like Price 1 but electricity (max. 20 %) is taken from the grid to fulfil daily production requirement (max. 20 %) - Price 3: Like Price 2, but subsidies, that conventional CSP plants receive are considered (DLR).
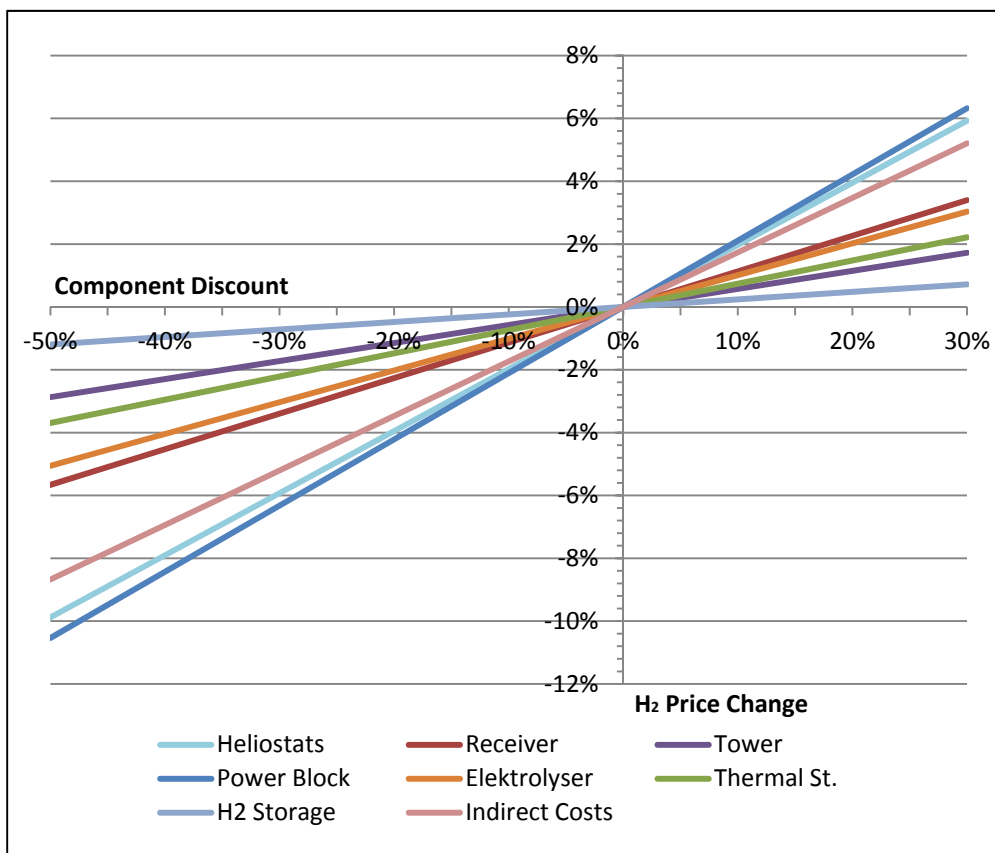
Figure 40: Sensitivity analysis of components.

6.7.3   Technology assessment of the coupling of a solid oxide cell unit and a linear Fresnel reflector

SOEC systems are characterized by the high temperature at which they work, and the requirement of feeding directly with steam. Therefore, for this work, a concentrating thermal solar system is proposed to deliver enough heat for the evaporation of the feed water. Based on their simplicity and the low cost of the components, a linear Fresnel reflector (LFR) and castable ceramic thermal energy storage (TES) were selected [97, 98]. Although LFR normally uses water as heat transfer fluid, thermal oil was retained as heat transfer fluid [99], this due to the characteristics of this system such as: no requirements of power production from the solar plant because the system is analyzed as an active grid balancing system, the level of temperature (above 300 ºC), the displacement on times of collecting and delivering heat, and the requirement of maximum simplicity to reduce cost.

In the present study, the proposed P2G plant is located near Seville, southern Spain. This is analyzed under a scenario where the Solid-Oxide unit is only used as steam electrolyser producing hydrogen that is directly sold to a hydrogen bus refuelling station. In relation with this scenario, the capability of the plant to feed 20 hydrogen metropolitan busses, which requires among 400-600 kg/day of hydrogen has been analysed [100]. In the scenario, where hydrogen is directly sold to a buss refuelling station, the hybrid plant is used to minimize the reduction of the Spanish demand during night hours. Lastly, all the simulations have been carried out with Ebsilon Professional software [101].

The P2G plant proposed in this work is presented in Figure 41. At the upper section, it can be seen concentrating thermal solar system; while at the bottom, the SOE/FC system (operating as electrolyser) is shown. In both scenarios, hydrogen is compressed up to 30 bar before it is delivered to the refuelling station or stored for later used in fuel cell mode. The compressor has five stages. Each of them has a nominal compression ratio of two that result in a maximum outlet temperature of 120ºC. Before entering the next compression stage, the gas is cooled down to 45 ºC with water, and the condensed steam is drained.
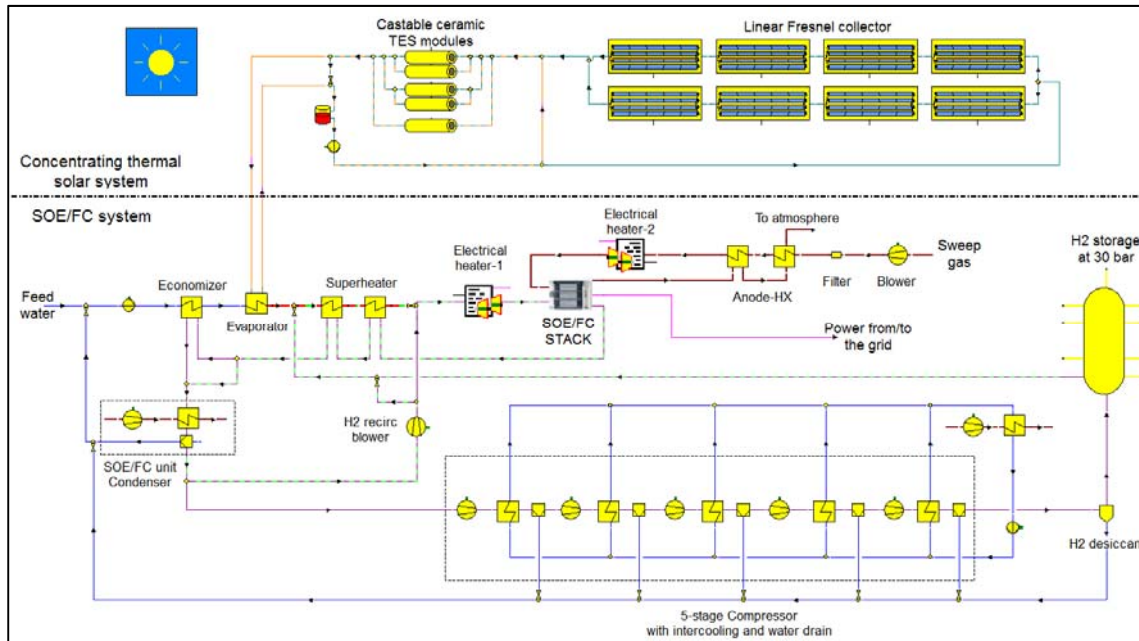
Figure 41: Scheme of the hybrid plant.

The solar system consists of several LFR collectors and a number of castable ceramic TES modules, five in the scheme shown in Figure 41. Concerning the LFR collectors, among the different models implemented in Ebsilon Professional, mirror LFR collectors are well suited for the proposed plant due to its modularity, the use of PTR 70 receiver manufactured by Schott Solar GmbH, which allows reaching high temperatures, up to 400 ºC at a maximum pressure of 40 bar; and its previous use in thermal applications like the one study in this work [99]. A total of eight mirror LFR collectors, grouped into two lines of four collectors in series were implemented. Regarding the TES modules, it has been simulated based on the methodology proposed by Tamme et al., and the experience presented by Laing et al. [102, 103]. Each TES module is 10 m long and has a square section of 4.84 m². It has been simulated as a unique pipe of 350 m long that makes 36 passes along the module. Thermal losses are considered negligible. Specifications of the LFR and the TES modules are presented in Table 17.

Table 17. Concentrating thermal solar system characteristics.

Mirror Linear Fresnel reflector		Storage material properties		Storage module	
Collector length	65 m	Storage medium	Castable ceramic	Module length	10 m
Gross aperture	7.5 m	Thickness of storage (around the pipe)	0.062 m	Section	2.2 x 2.2 m
Net aperture area	351 m	Density	3500 kg/m³	Number of passes	36
Focal length	4 m	Specific heat capacity	866 J/kg K	Pipe length	350 m
Absorber inner diameter	0.0656 m	Thermal conductivity	1.3 W/m K	Pipe inner diameter	0.04 m

The solar system carries out two operation processes along the day: the charge of the TES (green and green-orange dash lines), and the discharge (orange and green-orange dash lines). During the charging process, a constant mass flow of 8 kg/s of thermal oil are sent from the reservoir tank to the LFR system where it is heated up. Afterwards, the mass flow is divided in equal parts to charge every TES module at the same time. Finally, the thermal oil goes back to the reservoir tank, and from there is recirculated to the system. On the other hand, during the discharge process, the thermal oil is sent directly to the TES through the orange pipe. After increasing its temperature, it is sent to the SOEC boiler, where superheated steam at 115 ºC is produced as demand of the electrolysis system.

Regarding the SOE/FC system, it is composed of two units of 2.5 MW$_e$. This consists of 38400 cells, with an active area of 80 cm^2. As can be seen in Figure 42, these cells are grouped into 192 stacks of 200 cells. Two columns of 8 stacks in series form a single module. The final unit has 12 modules grouped into two levels, each one with 6 modules set together as it is shown at the right of Figure 42.

Concerning the performance of the cells, some hypotheses were assumed according to the FCH-JU ADEL project: The electrolyser stack operates at 700 ºC, at the thermoneutral voltage, which corresponds with a cell voltage of 1.281 V and a current density of 0.63 A/cm^2. Furthermore, to prevent the degradation of the cathode, reducing conditions have been ensured recirculating a fraction of hydrogen into the cathode feed steam, yielding to 10 % vol hydrogen content; and limiting the steam conversion in the stack at a maximum level of 60 % [93]. In addition, equal molar flow rated on the cathode and sweep loops was assumed. Under these conditions, the stack achieves a nominal efficiency of 97 %.

| Cell | Stack | Module | ½ Unit (Two levels) |
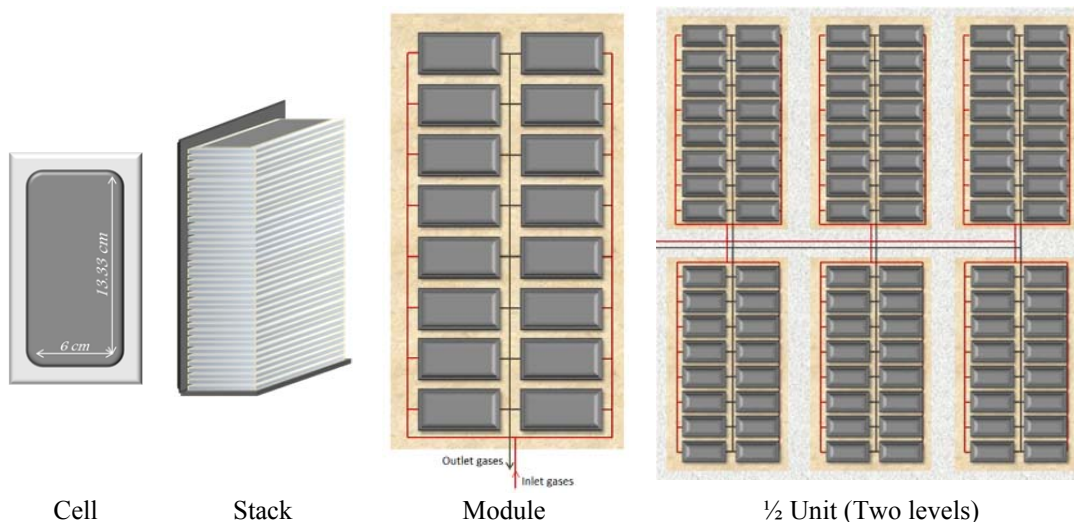
Figure 42: Scale-up of the cell to the 2.5 MWe SOE/FC unit.

Concerning the SOE/FC unit, it consists of two differentiated gas loops: the cathode loop for feeding the steam or hydrogen (see Figure 41- down on the left); and other for the sweep gas, which removes the produced oxygen called sweep loop (down on the right). Both loops include a heat recovery system to make the most of the heat that contains the electrolysis

exhaust gases. Thanks to this system, the external heat supply is exclusively used to carry out the evaporation of the feed water of the electrolyser. In SOEC mode, liquid water is pumped to the system, preheated in the economizer and evaporated in the boiler by means of hot thermal oil. Afterwards, the steam is superheated and mixed with a hydrogen enriched stream to maintain reducing conditions at the cathode [104]. Then, the resulting mixture is finally heated up to the stack temperature, 700 ºC, by electrical heater-1. Lastly, the mixture enters to the electrolyser, where 60 % of the inlet steam is electrically reduced, producing hydrogen at the cathode, and oxygen at the anode. The resulting exhaust gas of the cathode is routed through the superheater and economizer of the heat recovery system. Along this process, the exhaust mixture reduces its temperature from 700 to 71 ºC. To remove most of the water before the compression process, the gas is further cooled to 45 ºC into an air-cooled condenser, yielding to a 90 %vol hydrogen mixture. Afterwards, 15 % of this mixture is recirculated and mixed with the inlet stream, as explained previously. The rest of the hydrogen enriched mixture is compressed into a five intercooler-stage compressor up to 30 bar. After each intercooling stage, the condensed water is removed to avoid the erosion of the turbine blades. Lastly, a molecular sieve desiccant is used to remove the rest of the moisture before the hydrogen is stored. Under SOFC mode, the hydrogen stream flows as the purple-clear green dash line shows. Main differences with the SOEC mode are that: (i) the economizer, the evaporator and the compressor are not used, and (ii) that the un-reacted hydrogen is injected into the inlet stream, before the superheaters of the heat recovery system.

Besides the steam/hydrogen loop, there is the sweep gas loop shown in the center-right of Figure 41. This is used to remove or supply the oxygen produced or consumed depending on the system operation mode, as SOEC or SOFC respectively. The air is blown in the system with a blower. Firstly, a filter removes particles and poisonous gases from the air. Then, this is preheated through the anode-HX and also through the electrical superheater. Afterwards this enters the stack. Before it is sent to the atmosphere the exhaust gas flows through the anode-HX system.

Finally, power is taken or injected into the grid as function of the operation mode of the SOE/FC units.

Analysis of the results

The proposed P2G plant has been analyzed to feed a hydrogen bus refuelling station, at the same time that the system helps to minimize the reduction of the grid demand during night hours. For analyses, it was assumed that the electrolyser operates between 1:00 and 6:00 a.m. This corresponds with hours at which the demand falls to its minimum values. The availability of the system has been analyzed as function of the thermal storage capacity. Within the analysis, the number of TES modules has been varied from 4 to 10.
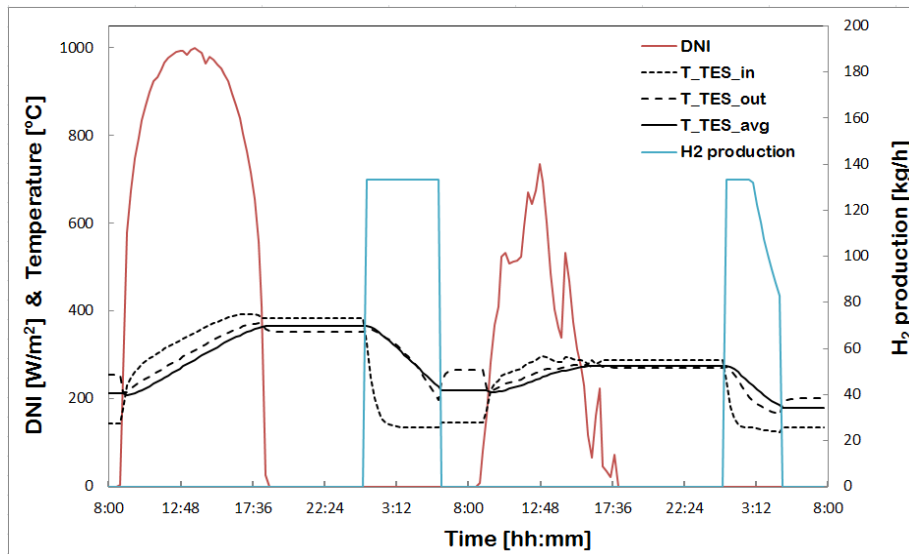
Figure 43: DNI, temperature in the thermal storage and hydrogen production profiles in two representative days.

Figure 43 shows the profile of the DNI, the temperature at the inlet and outlet of the TES, as well as the storage average temperature, and hydrogen production profile along two representative days. As can be seen, during a day with good radiation, the TES modules can be completely charged and reach temperatures above 350 ºC. This makes possible to operate the SOEC at full load along the 5 hours, producing a total amount of 666.3 kg. However, it can be seen that during cloudy periods the TES reach lower temperature levels, even though the previous day it was not completely discharge. Due to the poor charge level of the storage, the SOEC is able to work at full load only the first two hours. Afterwards, starts the operation at partial load during the next 1h 45 min. Under this condition, the mass flow of hot oil towards the boiler of the electrolyser is limited to 10 kg/s, and the heat transfer decreases with the time as function of the temperature of the TES. Finally, the last 1h and 15min the SOEC reaches its minimum capacity level (60%) and has to be switched off.

Concerning the assumed scenario, hydrogen production is analyzed as function of the number of TES modules. Table 18 shows the annual hydrogen production, which reaches levels above 200 ton/year. Due to cloudy periods, the best production level is 90 % of the maximum possible production. In Figure 44 it is shown the average daily production of the electrolyser. As it is seen, the amount of hydrogen that the proposed system is able to deliver is in the range given for 20 buses by Zaetta and Madden, 400 to 600 kg/day [100]. Additionally, above 5 storage modules, hydrogen production exceeds 550 kg/day. Thus, a slightly larger number of busses might be fed with this plant.

Table 18. Annual hydrogen production.

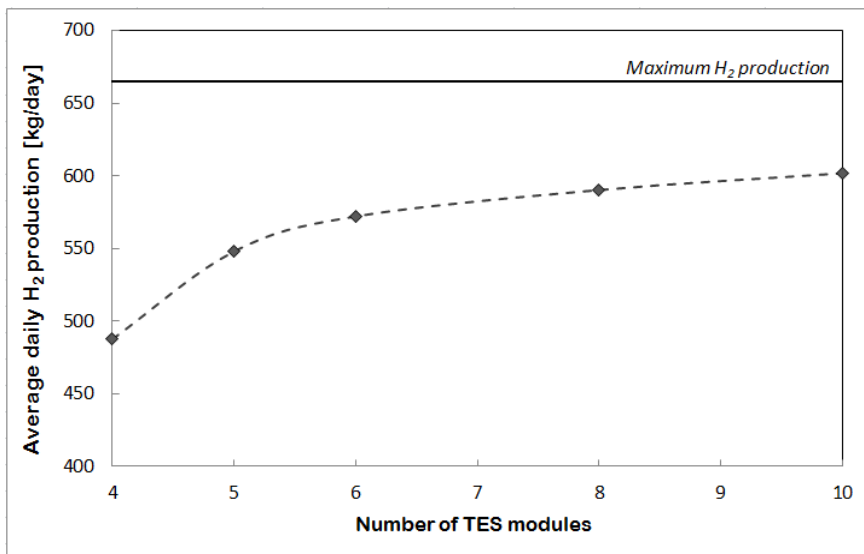| Nº TES	Annual hydrogen production (ton)
4	177
5	199
6	208
8	215
10	219
Max. possible production	242

Figure 44: Average hydrogen daily production.

The increase of hydrogen production with the number of storage modules is due to the improvement of the availability of the plant with larger number of TES modules. As can be seen in Figure 45, just increasing the number of modules from 4 to 5, the number of days that the SOEC units work at partial load decreases enormously, more than 150 days. Additionally, 200 days become days where the SOEC system is able to work at full load along the whole night. Thus, it can be concluded that four TES modules would be insufficient to deliver the heat demanded by the SOEC units. Moreover, oversizing the TES makes possible to store heat from sunny days for later use in following cloudy days, increasing the number of days at which the SOEC is able to work at full load. However, this capacity gain achieves lower relevance with the increase of the number of TES modules. On the other hand, the number of days, at which the proposed plant is not available for grid balancing, does not decrease significantly with the storage. Thus, from the point of view of the availability as an active grid balancing system, it might not be interesting to install more than 5-6 modules.
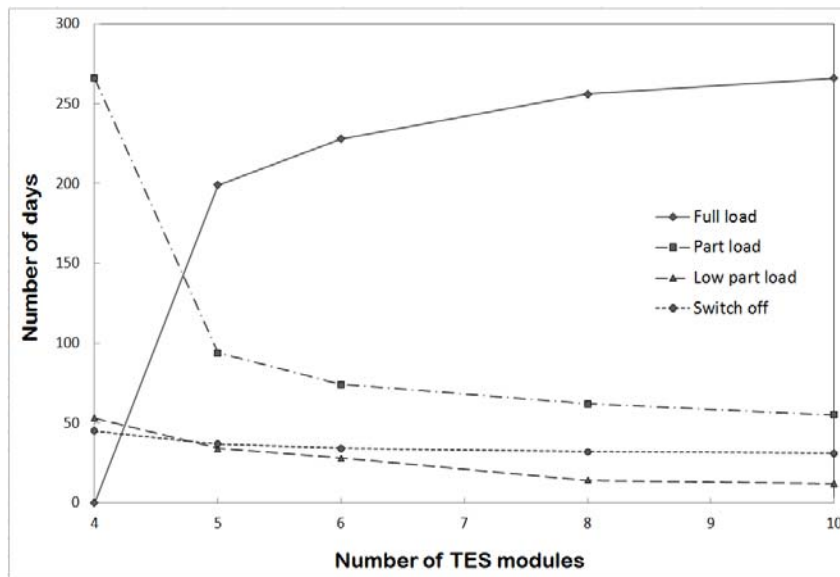
Figure 45: Description of the availability of the plant.

From the study carried out, it was found that the proposed plant is capable to supply fuel to a hydrogen refuelling station with a capacity higher than 20 metropolitan busses. It was also seen that the system might achieve a high enough availability level to be useful to the power grid. Multiple plants would be able to minimize the great demand difference that occurs between peak and off-peak demand periods, and to make the most of the excess electricity producing hydrogen that later on can be reconverted to power whenever it is needed, used directly into a vehicle, or injected into the gas distribution system with or without previous conversion to methane.

Lastly, it is clear than, for the system proposed in this study, it is necessary to implement more than 5 castable ceramic TES modules. Nevertheless, it should be mentioned that the gain achieved with the increment of TES modules is lower and lower with the number of them; and for example, the number of days that the system is not available at all is almost constant. Thus, the best solution might be the integration of 6 castable ceramic TES modules. However, further economic studies would be necessary to define which number of modules is the best.

6.8 Molten carbonate electrolysis

6.8.1 Process description

In order to reduce the temperature gap with current solar thermal fluids, development of electrolysis processes within the 500-600°C range would be a desirable option. In this context, molten salts could be seen as an ideal medium for lowering process temperatures with respect to solid oxide electrolyzers (SOE) since overall ionic conductivity and transport numbers of liquid salts are usually higher than solid-type electrolytes. Recently, alkali molten carbonate salts have gained a return of attention as versatile electrolytes for conducting electrochemical conversion processes of mineral ores and CO_2 gas at moderate temperature [105, 106].

In this context, molten carbonate electrolysis (MCE) to produce hydrogen from water is another process that has been recently mentioned in literature [107]. This process proposed by Frangini et al. (2014) [108] is schematized in Figure 46. Steam and carbon dioxide are fed to the cathodic space with a molar ratio $1:s_{CO_2}$. Due to the electrochemical reaction, a fraction X (steam conversion) of the water fed to the electrolyser is split into H_2 and O_2, which are produced at the cathode and anode, respectively. Carbon dioxide takes part in the electrode reactions and is required to keep the carbonate salts stable; however, no net production/consumption of CO_2 occurs in the electrolyzer. The outlet cathodic gas contains H_2 together with unreacted H_2O and CO_2, while the outlet anodic gas contains only O_2 and CO_2 with a molar ratio 1:2.
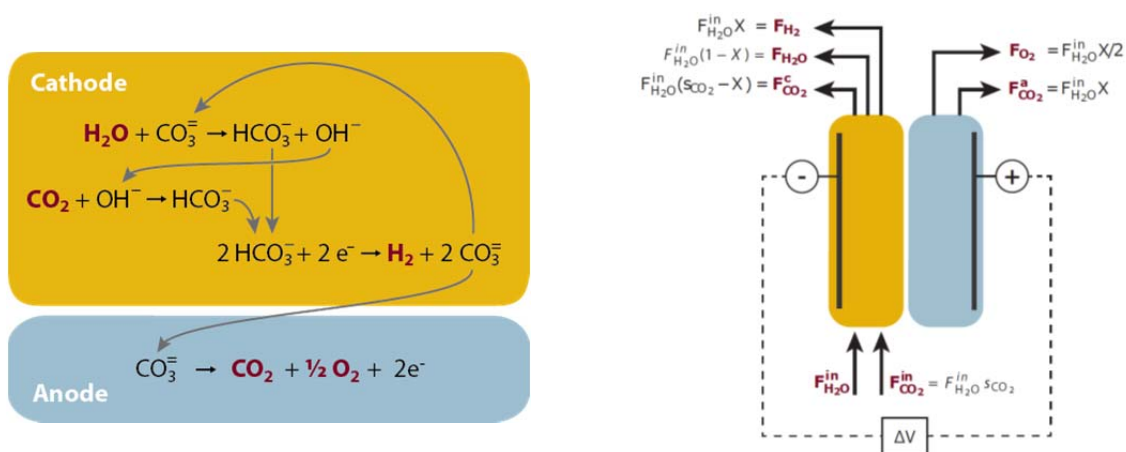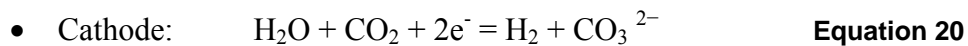

Figure 46: Description of MCSE process. On the left: main reactions involved in the chemistry of the process at 500 °C [108]. On the right: schematics of the electrolyser with inlet and outlet streams.

Only very recently, the feasibility of a MCE process for hydrogen production has been demonstrated on laboratory scale experiments in the 600-675 °C range using a Molten Carbonate Fuel Cell (MCFC) operated in a reverse (electrolysis) mode [109].

The present analysis is focused onto Ni-based MCFC electrodes since they behave as efficient bi-functional electrocatalysts, although long-term and more detailed studies are warranted, especially to evaluate the electrolysis corrosion effects on MCFC electrodes and thus to demonstrate the feasibility of a reversible MCFC concept.

The overall electrolysis reactions can be written as:

- Cathode: $H_2O + CO_2 + 2e^- = H_2 + CO_3{}^{2-}$ **Equation 20**

- Anode: $CO_3{}^{2-} = CO_2 + \frac{1}{2} O_2 + 2e^-$ **Equation 21**
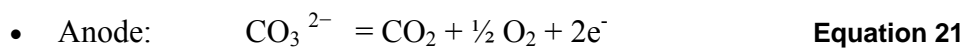
Several peculiar aspects of a water MCE process are worthy of note. Firstly, it may be observed that the anode reaction does not produce pure oxygen, but a CO_2:O_2 gas mixture, which is ideal for use in oxycombustion processes. In fact, the anodic off-gas is composed of a 2:1 CO_2:O_2 mixture that is comparable in terms of adiabatic temperature to an air stoichiometric combustion [110]. Secondly, since the cathode reaction needs a CO_2 source, an integrated electrolysis-oxycombustion process could easily realize a CO2 closed-loop system with CO2 capture. Part of the postcombustion CO_2 could be, in fact, re-injected to the cathode, whereas the excess CO_2 could be easily captured or used. Other researchers are proposing CO_2 reduction to CO for its later use in methanol production [36]. Versatility of molten carbonates electrolyzer is summarized on Figure 47.
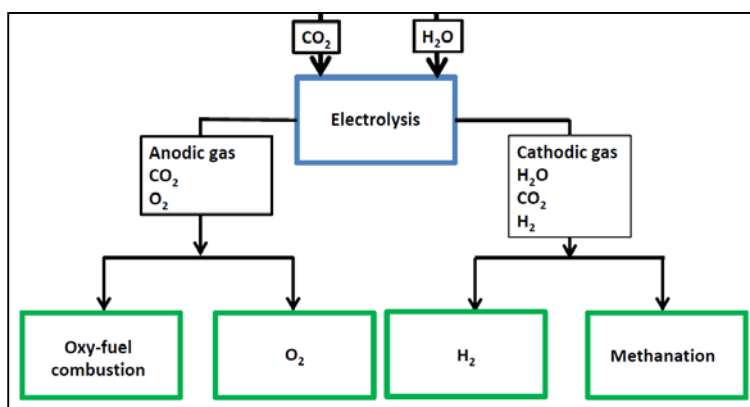

Figure 47: Versatility of molten carbonates electrolyzer.

According to chemical reaction shown on equation 21, water steam (H_2O) and carbon dioxide (CO_2) are reduced what produces hydrogen (H_2) and carbonate ion ($CO_3{}^{2-}$) which diffuses through the electrolyte towards the anode where carbonate ion is reduced producing CO_2 and O_2 [108, 109]. Cathode is made of Ni-based alloy with chromium and aluminium in a concentration of 2-10 % for thermal stress resistance increasing [109]. Anode is made of NiO

with intercalated lithium and MgO for corrosion prevention [109, 111]. Ceramics matrix made of $LiAlO_2$ is separating cathode and anode and is the housing for the electrolyte which consist on ternary eutectic mixture of molten carbonates Li_2CO_3-Na_2CO_3-K_2CO_3 (shortened as LiNaK hereinafter) [108, 109] with molar distribution of 43,5-31.5-25.0 % respectively and melting temperature of 397 ºC.

The Molten carbonates electrolyzer technology is still at applied research stage with first laboratory tests completed by ENEA and has a TRL of 3. Moving from proof-of-concept level towards small scale prototype (TRL 4) and large scale prototype (TRL 5) tested in intended environment will be crucial for technology deployment.

6.8.2 Technology assessment

A series of experiments were performed by ENEA group using a small laboratory prototype tested with dry CO_2 and wet composition 50:50 (P_{CO2}=0.5 atm; P_{H2O} =0.5 atm) fed at 120 ºC with volumetric flow of 60 mL/min. Results from galvanostatic experiments of the electrolyzer run at cell temperature between 500-600 ºC are needed for voltametric equations fitting of the MCE developed model.

Figure 48 shows the solving procedure that has been proposed for modelling the molten carbonates electrolyzer. Modelling scheme shown below has been programmed into MATLAB routines code for validation purposes and sensitivity analysis. Later, this code has been adapted into FORTRAN code language for its final application into TRNSYS simulation environment coupled to concentrating solar plant.
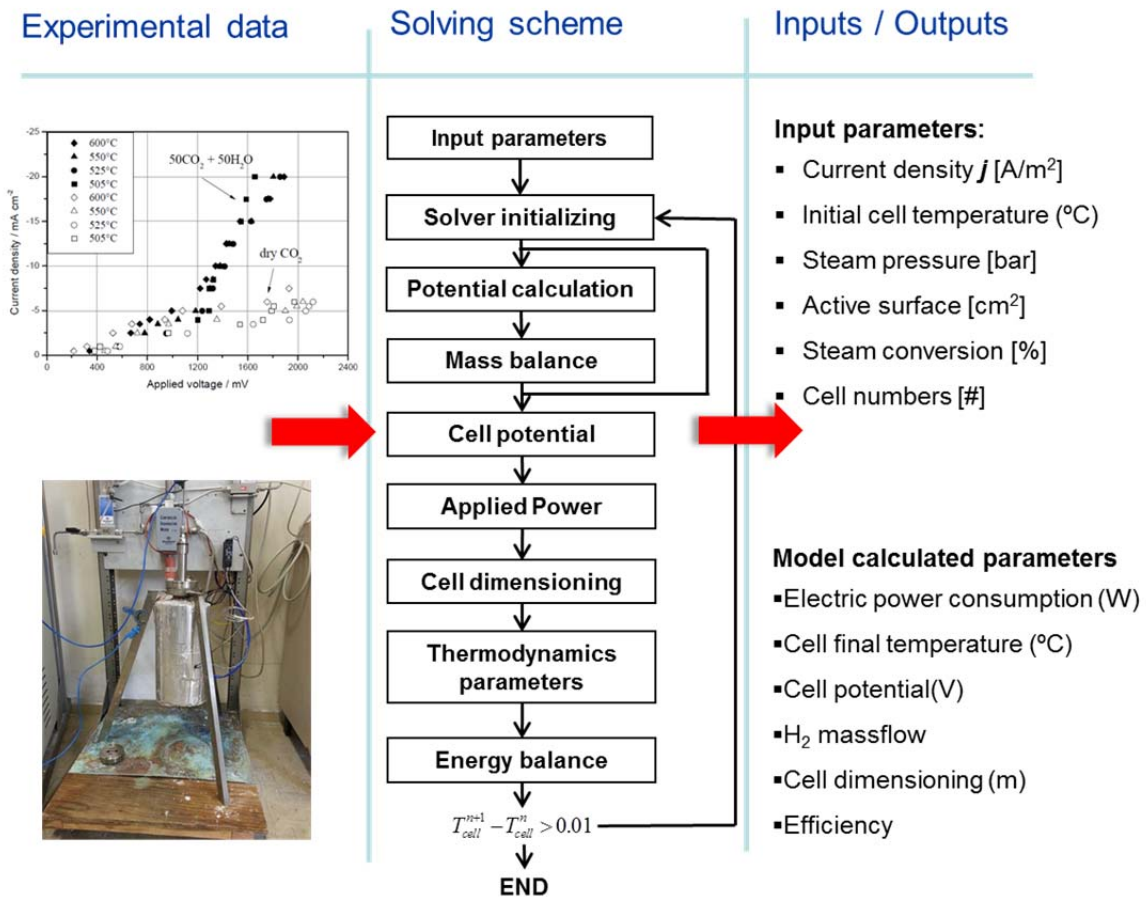
Figure 48: MCE solving diagram.

<u>Equations description</u>

1. Nerst, reversible and thermoneutral potential calculation

Reversible potential of a cell depends on Gibbs free energy which changes with cell temperature [112] and can be calculated from equation 22.

$$E_{REV} = \frac{\Delta_r G_T^0}{2 \cdot F} \qquad \qquad \textbf{Equation 22}$$

$$\Delta_r G_T^0 = 244800 - 49.18 \cdot T - 2.72 \cdot 10^{-3} \cdot T^2 \qquad \qquad \textbf{Equation 23}$$

Nerst potential is affected by cathode and anode composition [113] and can be calculated from equation 24.

$$E_N = E_{REV} + \frac{R \cdot T}{2 \cdot F} ln \left[\frac{P_{H2,cat} \cdot P_{O2,an}^{1/2} \cdot P_{CO2,an}}{P_{H2O,cat} \cdot P_{CO2,cat}} \right] \qquad \qquad \textbf{Equation 24}$$

Thermoneutral potential can be determined from reaction enthalpy [40], equations 25 and 26.

$$E_{TN} = \frac{\Delta_r H_T}{2 \cdot F}$$ **Equation 25**

$$\Delta_r H_T = 238200 + 13.12 \cdot T - 3.53 \cdot 10^{-3} \cdot T^2$$ **Equation 26**

2. Mass balance

In order to determine hydrogen production from the electrolyzer, mass balance was proposed using Faraday law, steam conversion given and partial pressures applied to each species.

3. Overpotential calculation

Working potential of the electrolyzer (E) is the result of all irreversibilities of the system as it is shown in Equation 27. These are the ohmic losses (E_{ohm}), activation overpotential η(j) and Nerst potential.

$$E = E_N + E_{ohm} + \eta(j)$$ **Equation 27**

Ohmic losses can be determined by means of Ohm law and the overpotential using Butler-Volmer expression [113] given in equation

$$\eta = \frac{R \cdot T}{2 \cdot \alpha_A \cdot F} \cdot \sinh^{-1} \cdot \left(\frac{j}{2 \cdot j_{0,an} \cdot S} \right) + \frac{R \cdot T}{2 \cdot \alpha_C \cdot F} \cdot \sinh^{-1} \cdot \left(\frac{j}{2 \cdot j_{0,cat} \cdot S} \right)$$ **Equation 28**

Parameters from this equation have been fitted to experimental data available from experiments shown on Figure 48.

4. Electric power calculation

Electric power applied is calculated as the multiplication of applied voltage (E), current density (j), active surface (S) and the number of cells.

5. Energy balance

Energy balance will be applied to the insulating material of the MCE in order to determine the energy losses and the accumulated energy inside the stack. The energy balance is described in equation 29.

$$K_s \cdot \frac{dT}{dt} = (E \cdot j \cdot S \cdot (1 - \eta)) - \frac{(T - 25)}{R} - \dot{n}_{H2O} \cdot cp_{H2O}(T - T_{IN}) - \dot{n}_{CO2} \cdot cp_{CO2}(T - T_{IN})$$ **Equation 29**

Where the left hand side represents the temperature variation along the time, while the first bracket term on the right hand side accounts for the gained thermal energy while the rest account for thermal losses.

6. Cell efficiency

Cell efficiency is calculated as the ratio between thermoneutral potential and the total one, as it is shown in equation 30.

$$\eta = \frac{E_{TN}}{E}$$
Equation 30

Modelling results

Results presented on Table 19 were obtained for current density of 0.014 mA/cm^2 (as it was proposed from experimental tests). As it can be seen, scaling factor of 10 was found between both production scenarios. However, applied electric power did not follow that factor due to different cell geometries and lower thermal losses when working at higher temperature.

Table 19. Modelling results for production scenarios studied.

Parameter		Unit	Refilling station	Industrial application
Target	H$_2$ Production	[kg/day]	400	4000
Estimated	Current density	[mA/cm^2]	0.014	0.014
	Steam conversion	[-]	0.6	0.6
Calculated	Temperature	[ºC]	539	548
	Steam needed	[kg/h]	248.2	2482
	CO$_2$ needed	[kg/h]	606.4	6064
	Applied voltage	[V]	1.62	1.61
	Cell number	[#]	319000	3190000
	Electric power	[kW]	726.2	7205

Sensitivity analysis

Figure 49 shows the effect of electrolyzer working conditions (current density and steam conversion) on electric power required and cell temperature. As it can be observed from the figure on the left, the higher the steam conversion the lower the electric power needed for the electrolysis process for any current density. These conditions correspond to higher operating temperature of the electrolyzer cell that is translated into higher efficiency. In addition, the lower the current density the lower the electric power required for the electrolysis process for any steam conversion. In conclusion, it is desirable to work in the region of low electric

power requirements for the electrolysis process corresponding to high steam conversion ratios and low current densities. As it was abovementioned, melting temperature of molten carbonates used for this electrolyzer is around 400 ºC what is liming the working region of the electrolyzer.
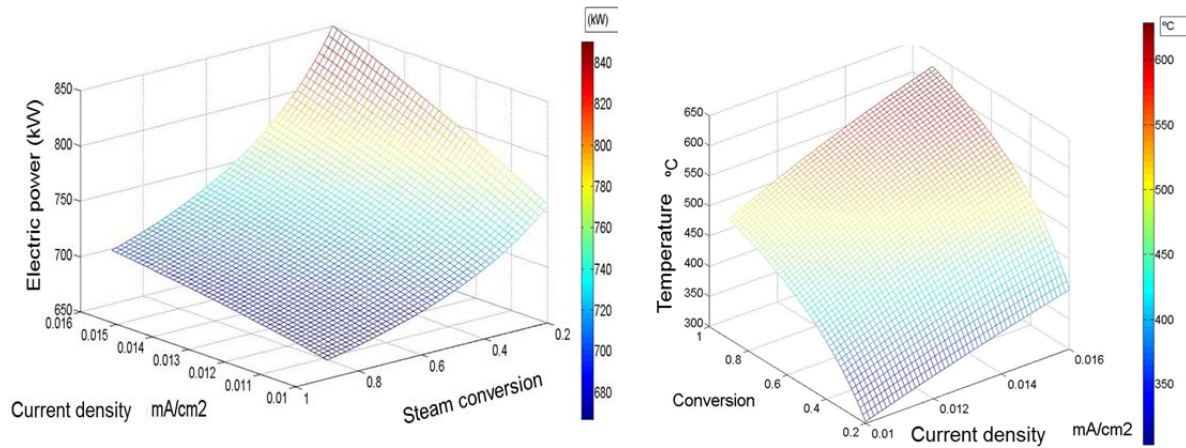

Figure 49: Electric power applied to MEC dependence with steam conversion and current density. Left: electric power needed. Right: cell temperature.

In the proposed scheme a Linear Fresnel system like the one used in the previous section for SOEC is modified to extract some heat from the storage to produce the steam needed at a molten carbonate electrolyzer.
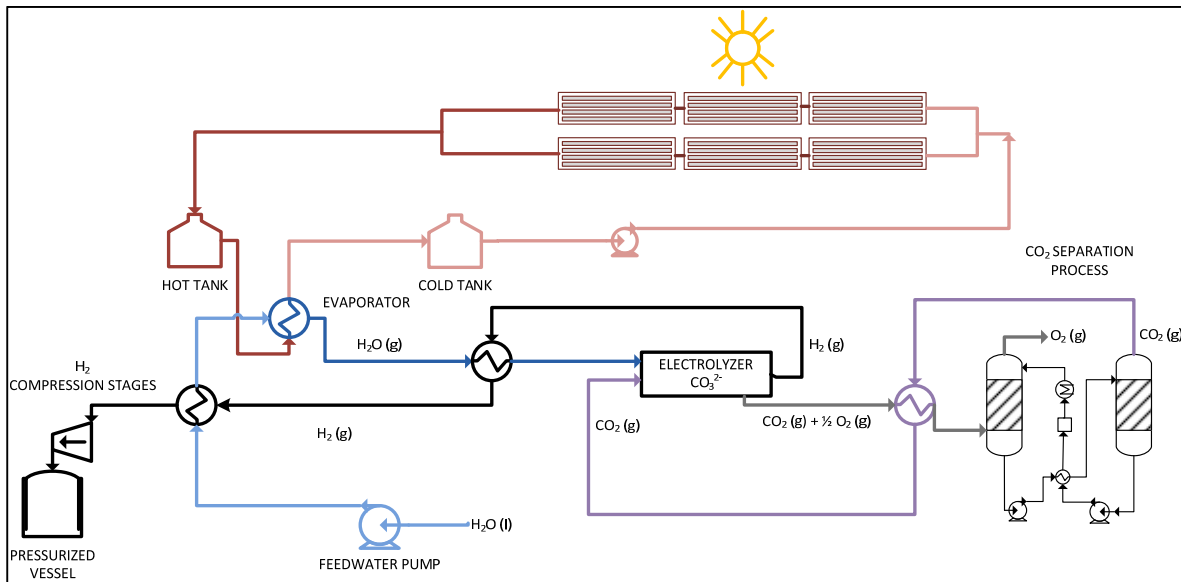
Figure 50: Scheme of the solar-hydrogen plant with a Linear Fresnel collector field and an molten carbonate electrolyzer.

Figure 51 shows process flow diagram in detail for MCE coupling to an external thermal source, in this case Linear Fresnel collector plant. Main elements from the diagram are the electrolyzer (marked as MCEC), the external heat addition connection (marked as E-102), the energy recovery network (red box) and cooling system (blue box) that is needed prior CO_2 separation process (green box).
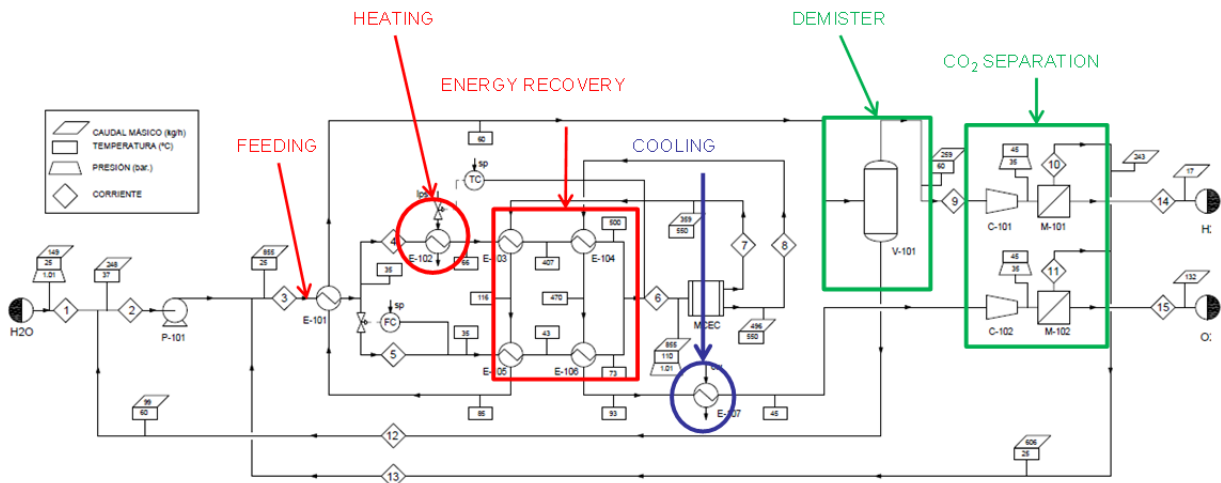
Figure 51: Coupling process flow diagram (detail).

Cathodic current is preheated using heat exchanger E-101, this current is later divided into two uneven streams (60% and 40%) for its heating up to 110 ºC using heat exchangers E-102 and E-106 which are recovering part of the high temperature from electrolyzer outlet streams. Anodic and cathodic streams are cooled down and water and CO_2 are separated for feeding back the electrolyzer. O_2 and H_2 streams could be purified using amines or membranes separation. In both cases, electrolyzer streams should be cooled down below safety temperature for both amines and membranes materials (around 100 ºC) [114]. Oxygen and hydrogen streams should be compressed in a range from 35-42 bar for separation process using membranes. Solar plant will be coupled to the electrolyzed by means of heat exchanger E-102 what will provide thermal energy required for ensuring electrolyzer inlet temperature at working conditions (540 – 550 ºC).

Table 20 shows modelling results of the electrolyzer coupled to linear Fresnel plant assuming current density of 0,014 mA/cm^2, steam conversion of 60%, feeding temperature of 120 ºC and cell working temperature of 550 ºC.

Table 20. Modelling results for MCE coupled to linear Fresnel plant.

Equipo	400 kg/day H_2	4000 kg/day H_2
MCEC, electric power (kW)	726.2	7205
E- 102 external heat power (kW)	40	359.5
E-102 water steam, *lps*, (kg/h)	39.5	589.3
E-107 rejected thermal power (kW)	6	62
E-107 water mass flow, *cw*, (m^3/h)	1.036	10.7

Results of Table 20 are corresponding to exothermic working region of the electrolyzer. Electric power required could be further reduced towards thermoneutral behaviour. In that case, results have shown for the case of 400 kg/day that electric power could be reduced to 590 kW in exchange of increasing thermal power required by 4 times (up to 160 kW).

Due to the very limited experimental information for this kind of technology, a mathematical model has been developed for reproducing MCEC behavior. This model has been validated against laboratory scale experiments and used later to explore its coupling to solar plant. Main conclusions found from model analysis are as follows:

- Technology can be used for a wide range of operative conditions in terms of steam conversion and current density. Nevertheless, it is preferred high steam conversion and lower current densities for reducing electrical power applied.
- Electrolyte nature is limiting the working temperature of the cell above 400 ºC to prevent from molten salts freezing.
- Electric power requirements can be reduced by increasing external thermal power

Flow sheeting

The block diagram of the whole MCSE process considered in the techno-economic analysis is schematized in Figure 52. MCSE is assumed to be carried out at 500°C, pressure slightly above 1 atm and close to thermoneutral conditions (the thermoneutral potential at 500°C is 1.28 V). Processing of the outlet gases is required in order to recover pure hydrogen and oxygen from the electrolyser products. Both outlet streams are cooled down to 40 °C and the heat recovered is used to pre-heat the feed streams to 480°C. Water is condensed from the cathodic gas and each outlet stream is sent to a separate amine (MDEA based) absorption column to remove CO_2, which is recycled to the electrolyser feed. A single column is used to regenerate the rich amine stream coming from both absorption columns.
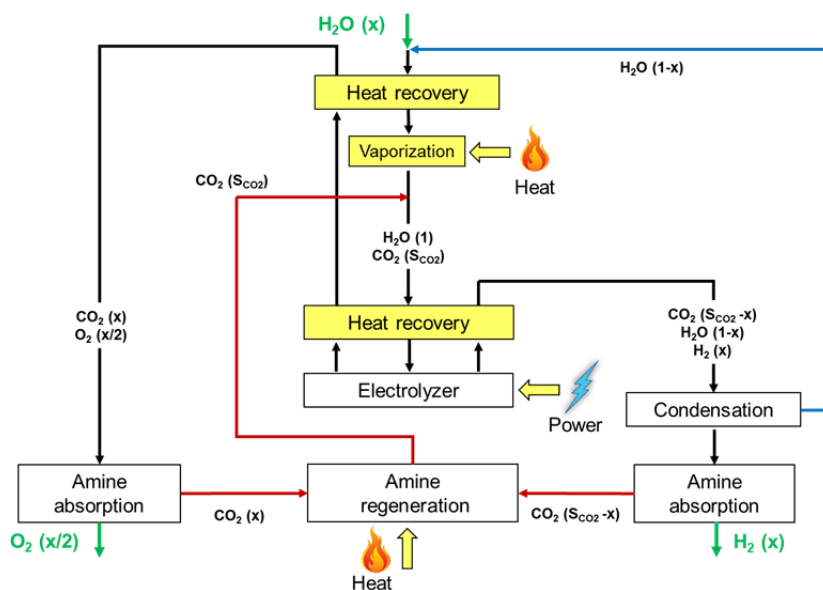

Figure 52: Block diagram of the whole MCSE process used for technology assessment.

A flowsheet of the whole process (Figure 53 and Figure 54) was developed with the software AspenPlus and used to simulate the operation and calculate the energy requirement of the plant. A plant capacity of 4000 kg/d of hydrogen with a purity of 99.996% on a molar basis was considered in the simulations and a parametric study was carried out for steam conversion in the range 60-80%.
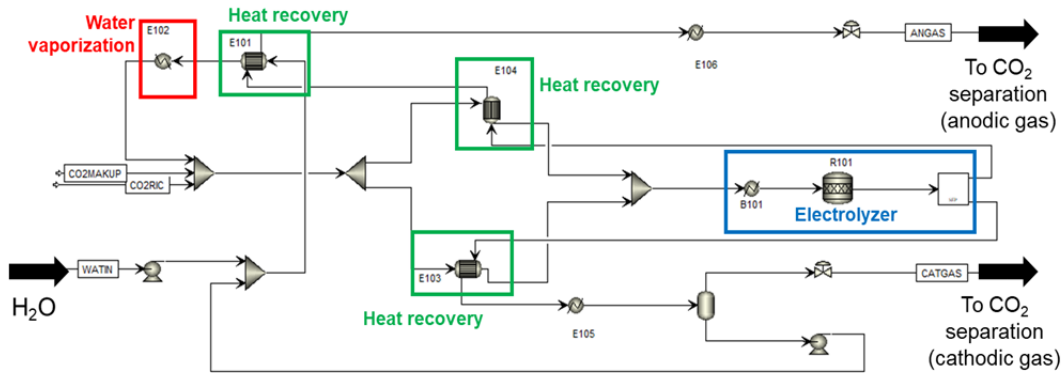

Figure 53: Flowsheet of the MCSE process used for technology assessment (electrolysis section). Units highlighted in red require low-temperature heat from a utility.
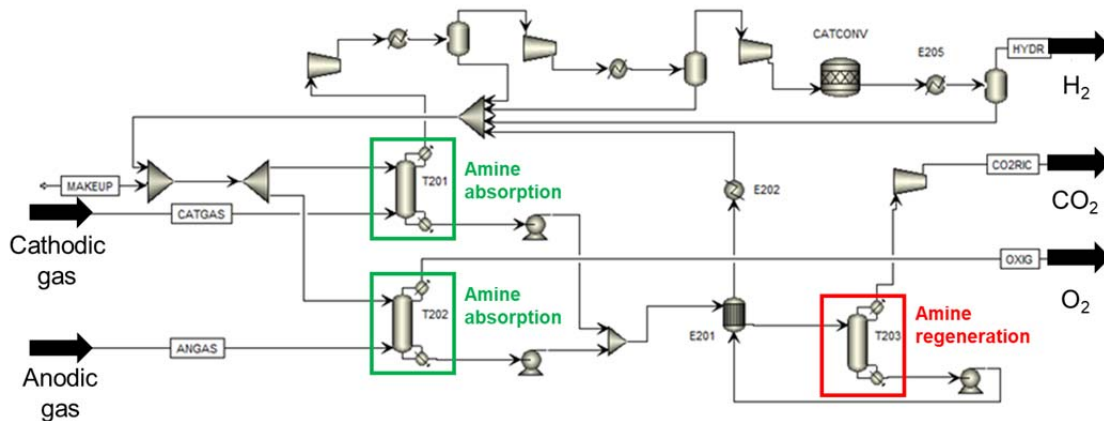
Figure 54: Flowsheet of the MCSE process used for technology assessment (CO_2 separation section). Units highlighted in red require low-temperature heat from a utility.

Continuous hydrogen production by the proposed flowsheet requires about 12.5 MW, 51% of which as low-temperature heat and 49% as power. Heat is required for steam production (18%) and amine regeneration (82%). Power is used for electrolysis (93%) and pumps and compressors (7%).

Integration with CSP

A first attempt was carried out to explore the possibility of coupling the MCSE plant with a CSP plant to fulfil both the heat and power requirements. In this first attempt, the integration strategy was aimed at causing the smallest possible perturbation to the CSP plant configuration and performance. A 50 MW parabolic trough plant using molten salts as heat

transfer fluid was considered. The CPS plant has a solar field (SF) of the same type as the Archimede plant in Priolo Gargallo (Italy) and Akesai Solar Thermal Power Plant (China) [115], which provides heat to a superheated steam cycle; furthermore, the plant is equipped with a two-tank molten salt thermal energy storage (TES) system. The CSP plant is oversized compared to the power requirement of the MCSE plant, so that grid export is also envisaged. The heat requirement of the MCSE plant is fulfilled with service steam (saturated, 130°C) produced with molten salts from the cold tank (CT, Figure 55) through an intermediate thermal oil circuit.
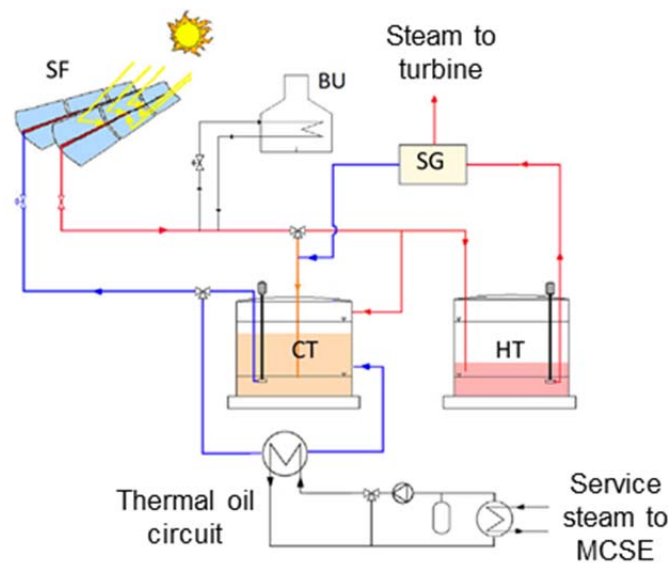
Figure 55: Strategy proposed for the integration of the CSP and MCSE plants.

In the proposed integration strategy, the H_2 production plant is assumed to work continuously. When the solar plant is not operating or the cold tank temperature is too low (<280°C), electricity is drawn from the grid and heat produced with a methane burner (BU). As a consequence, a fraction of the yearly hydrogen production is obtained with non-renewable energy. It is worth noting that, for molten salt freezing prevention, the burner is in general present in the CSP plants of the type considered; therefore, oversizing the methane burner is the only modification to the CSP plant required by the proposed integration strategy.

The plant was assumed to be located in Ben Guerir (Morocco), with a SF size of about 454,500 m^2 and 10 h nominal TES capacity. This scenario was selected as the best out of 3 options and not based on a thorough optimization activity. Therefore, the results obtained should not be considered as optimal, and there is margin for improvement.

One year operation of the solar plant was simulated with a 0.5 h time step, accounting for changes in Direct Normal Irradiance (DNI) and local atmospheric conditions. The results obtained for some key performance indicators are summarized in Table 21. Where applicable, the performance of the CSP plant alone is compared with the integrated CSP-MCSE plant.

Table 21: Key performance indicators of the CSP and CSP-MCSE plants (1 year operation, 60% steam conversion).

Indicator	Units	CSP	CSP-MCSE
Collected solar energy	GWh	545.5	553.8
Dumped solar energy	GWh	11.1	6.5
Thermal losses	GWh	50.6	45.8
Energy from methane combustion	GWh	3.8	31.4
Power production	GWh	202.0	195.8
Power to grid	GWh	202.0	171.3
Overall efficiency	%	18.8	20.2
Renewable energy in H_2	%	N/A	48.3

Preliminary economic analysis

Considering the very low technological maturity of MCSE, a detailed economic analysis of the process cannot be carried out with the currently available information. However, a preliminary effort was done in order to provide a first evaluation of the potential of this technology and orient future choices for its development.

The highest source of uncertainty is related to the cost of the electrolyser, since no significant scale demo is currently available for this device. In the present analysis, the baseline cost of the electrolyser was estimated based on the cost of a molten carbonate fuel cell (MCFC) stack of the same rated power. To that end, investment costs declared by FuelCell Energy in 2013, i.e. 2500 $/kW, and reported by the DoE in its annual Fuel Cell Technologies Market Report [116] were considered. Assuming that about one third of the investment cost is related to the stack and the rest to BoP, a cost of 850 $/kW was assumed. It is worth noting that such reference costs may be currently lower based on 2013 cost reduction projections. In order to account for the uncertainty in the cost of the electrolyser, a sensitivity analysis was carried out by increasing the baseline cost by up to 50%.

To determine the total investment cost of the MCSE plant, the other process equipment (i.e., heat exchangers, absorption columns, etc.) was sized for 4 t/d hydrogen production and costed with heuristic rules.

The cost of the solar electricity produced with the CSP plant was estimated with the same approach followed by Liberatore et al. [117] for a similar condition. The assumed baseline costs of grid electricity and methane were about 5.3 c€/kWh and 1.9 c€/kWh, respectively.

The resulting hydrogen production costs are reported in Figure 56, which also shows a sensitivity analysis on some input cost items, in particular the electrolyser cost. Only the results related to the more conservative condition of 60 % steam conversion are reported. For 80% steam conversion, the obtained hydrogen prices are in the range 6.34-7.54 €/kg.
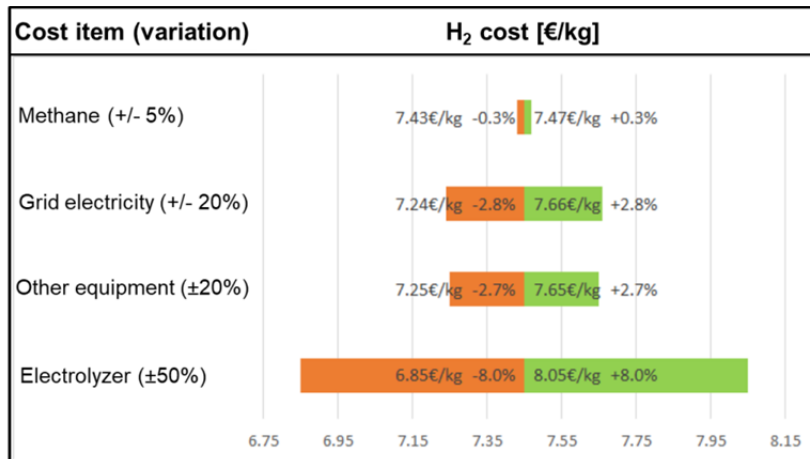
Figure 56: First estimation of the hydrogen production costs with the integrated MCSE-CSP plant considered (60% steam conversion: conservative assumption). A sensitivity analysis on some input cost items is also reported.

The approach proposed for the integration with the MCSE plant requires virtually no change to the CSP plant configuration, leads to a better exploitation of the SF (+1.5% solar energy collected) and reduces the thermal losses (-9.6 %); however, a minor reduction of the total power production is observed (-3.1%). Nearly 50% renewable H_2 production can be achieved even with continuous operation of the MCSE plant.

The results are encouraging and even better performance figures can be expected if the SF and TES size are optimized for the integration with the MCSE plant and higher steam conversion rates can be attained.

6.9 Solar gasification of carbonaceous materials and wastes

6.9.1 Process description

Allothermal steam-based thermochemical gasification of solid carbonaceous feedstock to syngas can be described in the ideal case by the simplified overall reaction:

$$CH_xO_{y\,(s)} + (1-y)\,H_2O + ash \rightarrow (1+x/2-y)H_2 + CO + ash \qquad \textbf{Equation 31}$$
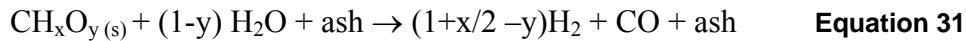
where x and y are the molar ratios of H/C and O/C in the feedstock. The produced syngas can be consumed as a combustion fuel or can be further processed to many conventional gaseous and liquid fuels. Here we target the production of hydrogen, which includes the conversion of CO to H_2 in a shift reactor. Figure 57 sketches the process.
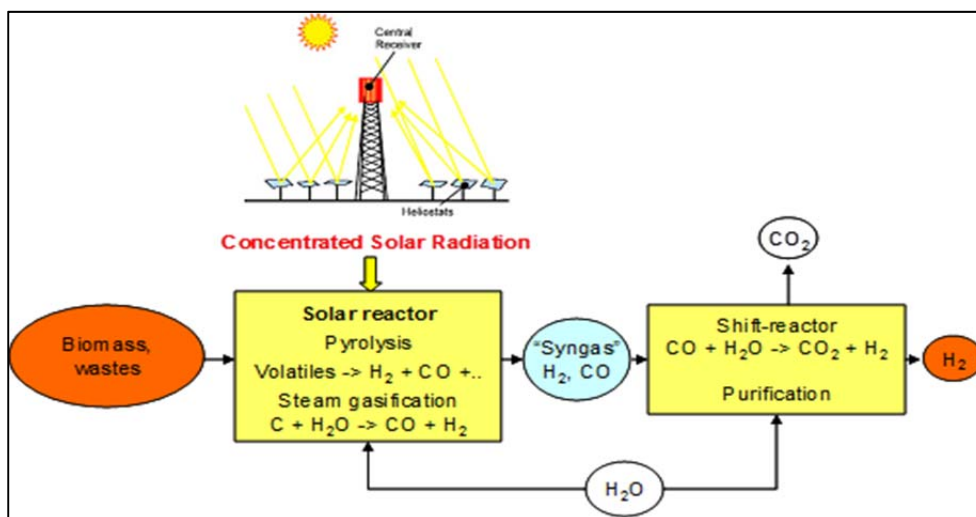
Figure 57: Simplified basic scheme of solar steam gasification with further processing to hydrogen.

The advantages of solar-driven vis-à-vis autothermal gasification are manifold [118]: (i) It delivers higher syngas output per unit of feedstock, as no portion of the feedstock is combusted for process heat, (ii) it avoids contamination of syngas with combustion by-products, and consequently reduces costly downstream gas cleaning and separation requirements, (iii) it produces syngas with higher calorific value and lower CO_2 intensity, as the energy content of the feedstock is upgraded by up to 33% through the solar energy input – solar-produced syngas has about two times higher calorific value per feedstock unit than syngas from conventional autothermal gasification –, and (iv) it easily allows for higher gasification temperatures exceeding 1100 °C, resulting in faster reaction kinetics and higher quality of the syngas produced with very low tar content or tars even being completely absent.

The solar driven gasification process has been studied intensively in several solar reactor types [119]. The most advanced development is based on an indirectly heated packed bed reactor design, often called two-cavity reactor design. This design has been tested and demonstrated with very different carbonaceous feedstock and wastes first on laboratory scale

[120] and later on on pilot scale [118]. The current technology assessment is based on this reactor concept.

The two-cavity solar reactor (Figure 58) features two cavities in series, separated by a thin ceramic absorber, often in the form of a plate ("separation plate"). The concentrated solar irradiation enters the "upper cavity" of the reactor from the top through a windowed circular aperture, gets absorbed and is reradiated by the other side of the hot separation plate towards a packed bed of solid reactants placed in the "lower cavity" forming the reaction chamber. The product gases leave the lower cavity through an outlet port located on the lateral walls of the lower cavity above the packed bed. This reactor concept requires beam-down solar radiation as e.g. realized by reflecting the radiation of a heliostat field downwards with a hyperbolic mirror. A further concentration of the beam with a compound parabolic concentrator (CPC) is needed to provide flux concentrations of around 1000 suns or more as required for solar gasification. For larger solar reactors the use of an array of 7 CPC's is proposed [63].
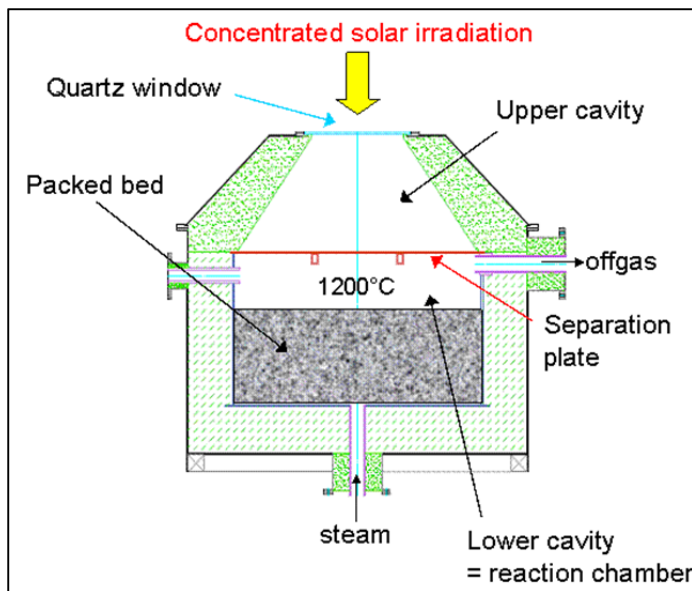

Figure 58: Schematics of solar two-cavity reactor.

A first 5 kW$_{th}$ solar reactor prototype was tested in the solar simulator of the PSI, Switzerland at a temperature up to 1215°C resulting in high quality syngas. The solar-to-chemical efficiency varied between 15.9 and 29% [120].

The technology was up-scaled and a 150 kW$_{th}$ solar gasification pilot plant was then operated in batch mode. Up to 30 Nm³/h syngas was already achieved in this indirectly heated packed bed batch reactor operated at Plataforma Solar de Almeria, Spain. A process efficiency between 22 and 35% was demonstrated [118] and an efficiency of approx. 60% is expected for full scale.

The packed bed solar gasification technology has been demonstrated at TRL 5 for a number of very different carbonaceous feedstock (pilot scale tests at Plataforma Solar de Almeria with 150 kW solar radiative power input [118]).

Important note: This solar gasification process has primarily been developed for production of syngas for direct combustion (e.g. in a cement kiln) or for further processing to liquid fuels. Since here the focus is on the production of solar hydrogen, a shift reactor and a PSA has been added. This application may not be the most beneficial for this technology. Nevertheless, it might be of interest for certain scenarios depending on specific project settings.

6.9.2   Technology assessment

The following information regards the solar reactor including the specific optical system (beam down). This information is based on the experience with the pilot scale installation in Almeria [118] which has been realized within the project Solsyn by Holcim (now LafargeHolcim), PSI and ETHZ and further (unpublished) investigations within this project. These included conceptional design work of the technology for 6 MW_{th} input and (less detailed) for 30 MW_{th} input relating to about 30% and 150% of the size required for a 4000kg/d solar hydrogen production plant under study here. This design work in turn made use of conceptional design work performed in the EU-project SOLZINC for carbothermal production of Zinc from Zinc Oxide [63], which was based on a similar two-cavity reactor technology (see section 6.3 on carbothermal ZnO/Zn cycle).

The solar production of syngas with the packed bed two-cavity reactor has been demonstrated with a number of very different feedstock in terms of volatiles content, humidity, size distribution and others. In spite of these differences, key parameters relevant for the technology assessment are very similar.

For this technology assessment a "typical feedstock" is considered, based on an average of the pilot test performance of the three feedstocks Beech charcoal, Low Rank Coal and bagasse [118]: It is approximately characterized by the chemical expression $C_7H_6O_2$, one mol of which is reacted together with $>\approx 7H_2O$ in the form of steam. Per mol about 0, 4 and 7 mol H_2O are additionally contained in beech charcoal, low rank coal and bagasse, respectively. At least the difference has to be fed as steam into the reactor. For example, low rank coal contains about 4% ash and 35% water, resulting in an LHV of about 16 MJ/kg (wet) or 25 MJ/kg (dry).

The resulting syngas composition for the typical feedstock can be approximately written as about 1 mol H_2 + 0.5 mol CO + 0.2 mol CO_2. Consequently a very approximate *real* overall reaction is

$$C_7H_6O_2 + 7\ H_2O + ash \rightarrow 10\ H_2 + 5\ CO + 2\ CO_2 + ash \qquad \textbf{Equation 32}$$
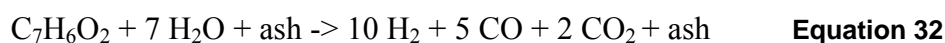
The solar upgrade Q_{syngas} (hot)/$LHV_{feedstock}$ is about 1.4 for these "good" feedstocks, which translates to about 1.25 for the cold syngas ($LHV_{syngas}/LHV_{feedstock}$).

Table 22 lists the key assumptions that are made for a very simplified analyses, results of which are summarised Table 23. A very important parameter is the specific syngas power per

bed surface area. More than 100 kW/m^2 had been reached in the laboratory scale tests [120], while just about 60 kW/m^2 were demonstrated on pilot scale [118]. This discrepancy is attributed to (1) the somewhat lower operation temperature on pilot scale due to the limited solar power input that could be realized by the chosen simple optical system for generation a beam-down radiation [118] and (2) the imperfect steam distribution in the bed realized by the 4 steam injection nozzles into the pilot gasification reactor [118]. Only in few last pilot scale tests an improved steam distribution was realised due to the use of a distribution plate with holes. The calculations use the fair assumption, that 100 kW/m^2 can be realised on larger scale as well, especially in case a good steam distribution is realized.

Table 22: Key assumptions for technology assessment.

	Value	Unit	Remarks
Syngas power (hot)	20	MW	
Energy content syngas (hot)	12	MJ/Nm^3	Assumes no major N_2 (use of syngas for window etc.)
Specific syngas power production (hot)	100	kW/m^2 bed surface area	
Solar upgrade (hot)	1.4	-	Upgrade cold about 1.25
Concentration aperture	2400	kW/m^2	Defines aperture size (exits of 7 CPC's [4])
Mean absorber plate temperature	1350	°C	Determines re-radiation losses
Reactor height	2	m	
Specific wall energy loss	7.5	kW/m^2 wall area	
Thermal mass per wall area	15	kWh/m^2	Required for heat-up
Thermal mass per column (holding absorber structure)	20	kWh	Required for heat-up (16 columns in quadratic reactor)
Operation time eff.	8	h/d	
LHV Feedstock (dry)	25	MJ/kg	Value does only influence feedstock conversion rate

Table 23. Key results for 4000 kg/d H_2 production.

	Value	Unit	Remarks
Bed surface	200	m^2	
Solar input to apertures	13.0	MW	$Q_{solarin}$
Thermal efficiency	73	%	Q_{syngas} (hot)/(LHV$_{feedstock}$+$Q_{solarin}$)
Heliostats surface area	33'711[1]	m^2	Interpolated from optical design in SOLZINC project [63].
Cost estimate reactor	3.2	M€	Includes absorbers (1.0), bottom trays (0.6), reactor structure (1.6)
Cost estimate optics	6.11	M€	With 130 €/m^2 heliostat; 600€/m^2 hyperbolic mirror; 900€/m^2 CPC. Optical design interpolated from SOLZINC.
Feedstock feed rate (dry bases)	2.1	t/h	51.4/LHV$_{feedstock}$[MJ/kg] t/h (for 20 MW hot syngas and upgrade 1.4)
Syngas production	6000	Nm^3/h	with 12 MJ/Nm^3

[1]assuming 2880 h/a with 500 kg/h H_2 production at a location with 2138 kWh/m^2/a

The feedstock costs vary extremely depending on the specific material and are therefore a parameter for which a sensitivity analyses should be performed. A few respective indicative informations: Brown coal (a kind of low rank coal) costs about 10 €/t [121], translating into about 15 €/t dry bases. Bagasse costs vary in a broad range. A typical value in Brazil is about 30 €/t wet (about 50% H_2O) or about 60 €/t dry [122]. Also the case no or even negative feedstock costs appear worth to be studied (e.g. between -100 €/t up to 100 €/t).

Figure 59 represents the flow sheet of the process producing hydrogen. In addition to the solar gasifier described so far it includes the steam generator, the water gas shift and the PSA required to obtain the final hydrogen.
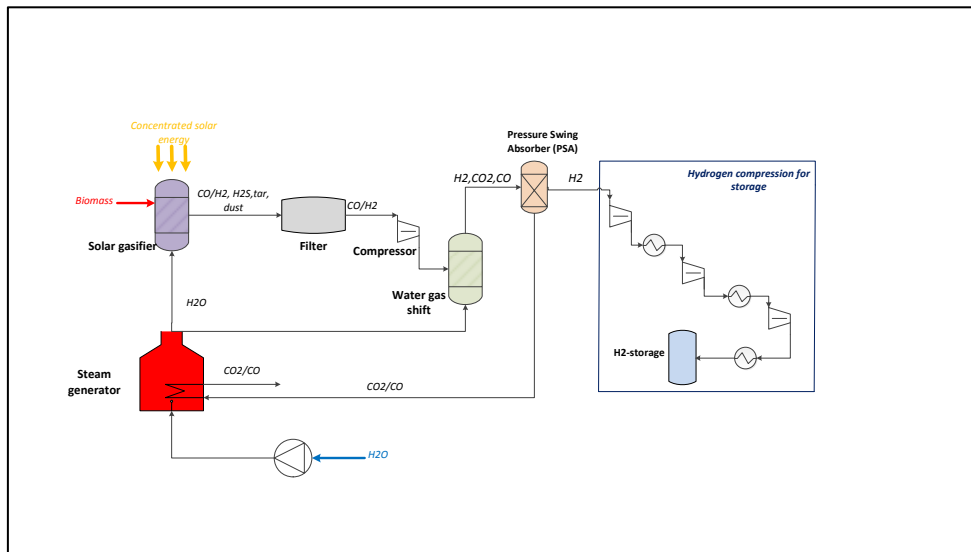
Figure 59: Flowsheet of the solar biomass gasification.

After the component sizing, the economic evaluation has been done. Table 24 shows the PEC of the major plant components required to produce the final hydrogen.

Table 24: Purchased equipment cost of the main equipment of the plant.

Summary of the main purchased equipment cost of the plant	[M€]
Compressors	4.9
Steam generation and WGS	0.5
Water and CO_2 separation	0.4
Hydrogen separation unit (PSA)	2.0
Solar part	9.3

Based on these purchase costs the total capital investment including costs for installation-, piping-, control-, electrical system-, building and service facilities as well as indirect costs has been calculated to be 61 Mio. €. Considering a plant life time of 25 years and discount rate of 8%, it results for a feedstock cost of 15 €/t in a hydrogen production cost between 5.4 and 7.2 €/kg depending on the percentage factors used for the economic analysis in the factor method (optimistic percentage factors vs. conservative percentage factors). For a feedstock which costs 60 €/t (dry bases) production costs between 5.6 and 7.4 €/kg are estimated.

6.10 Solar MS-heated hydrothermal liquefaction of wet biomass

6.10.1 Process description

The conversion of wet biomass into biofuels would be highly interesting but it is made unfavorable by the high heat demand to dry the raw material, as this energy cannot be recovered by heat integration in conventional processes. A possible solution to this drawback is the utilization of hydrothermal processes, which can be carried out in aqueous environment without the need of drying the feed. Particularly interesting would be the utilization of operative temperatures suitable to couple the hydrothermal process to a concentrating solar (CS) plant. As CS technology usually operates at temperatures lower than 500°C [123], the possibility to supply process heat to the chemical process by using a CS plant is an interesting option to be investigated. Microalgae are considered an interesting type of biomass feedstock for the production of biofuels, due to high amount of biomass produced in an year per used land unit, high energy content, possibility to be grown by using freshwater, seawater, wastewater depending on the algae species, and in marginal or partially polluted soils (e.g. close or inside industrial sites) [124]. In this section, our attention is focused on the hydrothermal liquefaction (HTL) of microalgae that is generally carried out between 280 and 400 °C, at pressures from 7 to 30 MPa. The target product of such a process is a bio-oil (from now on indicated as biocrude), i.e. a dark brown, viscous liquid, similar to petroleum, constituted by a complex mixture of several hundreds of organic compounds, mainly acids, alcohols, aldehydes, esters ketones, phenols, and guaiacols [125]. This product has a typical high heating value (HHV) of 35-39 MJ/kg and can be used as it is like fuel oil or it can be further upgraded to produce commercial liquid biofuels, such as diesel and kerosene. Other side products in the HTL of microalgae are: a) an aqueous phase containing volatile organics and nutrients (mainly phosphorous and nitrogen) which can be recycled to the microalgae cultivation stage [126]; b) a gas mixture mainly constituted by CO_2; c) a solid residue (biochar).

Here we present a conceptual analysis of the coupling of a concentrating solar power plant, based on parabolic through technology, with a plant for HTL of microalgae under the constraint of maximizing the thermal recovery from the hot reactor effluent. Part of the process heat is supplied by a molten salt stream, used as heat transfer fluid (HTF) and heated by the solar plant that is equipped with a storage tank of hot molten salt as thermal energy storage (TES) system. The proposed process configuration is based on the concept of indirect solar reactor i.e. a conventional chemical reactor that is heated by solar heat through the intermediary of the HTF. This strategy makes possible to optimize independently the performances of the solar and of the chemical plant and it is compatible with large scale continuous operation of the chemical plant despite the transient behavior of solar radiation. Another important feature is that it can be applied to any chemical process whose operating temperature is compatible with the stability interval of the molten salt mixture. By this approach, it is possible to operate the process at operating conditions difficult to have in directly irradiated solar reactors, such as high pressure and continuous processes.

The configuration of the proposed CSP-HTL plant was designed to allow continuous operation considering 10 kt/y of microalgae processed every year using a ternary nitrate mixtures, $Ca(NO_3)_2/NaNO_3/KNO_3$ 43/42/15 w/w, as heat transfer fluid and storage medium in the process temperature range of 340-410°C.

Compared to thermal oils, the ternary molten salts mixture is environmental friendly and cheaper; additionally, it has a lower freezing temperature (lower than 140°C) than traditional binary "solar salt" mixtures (with freezing temperature higher than 220°C) thus leading to easier management and higher performance of the linear CS plant.

The process layout is depicted in Figure 60.

The conceptual analysis was performed to decrease as much as possible capital and operating expenses and it allowed us to assess the most critical sections of the combined plants from the techno-economic point of view. With this strategy, we could estimate the minimum selling price of the produced biocrude, which resulted comparable with the cost of biocrude produced by more conventional biorefinery processes thus showing that the use of the solar plant, with the configuration proposed in this study, does not affect negatively the economic sustainability of the process.
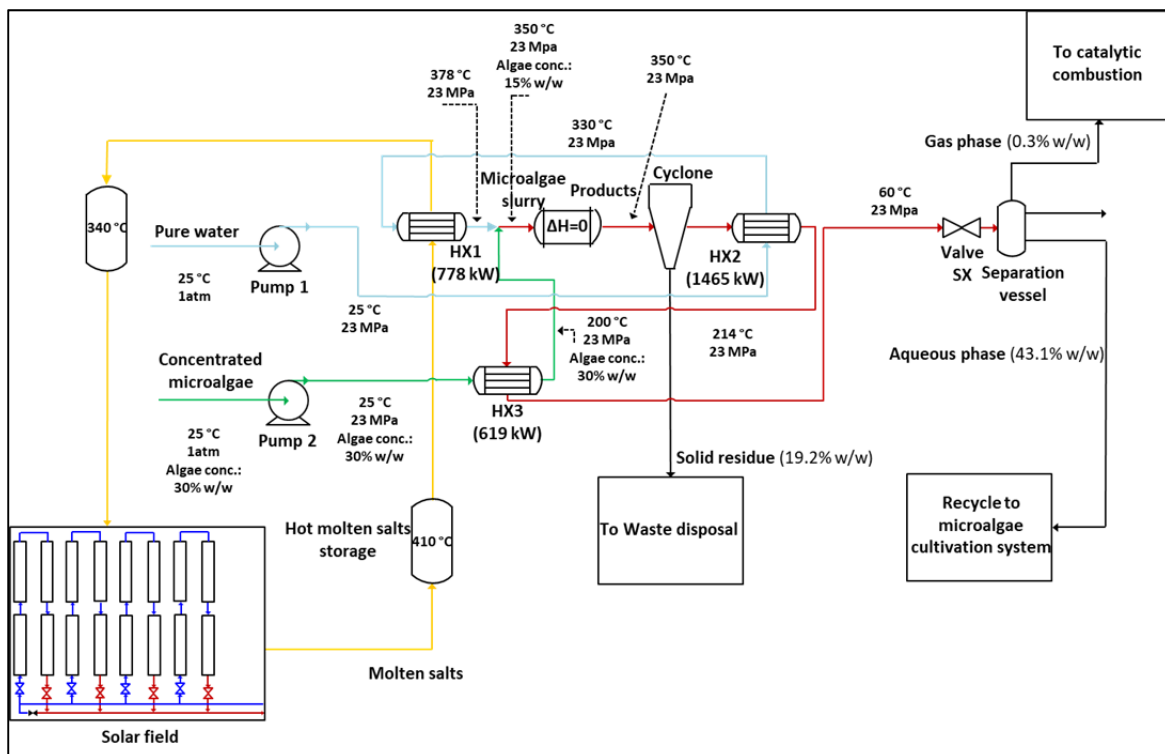

Figure 60: Schematic description of the solar-assisted hydrothermal liquefaction process.

The proposed plant configuration is based on the apparatuses used in experimental studies on the hydrothermal conversion of microalgae and ligno-cellulosic biomass in continuous lab-scale reaction systems [127-130]. Two feeding streams, pure water at 25 °C and 0.1 MPa (stream 1, mass flow rate 1.07 kg/s) and a concentrated microalgae aqueous slurry at 30%

w/w (stream 2, mass flow rate 1.07 kg/s) were considered. Both streams are compressed to 23 MPa at room temperature by pumps 1 and 2, respectively. Heat exchangers were configured to maximize the heat recovery from the hot stream exiting the chemical reactor, thus minimizing the size of the solar field. Stream 1 is heated in two consecutive heat exchangers, HX2 using the hot effluent exiting the cyclone, located after the reactor, and HX1 using as heating medium the molten salts heated by the solar field. Stream 2 is sent to heat exchanger HX3 to be pre-heated by the residual enthalpy stored in the effluent from HX2. After compression and heating, streams 1 and 2 are rapidly mixed to obtain a 15% w/w microalgae slurry at 350 °C that is sent to the reactor. According to the literature [131-133] for this process the heat effects inside the reactor were considered negligible and the reactor was modeled as a single tube adiabatic reactor.

Inside the reactor, microalgae are converted into the products: the target liquid biocrude, an aqueous phase, a gas phase and a solid residue. The stream exiting the reactor is sent to a cyclone, considered adiabatic, where the solid fraction is removed. The purified stream is then cooled in HX2 and HX3 to 145°C while still pressurized at 23 MPa. Under these conditions, the dielectric constant of water increases to about 46 and biocrude liquid phase separation was considered to be completed so that a two-phase compressed stream was sent to the flash valve (SX) to be expanded to the water vapor pressure at the expansion temperature.

The cooled products are finally brought to atmospheric pressure, and afterwards sent to a vessel where the three phases, biocrude, aqueous phase and gas, are separated by gravity. The gas phase is sent to a catalytic combustion step in order to completely oxidize it. The solids are disposed, and the aqueous phase is recycled back to the microalgae cultivation system.

For the proposed solar-assisted process for the production of liquid biofuel, via hydrothermal liquefaction (HTL) of microalgae coupled with CS plant using molten salts as HTF, the TRL can be indicated as 3 (experimental proof of concept) – 4 (technology validated in lab). Hydrothermal liquefaction of microalgae has already been performed in several laboratories in a range of operative conditions, using batch reactors [134]:

- temperature = 280-400 °C;
- residence time inside the reactor = 5-30 min;
- thermally activated process or in the presence of catalysts (homogeneous, heterogeneous);
- reactor volume: from some ml to about 1 liter.

Also continuous HTL process layout have been developed and presented [127, 128, 135].

Use of molten salts CS technology to energetically drive a chemical process has been already developed and proposed by ENEA for the low temperature MS-heated steam reforming process (see the previous subchapter in this document).

At UNIPA's a small lab-scale (10 ml reactor volume) continuous high pressure reaction system for the hydrothermal conversion of biomass feedstock has been developed and already tested with biomass model compounds [136].

6.10.2 Technology assessment

All calculations for the operative process conditions and techno-economic analysis were performed using Matlab® and Microsoft Excel® software. Thermodynamic and transport properties of water were obtained through the use of XSteam software. Mass and energy balances were performed in order to determine the energy inputs and outputs of the process; the obtained values were used to design the main equipment (reactor and heat exchangers). The required power, the chemico-physical and transport properties of the thermal fluid and its temperature variation between inlet and outlet of the solar field were used to calculate the number of solar collectors and their layout. In order to compute the yield of the products of HTL processing of microalgae, the kinetic model proposed by Valdez and Savage was used, where the biomass is modeled as a mixture of the three main biochemical constituents (proteins, carbohydrates, and lipids) and ashes, the latter being considered as an inert [137]. The estimation of capital cost for the HTL section of the plant was performed using Guthrie's method, where the CAPEX is estimated as a function of the cost of each single equipment of the plant. The price of each equipment was estimated from correlations found in the literature [3, 138], that relates the equipment cost with its size. The bare module cost (BMC), i.e. the total cost to be afforded to install each equipment taking in consideration labor cost, insurance, general expenses, etc., was estimated by multiplying the purchased equipment cost by a suitable correction factor that also consider that apparatuses were built in AISI 316 stainless steel and rated to work at high pressure.

The cost of the solar field was estimated by ENEA staff basing on internal expertise and tools and referring to previous projects; the estimated value was considered as the CAPEX for the solar field.

Several configurations of the CS plant were analyzed to study the effect of different design parameters on the cost of the biocrude produced by the HTL plant. Specifically, the following features of the CS plant were changed:
  a) the size of the solar field expressed by the number of collector rows (Ns) each 200 m long: solar fields with 2, 3 and 4 rows were considered;
  b) the capacity of the heat storage system: TES systems with different volume of the tank corresponding to heat storage capacity 0, 4, 6, 8 and 12 hours were considered.

The CAPEX-values of the HTL section and the solar field were added to obtain the value for the full plant.

The OPEX comprehends the costs associated with raw materials, waste disposal, utilities, labor and other; it was estimated from correlations reported in [138] using the CAPEX, the number of equipment pieces and mass and energy flows. The purchase cost of microalgae was considered to be 0.3 €/kg [139] and the cost of electricity was considered to be 0.173 €/kWh [140]; the cost of disposal of aqueous phase products was neglected, as it was assumed that these products were recycled back to the microalgae cultivation system [126]. The working capital (WC), i.e. the amount of money required to make operative the plant, was assumed to be 20% of the CAPEX.

In order to estimate the minimum fuel selling price (MFSP) of the biocrude, a cash flow analysis was performed. It has been taken in consideration a plant life of 25 years with production starting from the 3rd year, while the first two years are dedicated to the construction of the plant; the interest rate on the investment was taken to be 10% and the taxation rate on revenue 40%. The minimum selling price was calculated with the Excel solver by imposing the net present value (NPV) of the project at the end of its life to be equal to zero.

By optimization of thermal integration among the hot stream recovered from the hydrothermal reactor and the two cold streams fed to the process, it was found that the solar field should sustain the process with a thermal power of 800 kW necessary to heat the water in HX1 from 330°C to 378°C.

Table 25: Estimated capital costs C_T of process equipment constituting the HTL plant and estimated cost of manufacturing (OPEX) of the HTL plant.

Equipment	C_T (kUS\$) [1]
HX1	450
HX2	345
HX3	350
Slurry pump (2 units)	335
Pure water pump (2 units)	545
Reactor	760
Cyclone	180
Separation vessel	260
Total HTL Plant	3,230
OPEX HTL Plant	5,340

[1] All costs referred to 2014 in US\$. Chemical engineering plant cost index CEPCI=579.8.

Table 26: Estimated capital costs of process equipment constituting the CS plant and cost of manufacturing (OPEX) of the solar plant. Estimation of the minimum fuel selling price (MFSP) of the produced biocrude was performed considering different configuration of the solar field (number of collector rows and TES capacity), with the respective associated costs.

Number of rows	2		3			4		
TES capacity (h)	4	6	4	8	12	4	8	12
Molten salt volume (m^3)	57	85	57	113	170	57	113	170
Solar field (kUS$)	715	715	1,000	1,000	1,000	1,310	1,310	1,310
TES system (2 tanks) (kUS$)	195	285	195	370	545	195	370	545
Back-up heater (kUS$)	160	160	160	160	160	160	160	160
Instrumentation, BoP[2] and other costs (kUS$)	320	320	320	320	320	320	320	320
Installation and transport (kUS$)	210	225	265	300	335	325	360	395
Civil works, engineering, overhead and contingency (kUS$)	1,275	1,370	1,580	1,770	1,950	1,910	2,100	2,280
CAPEX CS plant (kUS$)	2,875	3,075	3,520	3,920	4,310	4,220	4,620	5,010
OPEX CS plant (kUS$)	67	69	82	94	101	88	107	120

[2] Balance of Plant (BoP) includes all the components required to complete the installation and to operate the plant (piping and connections, valves, etc...).

The effect of the different configuration of the solar field on the MFSP of the produced biocrude is visible in Figure 61. When the smallest solar field (Ns = 2 collector rows) was considered the cost of the fuel slightly increased when the TES capacity was increased from 4 to 6 hours, that is the maximum possible size of the storage system with this solar field size. Differently, in the case of larger solar fields constituted by Ns = 3 and 4 collector rows, the MSFP decreased with the storage capacity. This different trend is due to the fact that higher capital and operative expenses accompanying the increase of Ns and TES capacity in these plants are always overcompensated by the lower fraction of biocrude internally consumed for the energy back-up.
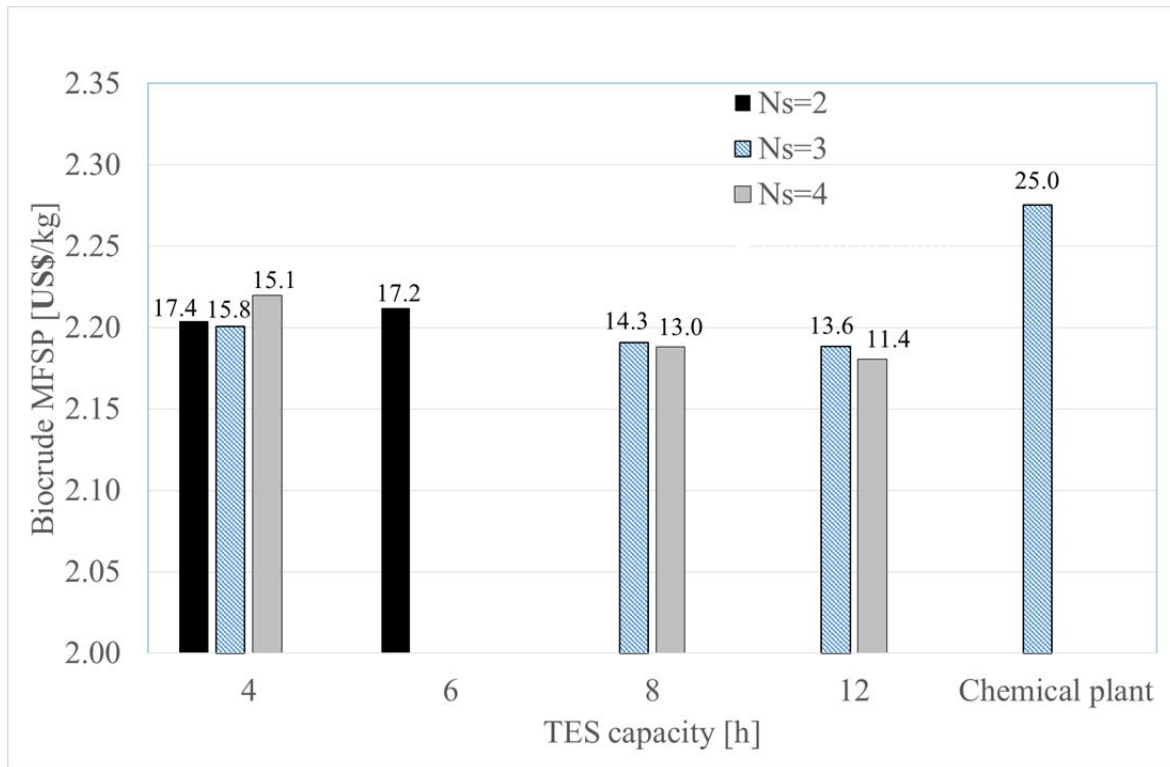
Figure 61: Minimum fuel selling price (MFSP) of biocrude as a function of the TES capacity and of the number of collector rows (Ns), compared with a pure chemical plant not powered by solar energy (i.e. energetically sustained only through the combustion of part of the produced biocrude). Numbers at the top of the bars are the fractions X (%) of the produced biocrude used for self-consumption in the back-up heater of the TES.

It can be observed that the lowest MFSP value of 2.19 US$/kg was obtained with the largest investigated configuration of the solar plant (i.e. with Ns = 4 rows and TES capacity 12 hours). Quite interestingly, the pure thermal process (i.e. non-solar process, using only part of the produced biocrude as energy source) was characterized by the highest estimated MFSP corresponding to 2.29 US$/kg. In general, it is clear from Figure 61 that the lower the fraction X of self-consumed biocrude, the lower the cost of production. This indicates that using solar heat it is possible to perform the process with an economic sustainability similar to that achievable with conventional chemical processes [141], but with a significant improvement in terms of environmental sustainability, since lower amount of fuel must be combusted to drive the plant and, thus, a higher amount of product can be put into the market.

As mentioned, microalgae are interesting type of biomass to be converted into biofuels; however, the production cost of this biomass is high and it has a strong impact on the economy of the entire biofuel production process.
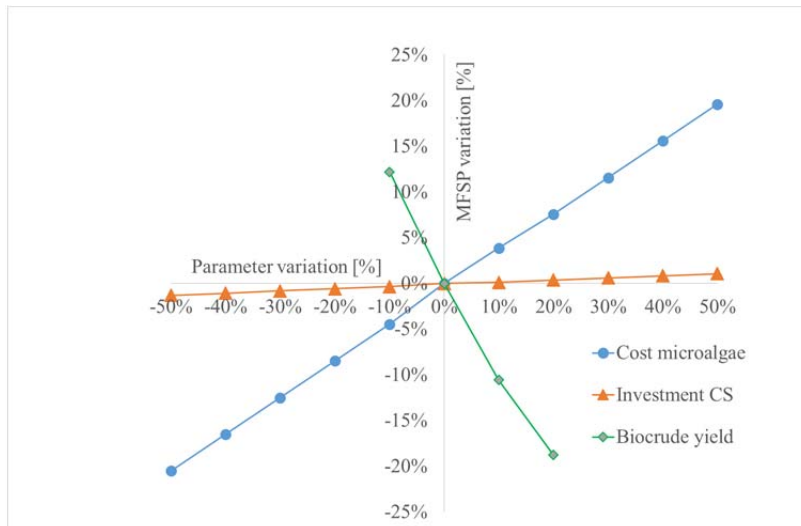
Figure 62: Sensitivity analysis for the MFSP of the produced biocrude, performed by changing the cost of microalgae, CAPEX of solar (CS) plant and biocrude yield.

This aspect is making evident by the sensitivity analysis performed on the process by evaluating the relative effect of the cost of the raw material, of the CAPEX of the CS plant and of the biocrude yield on the process economy. The results of this study are reported in Figure 62. We have found that the MFSP of the produced biocrude is slightly affected by the investment cost of the CS plant. Indeed, even if this cost changes by ±50%, the MFSP changes by only ±1%.

Differently from the CS plant investment costs, variations in the cost of the microalgae had a much more significant effect on the MFSP of the produced biocrude. When the cost of microalgae changed by ±50% the value of MFSP changed by about ± 20%. The strong impact of the cost of raw material reflects on the effect of the biocrude yield: an increase of yield at fixed cost of the microalgae has the same economic effect of a decrease in the cost of the raw material at fixed material efficiency of the process.

According to this analysis, biocrude yield should be maximized, as expected in general. Moreover, a more interesting scenario is represented by the use of waste streams as biomass process feedstock, such as sewage sludge, food industry effluents, etc... For example, if a null cost is associate to the feedstock, in case of using a waste as raw material, the MFSP of the biocrude would decrease to 1.31 US$/kg. Thus, this waste-to-fuel strategy would strongly increase the economy of the process, also providing the huge environmental advantage of waste valorization and reuse, to be pursued in the view of a circular economy. More information on the techno-economic analyses of the considered process can be found in [142].

7. Recommendation of R&D priorities: technology roadmap

Research priorities are proposed in order to improve the solar fuels production processes to get closer to their theoretical efficiency limits. Larger scale demonstration activities are necessary to get the technologies closer to market application. The following step is the first market introduction that will prepare the entry into the market learning curve that will finally lead to the cost reduction to be competitive. This roadmap includes new processes (i.e. molten carbonate electrolysis) which have not been investigated within previous roadmaps and which were selected here because of their interesting and promising first results.

7.1 Non-volatile metal oxide cycles

Non-volatile metal oxide cycles presently are in the TRL range of 5-6. The achieved developments are very promising for a fast deployment of this technology. To increase the TRL larger scale demonstration activities in the MW range are necessary.

The current challenges concerning the thermal management and the gas separation are solvable in the mid-term future. Moreover, many problems are of conventional nature (e.g. thermal management) and have not been treated intensively with state-of-the-art technologies known from the conventional power plant technology.

Present solar towers for power production are designed for much lower temperatures and therefore concentrations. Solar towers for fuel production must achieve concentration factors of over 2000 and need a control strategy that prevents temperature variations in the receiver-reactor to operate the chemical process efficiently. The receiver reactors must be further developed to minimize inert heated mass like structures and flushing gases. Also more active redox materials need to be developed. To solve the problems on the conventional part, detailed transient models should be employed to predict the performance of alternative concepts of thermal management including storage and separation of heat generation and chemical reaction. Prior to demonstrate the feasibility of a whole plant the required "side technologies" needed for water splitting like gas separation and plant design should be developed separately.

Items like process control, automation and "continuous generation" should be moved in the focus of R&D work. Lab-scale research on alternative materials as REDOX-systems should take place and scale effects should be investigated theoretically.

7.2 ZnO/Zn cycles

Concerning the <u>carbon-free ZnO/Zn thermochemical cycle</u> process major issues have been identified in the research up to now. In the currently explored approach for separation of Zn and O_2 these issues specifically include the need of a large amount of inert gas for quenching the $Zn(g)$-O_2-mixture and - related to this - the need to separate the inert gas from O_2. Guided by this we suggest not to focus on this research line as long as no breakthrough technology option regarding Zn-O_2 separation and/or inert gas-O_2 separation has been identified.

However, it appears to be justified to foresee a limited activity to search for such breakthrough technology options.

Based on the above reasoning research in the following two fields should be considered (in this priority order):

1) Research on effective separation of O_2 and inert gas (relevant for other thermochemical cycles, as well).

2) Fundamental research for alternative $Zn(g)$-O_2 separation processes (membranes? Quenching with liquid nitrogen? ..)

Only in case very significant progress is made in at least one of these fields a continuation of the solar reactor development for ZnO dissociation is recommended (e.g. tackling topics like optimised gas patterns in the reactor for effective transport of the dissociation products for improving the reacting rate).

The <u>carbothermal ZnO/Zn cycle</u> avoids these issues due to the production of a gas mixture of $Zn(g)$ and CO well known in Zn metallurgy. However although the pilot scale carbothermal ZnO reduction tests were quite successful, no direct follow up activity could yet be realized. E.g. an EU-proposal with focus on the production of H_2 (in contrast to the preceding SOLZINC project), which was not successful due to the very strong competition in the specific call. Now, that major issues with the ZnO dissociation cycle have been identified and other thermochemical cycles suffer from still rather moderate efficiencies, the reconsideration of the carbothermal ZnO cycle appears to be advisable.

Three types of R&D work are recommended:

(1) <u>Work for improvement of the solar reactor.</u> Since basically the same two-cavity reactor is also under development for solar steam gasification of carbonaceous materials (see separate chapter on gasification) the activities suggested there are also relevant here. These include the avoidance of the quartz window and modifications to feed material into the hot reactor (e.g. semi-batch).

(2) <u>The hydrolysis step</u> should be developed further with special emphasis on the interface topics; that is trying to optimize the materials in each of the two steps of the thermochemical cycle for use in the other step.

(3) <u>Basic study</u> of a more direct path to solar H_2 via this cycle by investigating options to <u>integrate Zn hydrolysis and CO shift into the quenching</u> of the produced Zn(g)-CO mixture (see sketch in Figure 63). Due to the underlying thermodynamics complete conversion of H_2O to H_2 simultaneously with conversions of CO to CO_2 is not expected to be possible, but maybe by using several steps (like hydrolysis first followed by a separate CO-shift step) one might approach this ideal target. If successful this process would be significantly simplified, however at the expense of losing the advantage of optional flexible storage of Zn-powder prior to it's processing to H_2 and ZnO.

An important source of knowledge for points (2) and (3) exists in the extensive work on solar ZnO/Zn hydrolyses that has e.g. been performed at ETHZ (mainly related to ZnO-dissociation, but also being relevant for the solar carbothermal ZnO reduction) (e.g. [51]).
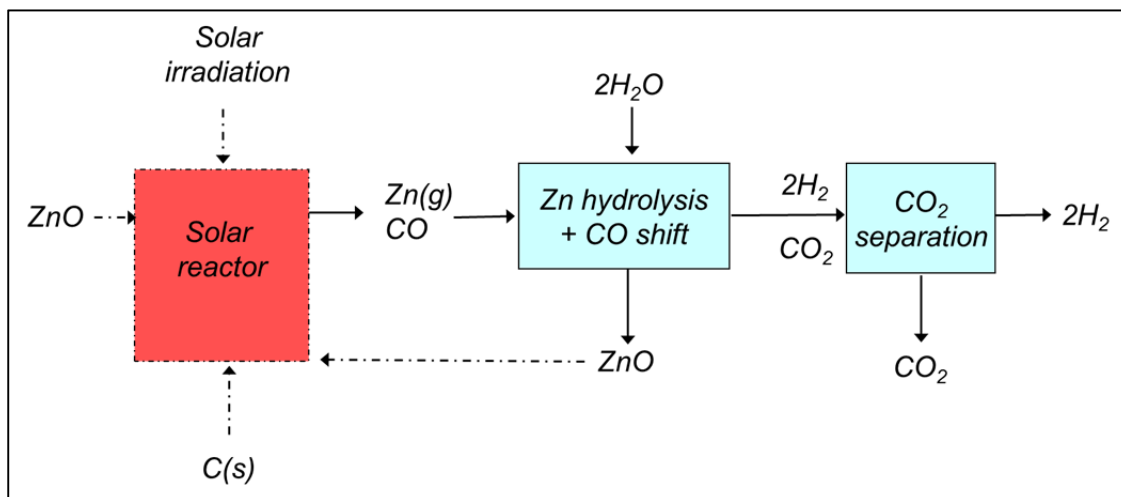
Figure 63: Sketch of a process variant worth evaluating for direct H_2 production from carbothermal ZnO reduction gas.

Regarding further test installations and scale-ups, it is recommended to start a new initiative to win industrial partners for scaling-up of this technology by reactivating old industry contacts and by initiating new ones. The realization of a prototype demonstration at the level of a few MW should be targeted. A conceptual design for such a plant had already been worked out at the end of the Solzinc project [63]. This might be updated to include latest improvement of the reactor technology (e.g. regarding windowless design) and then be used as a starting point for this new initiative.

7.3 Hybrid sulphur cycle

The solar heated hybrid sulphur cycle has actually achieved a TRL of 5 and is a very promising technology for solar hydrogen production. This TRL could increase by larger scale demonstration activities with further scaling of the sulphuric acid splitting section in the MW-range. Other factors to be further researched is the pressurization of the sulphuric acid splitting reactor (e.g. 10 bar), the development of a suitable high temperature heat storage (i.e.

900 °C) for continuous operation of the sulphuric acid splitting as well as the development of the heat recovery system between outlet (850 °C) and inlet of sulphuric acid splitting (i.e. between hot $SO_2/O_2/H_2O$-stream and cold H_2SO_4/H_2O-stream) and the gas separation after sulphuric acid splitting for efficient recovery of O_2 as by-product/off-gas.

Regarding the sulphur dioxide electrolyser (SDE) section, it has to be further optimized to avoid/reduce/control the sulphur formation. This SDE should be further scaled and on-field demonstrated at relevant scale. Another development factor is the pressurisation of SDE (e.g. 10-20 bar).

Concerning the materials development, research on optimization of the catalysts for sulphuric acid splitting has to be done as well on research on protective coating to reduce corrosion of steel components in sulphuric acid splitting reactor. Regarding SDE, the bipolar plates should be optimized and potential of reduction of sulphur formation in SDE should be further researched.

7.4 Solar steam reforming (high and low temperature)

The solar steam reforming has actually a TRL of 5-6, which is very promising for a further deployment of this technology. Industrial partners from different areas have to be involved in sunbelt countries to build a demonstration plant to achieve TRL 7. Demonstrated on such a level the plant can be optimized and the system can be tested and qualified in operational environment.

7.5 Solar driven solid oxide electrolysis

The solid oxide electrolysis coupling with solar concentrated energy is a highly promising technology for future hydrogen production. SOE systems need to be developed closer to commercial hydrogen production. This means larger cells and stacks as well as long term operation tests and coupling to appropriate heat sources. With an increasing hydrogen demand for mobility and industry, the SOE coupled with CSP could play a big role in renewable hydrogen production.

At present, the FCH JU supports RD&D of SOE with 20.1 €M. The call of 2014 funded two projects, HELMETH and SOPHIA. In the MAWP (FCH JU2) high temperature electrolysis was acknowledged as having the potential to reduce electricity consumption, once stability of stack and materials is improved. Key Performance Indicators were provided for the efficiency, CAPEX and OPEX, delivery pressure and life-time [143]. Topics covering SOE technology development were included in the Annual Work Plan (AWP) of 2014 leading to project SELYSOS and 2015 leading to project GRINHY. Also under AWP 2015 a topic on high temperature co-electrolysis of water with CO_2 for the production of synthetic CH_4 funded the project ECO.

Project HELMETH [144] will demonstrate the thermal integration of a high temperature SOE with a CO_2 methanation step aiming for conversion efficiencies of >85 % from renewable electricity to methane by utilizing the process heat of the exothermal methanation reaction in the high temperature electrolysis process.

Project SOPHIA [145] aims to design, fabricate and operate on-sun a 3 kW_e pressurized SOE system, coupled to a concentrated solar energy source, for the coelectrolysis of H_2O and CO_2 to produce syngas (H_2+CO) as an intermediate step for the production of synthetic CH_4. The solar receiver has been built and tested. Single repeating units and stack tests have been done in electrolysis and co-electrolysis mode at atmospheric and pressurized conditions (15 bar).

Project SELYSOS [146] aims to develop new, more efficient electrodes and to understand the reaction mechanisms and processes that cause degradation on both SOEC electrodes combining experiments/theoretical modelling, eventually identifying the design parameters to guide the development of new SOECs less prone to degradation with better performance and stability.

Lastly from AWP 2015, project GRINHY [147] is developing and demonstrating a 6-stack 120kW SOE to a steel industry, where the H_2 will be used in the annealing process of steel. The project aims to prove that efficiencies of > 80 %LHV (ca. 95 %HHV) can be reached plus a lifetime of > 10,000 h with a degradation rate < 1 %/1,000 h. Integration and operation for at least 7,000 h meeting the hydrogen quality standards of the steel industry is one of the targets.

Project ECO aims to develop a highly efficient coelectrolysis process for the conversion of excess renewable electricity into distributable and storable hydrocarbons via simultaneous electrolysis of steam and CO_2 through SOE. The project plans to investigate durability under realistic co-electrolysis operating conditions that include dynamic electricity input from fluctuating sources, with the aim to achieve degradation rates below 1%/1000h at stack level.

As a conclusion, until now the FCH JU has provided noticeable R&D support to this technology, leading to more efficient and durable units, helping European SOEC industry become the most advanced globally. Durability beyond 10,000 h and efficiencies above 80% are the main priorities in the roadmap of the technology by 2030, together with scaling up of stacks and integration of replicating units with different energy sources, among them concentrating solar thermal. Systems with capacities higher than 100kW that can operate in reversible mode are currently being developed for demonstration at industrial sites.

Follow up projects should target the demonstration of SOE units with solar thermal plants. In particular, after the analysis herewith it is proposed the demonstration of a system integrating SOE and a Linear Fresnel solar thermal plant and producing 400-600kg H_2/day. Similarly, high temperature reversible fuel cells taking advantage of near-by NG grids could also be applicable in P2P applications.

The objectives of the innovation activities will be focused on improving the efficiency of hydrogen production and reducing costs, increasing the yield of purification methods and improving carbon dioxide removal from production pathways.

7.6 Molten carbonate electrolysis

The technological maturity of the MCSE is currently low (TRL 3) and the available information on the process was obtained in preliminary experimental campaigns with commercial MCFC operated in electrolysis conditions and with an alumina crucible laboratory cell. Therefore, the short to medium-term R&D efforts should be focused on raising the TRL to at least 5 by developing and testing a significant scale electrolyser prototype in relevant operating conditions.

To that end, one of first issues to be solved is the selection of appropriate corrosion resistant materials both for the electrolyser shell and for the electrodes; such materials must be able to withstand corrosion in the harsh molten carbonate environment for long operating times. Indeed, the preliminary tests on reversed MCFC suggested that the conventional electrode materials used for such devices may not be suitable for operation in electrolysis mode. Once the materials selected, it will be possible to realise and test new laboratory reactors, which will allow studying the process under more realistic conditions.

Accurate mathematical models of the process will have to be developed and used to select the electrolyser configuration and optimize its design before developing the first TRL 5 demonstrator.

Further work is required also on the system analysis and integration side. Gas handling and separation operations required downstream of the electrolyser are energy consuming and currently bottleneck the efficiency of the process. New solutions should therefore be evaluated for this section of the MCSE plant. In parallel, alternative uses of the electrolyser outlet gases, which avoid CO_2 separation, should be evaluated: as an example, the composition of the anodic gases makes combination of MCSE with a methanation process very appealing.

Furthermore, the integration strategy of MCSE with CSP plants should be optimized.

7.7 Solar gasification of carbonaceous materials and wastes

The promising results of the tests so far as well as the simplicity and versatility of the reactor design offering the potential to convert basically all carbonaceous materials to high quality syngas without major pre-treatment qualifies this process for a further development.

Two topics of specific interest to be studied are the following:

(1) Up to now, the process has been successfully demonstrated in batch mode (1 batch per day). For certain feedstock a "tar cracker" is required *during the heat-up phase* of the reactor (once the reactor is on operation temperature of around 1100°C any tar forming components are thermally converted into H_2 and CO, the main syngas components, anyway). A key improvement would be reached by realizing a transport of the feedstock into a *hot* reactor, thereby making a tar cracker obsolete. An interesting realization might make use of a pushing furnace principle (the bottom part can be replaced for introduction of a new feedstock batch into the reactor and the replacement of a processed batch (ash remaining) by a new one). This also allows processing smaller batches with reduced height, thereby relaxing the requirements on the feedstock with respect to ash content (option to process several batches per day).

Conventionally heated pushing furnaces are well known in metallurgical processing [148]. Considerations for a solar pushing furnace have been performed and it is recommended to study the respective critical issues like opening/closing during feedstock entry/ash removal first on a lab scale. A rough design of a laboratory scale two-cavity pushing furnace is available.

(2) Another major improvement compared to the demonstrated state of the art concerns the omission of the quartz window. Instead of the established sealing of the reactor towards ambient air at the water-cooled holding structure of the window, in this case the sealing has to be performed at the ceramic absorber. Furthermore, the absorber material must be stable in air as well as the gasification gas at up to about 1400°C and withstand the mechanical stresses due to thermal gradients etc. Such a windowless design has been successfully demonstrated on lab-scale using differently shaped absorbers from different materials [149]. It would be valuable to further improve this design in terms of material choice as well as hot sealing. The successive logical step would then be the design and realization on pilot scale. This provides further challenges like the ones caused by the limited ceramic sizes available for the solar absorber, asking at least for very large installations for a gas tight construction combining several ceramic absorber pieces.

Currently a 5 kW laboratory solar two-cavity reactor at PSI and the 150 kW pilot gasification plant installed on the CESA tower at the Plataforma Solar de Almeria are available for further tests and for investigations of improvements. The next development step should involve design and realisation of a prototype demonstration plant of a few MW. Significant preparatory work for this step has already been performed in the Solsyn project together with Holcim (now LafargeHolcim).

7.8 Solar molten salt heated hydrothermal liquefaction of wet biomass

Even if the proposed process to not lead to hydrogen production it offers several advantages, with respect to traditional non-solar processes or to the most studied solar reactors to use solar heat to perform chemical processes:

- wet biomass containing streams (also waste biomass) can be converted into renewable biofuels;
- continuous operation is possible to produce large amount of fuel commodity;
- high pressure (up to 30 MPa) processes can be performed, due to the physical separation between the plant section devoted to the reaction (reactor) and that used for solar heat storage and transfer (molten salt stream);
- enhanced versatility of the chemical reactor (for the same reason of the previous point).

For the development of this technology to higher TRL values, the following steps are considered necessary:

- investigation of the process in lab-scale continuous systems heated by molten salts.
- investigation of the design of the solar plant to adapt it to the chemical process.
- preparation of demonstrative plants at small scale to demonstrate technological feasibility in operational environment.

Figure 64 and Figure 65 summarize the proposed R&D actions for all processes as well as the scale-up strategy with stop and go actions.

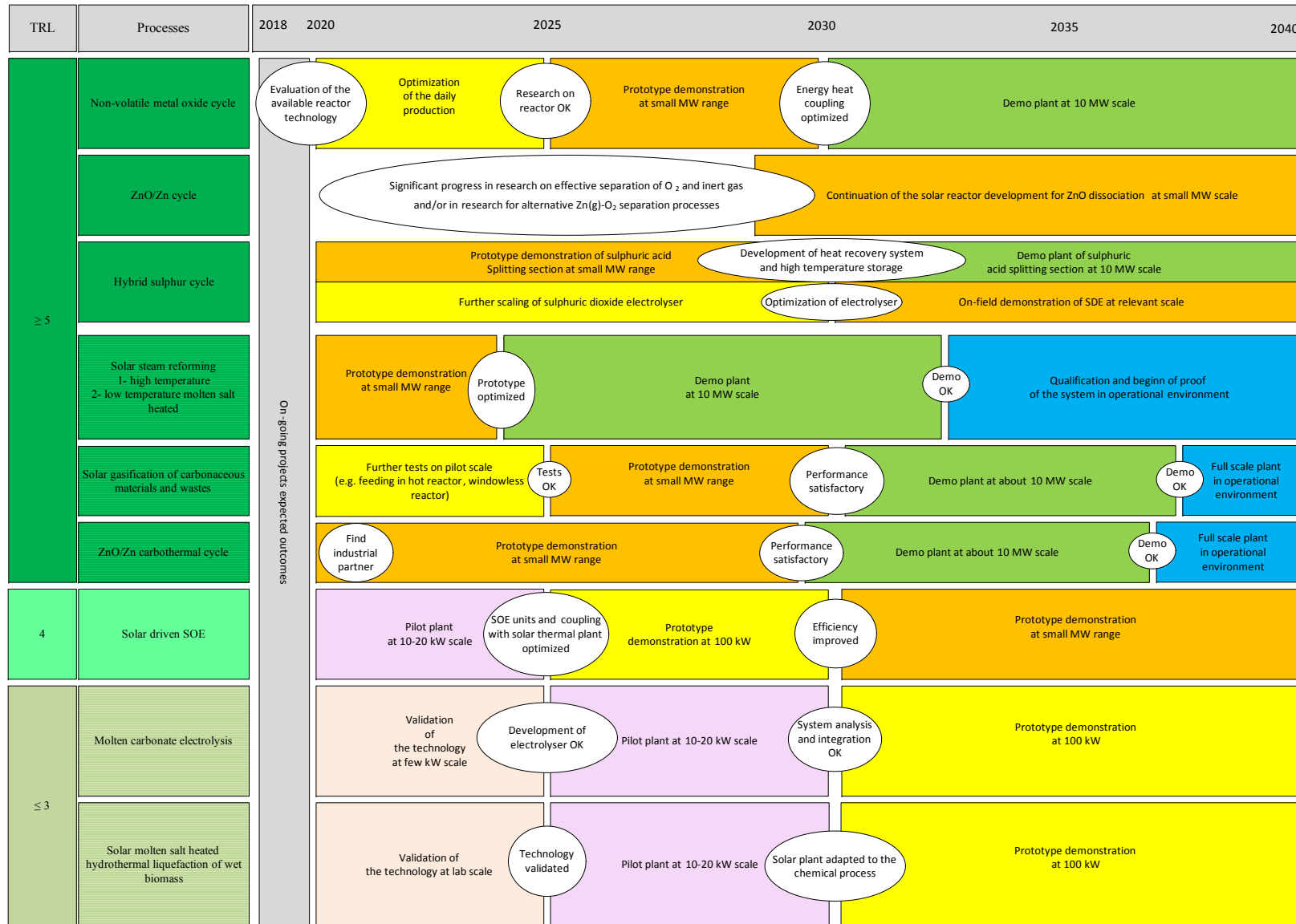**Figure 64: Summary of the R&D strategy Roadmap.**

Figure 65: Summary of the scale-up strategy Roadmap.

8. Conclusions

Concentrated solar technologies have the potential to produce hydrogen from renewable energy efficiently. Thermochemical cycles as well as high temperature electrolysis and solar fuels processes based on carbonaceous feedstocks have been investigated. Technology maturity and the current state of the art were assessed for each solar fuel production process, including new processes like the molten carbonate electrolysis, as well as the TRL. This document shows electrolysis is not the only way to produce hydrogen using renewable energy efficiently. Naturally, the costs contain some uncertainties and can be decreased, especially concerning the concentration of solar radiation part. No commercial solar thermochemical plant is in operation yet and only a small number of MW solar tower power plants. Cost degression depending on cumulated installed capacity was not taken into account. A learning curve should be projected to the CSP technology and the hydrogen production costs will decrease automatically.

After the assessment of the different processes, R&D actions have been proposed for these processes. A complete roadmap for the development of hydrogen production via concentrated solar technologies has been drawn until 2040 with recommendation for future R&D priority work including a list of development areas in order to foster further development of solar fuels production processes and to facilitate scaling up the solar fuels technologies in a fast and efficient way. As is obvious based in the current knowledge we recommend to continue the research and development of most studied technologies, however with further actions with strongly differ between the technologies and with go/no-go milestones for the most costly further upscaling activities. Depending on the technology, some challenges are solvable in the mid-term future, which is very promising for the next deployment of these concentrated solar hydrogen production processes. However, a growing interest of industrial partners is required to invest in these technologies to build bigger demonstration plants.

9. References

1.   Edwards, P.P., et al., *Hydrogen and fuel cells: Towards a sustainable energy future.* Energy Policy, 2008. **36**(12): p. 4356-4362.

2.   Konstandopoulos, A.G. and S. Lorentzou, *Novel Monolithic Reactors for Solar Thermochemical Water Splitting* in *On Solar Hydrogen & Nanotechnology*, L. Vayssieres, Editor 2010, John Wiley & Sons, Ltd: Chichester, UK.

3.   Peters, M. and K. Timmerhaus, *Plant design and economics for chemical engineers* 2004: McGraw-Hill.

4.   Fletcher, E.A. and R.L. Moen, *Hydrogen and Oxygen from Water - The use of solar energy in a one-step effusional process is considered.* Science, 1977. **197**: p. 1050-1056.

5.   McDaniel, A.H., et al., *Nonstoichiometric Perovskite Oxides for Solar Thermochemical H_2 and CO Production.* Energy Procedia, 2014. **49**: p. 2009-2018.

6.   Rytter, E., et al., *Process concepts to produce syngas for Fischer–Tropsch fuels by solar thermochemical splitting of water and/or CO_2.* Fuel Processing Technology, 2016. **145**: p. 1-8.

7.   Agrafiotis, C., M. Roeb, and C. Sattler, *A review on solar thermal syngas production via redox pair-based water/carbon dioxide splitting thermochemical cycles.* Renewable and Sustainable Energy Reviews, 2015. **42**(0): p. 254-285.

8.   *https://www.hydrogen.energy.gov/pdfs/review16/pd114_weimer_2016_o.pdf*

9.   Romero, M. and A. Steinfeld, *Concentrating solar thermal power and thermochemical fuels.* Energy & Environmental Science, 2012. **5**(11): p. 9234.

10.   Säck, J.-P., et al., *High temperature hydrogen production: Design of a 750KW demonstration plant for a two step thermochemical cycle.* Solar Energy, 2016. **135**: p. 232-241.

11.   Agrafiotis, C., et al., *Solar water splitting for hydrogen production with monolothic reactors.* Solar Energy, 2005. **79**: p. 409 - 421.

12.   Hoffschmidt, B., et al., *Performance Evaluation of the 200-kW_{th} HiTRec-II Open Volumetric Air Receiver.* Journal of Solar Energy Engineering, 2003. **125**(1): p. 87-94.

13.   Agrafiotis, C., et al., *Evaluation of porous silicon carbide monolithic honeycombs as volumetric receivers/collectors of concentrated solar radiation.* Solar Energy Materials and Solar Cells, 2007. **91**(6): p. 474-488.

14.   Heck, R.M., S. Gulati, and R.J. Farrauto, *The application of monoliths for gas phase catalytic reactions.* Chemical Engineering Journal, 2001. **82**(1): p. 149-156.

15.   Roeb, M., et al. *Thermo-chemical production of hydrogen from water by metal oxides fixed on ceramic substrates.* in *Proceedings of the 16th World Hydrogen Energy Conference.* 2006. Lyon, France.

16.   Roeb, M., et al., *Solar Hydrogen Production by a Two-Step Cycle Based on Mixed Iron Oxides.* Journal of Solar Energy Engineering, 2006. **128**(2): p. 125–133.

17.   Roeb, M., et al., *Test operation of a 100 kW pilot plant for solar hydrogen production from water on a solar tower: SolarPACES 2009.* Solar Energy, 2011. **85**(4): p. 634-644.

18.   Roeb, M., et al., *Operational strategy of a two-step thermochemical process for solar hydrogen production.* International Journal of Hydrogen Energy, 2009. **34**(10): p. 4537-4545.

19.   Neises, M., et al., *Simulation of a solar receiver-reactor for hydrogen production.* in *Proceedings of the ASME 2009 3rd International Conference of Energy Sustainability (ES2009).* 2009. San Francisco, California, USA.

20.   Houaijia, A., et al., *Analysis and improvement of a high-efficiency solar cavity reactor design for a two-step thermochemical cycle for solar hydrogen production from water.* Solar Energy, 2013. **97**: p. 26-38.

21.   Hao, Y., C.-K. Yang, and S.M. Haile, *High-temperature isothermal chemical cycling for solar-driven fuel production.* Physical Chemistry Chemical Physics, 2013. **15**(40): p. 17084-17092.

22. Bader, R., et al., *Thermodynamic Analysis of Isothermal Redox Cycling of Ceria for Solar Fuel Production.* Energy & Fuels, 2013. **27**: p. 5533-5544.

23. Chueh, W.C. and S.M. Haile, *Ceria as a Thermochemical reaction medium for selectively generating syngas or methane from H_2O and CO_2.* ChemSusChem, 2009. **2**(8): p. 735-739.

24. Chueh, W.C. and S.M. Haile, *A thermochemical study of ceria: exploiting an old material for new modes of energy conversion and CO_2 mitigation.* Philosophical Transactions of the Royal Society A: Mathematical, Physical and Engineering Sciences, 2010. **368**(1923): p. 3269-3294.

25. Abanades, S., et al., *Investigation of reactive cerium-based oxides for H_2 production by thermochemical two-step water-splitting.* Journal of Materials Science, 2010. **45**(15): p. 4163-4173.

26. Abanades, S. and G. Flamant, *Thermochemical hydrogen production from a two-step solar-driven water-splitting cycle based on cerium oxides.* Solar Energy, 2006. **80**(12): p. 1611-1623.

27. Call, F., et al., *Thermogravimetric analysis of zirconia-doped ceria for thermochemical production of solar fuel.* American Journal of Analytical Chemistry, 2013. **4**: p. 37-45.

28. Mogensen, M., N.M. Sammes, and G.A. Tompsett, *Physical, chemical and electrochemical properties of pure and doped ceria.* Solid State Ionics, 2000. **129**(1-4): p. 63-94.

29. Singh, P. and M.S. Hegde, $Ce_{0.67}Cr_{0.33}O_{2.11}$ *A New Low-Temperature O_2 Evolution Material and H_2 Generation Catalyst by Thermochemical Splitting of Water.* Chemistry of Materials, 2010. **22**(3): p. 762-768.

30. Chueh, W.C., et al., *High-flux solar-driven thermochemical dissociation of CO_2 and H_2O using nonstoichiometric ceria.* Science, 2010. **330**: p. 1797-1801.

31. Bader, R., et al., *Thermodynamic analysis of isothermal redox cycling of ceria for solar fuel production.* Energy & Fuels, 2013. **27**(9): p. 5533-5544.

32. Diver, R.B., et al., *Solar Thermochemical Water-Splitting Ferrite-Cycle Heat Engines.* Journal of Solar Energy Engineering, 2008. **130**(4): p. 41001-41008.

33. Lapp, J., J.H. Davidson, and W. Lipiński, *Heat Transfer Analysis of a Solid-Solid Heat Recuperation System for Solar-Driven Nonstoichiometric Redox Cycles.* Journal of Solar Energy Engineering, 2013. **135**(3): p. 031004.

34. Lapp, J. and W. Lipiński, *Transient Three-Dimensional Heat Transfer Model of a Solar Thermochemical Reactor for H_2O and CO_2 Splitting Via Nonstoichiometric Ceria Redox Cycling.* Journal of Solar Energy Engineering, 2014. **136**(3): p. 031006-031006-11.

35. Bader, R., et al., *Design of a Solar Reactor to Split CO_2 Via Isothermal Redox Cycling of Ceria.* Journal of Solar Energy Engineering, 2015. **137**(3): p. 031007-031007-10.

36. Ermanoski, I., N.P. Siegel, and E.B. Stechel, *A New Reactor Concept for Efficient Solar-Thermochemical Fuel Production.* Journal of Solar Energy Engineering, 2013. **135**(3): p. 031002-10.

37. Scheffe, J.R., M. Welte, and A. Steinfeld, *Thermal Reduction of Ceria within an Aerosol Reactor for H_2O and CO_2 Splitting.* Industrial & Engineering Chemistry Research, 2014. **53**(6): p. 2175-2182.

38. Marxer, D., et al., *Solar thermochemical splitting of CO_2 into separate streams of CO and O_2 with high selectivity, stability, conversion, and efficiency.* Energy & Environmental Science, 2017. **10**: p. 1142-1149.

39. *http://www.sun-to-liquid.eu/.*

40. *https://www.psi.ch/lst/bfe-solarzinc-pandd.*

41. Loutzenhiser, P.G., A. Meier, and A. Steinfeld, *Review of the Two-Step H_2O/CO_2-Splitting Solar Thermochemical Cycle Based on Zn/ZnO Redox Reactions.* Materials, 2010. **3**(11): p. 4922-4938.

42. Felder, R., *Well-to-wheel analysis of renewable transport fuels: synthetic natural gas from wood gasification and hydrogen from concentrated solar energy.* Doctoral Thesis No. 17437, ETH Zürich, 2007.

43. Koepf, E., et al., *A review of high temperature solar driven reactor technology: 25 years of experience in research and development at the Paul Scherrer Institute.* Applied Energy, 2017. **188**: p. 620-651.

44. Koepf, E., W. Villasmil, and A. Meier, *Pilot-scale solar reactor operation and characterization for fuel production via the Zn/ZnO thermochemical cycle.* Applied Energy, 2016. **165**: p. 1004-1023.

45. Alxneit, I., *Assessing the feasibility of separating a stoichiometric mixture of zinc vapor and oxygen by a fast quench – model calculations.* Sol Energy 2008. **82**: p. 959–64.

46. Alxneit, I. and H.R. Tschudi, *Modeling the formation and chemical composition of partially oxidized Zn/ZnO particles formed by rapid cooling of a mixture of Zn (g) and O_2.* J Mater 2013: 718525 p. 1-9.

47. Gstoehl, D., et al., *A quenching apparatus for the gaseous products of the solar thermal dissociation of ZnO.* J Mater. Sci., 2008. **43**: p. 4729–36.

48. Jakober, R., E. Koepf, et al., *Technoeconomic Analysis of Industrial Plant for H_2 Production via the ZnO/Zn Solar Thermochmical Cycle.* to be submitted.

49. Stamatiou, A., A. Steinfeld, and Z.R. Jovanovic, *On the Effect of the Presence of Solid Diluents during Zn Oxidation by CO_2.* Industrial & Engineering Chemistry Research, 2013. **52**(5): p. 1859-1869.

50. Weibel, D., Z.R. Jovanovic, and A. Steinfeld, *Exploiting kinetics to unravel the role of the ZnO diluent in the production of CO via oxidizing Zn particles with CO_2.* Chemical Engineering Science 2017. **165**: p. 96-107.

51. Weibel, D., *The Reaction of Particulate Zn-ZnO Mixtures with CO_2 and H_2O for the Production of CO and H_2*, Doctoral thesis No 23357, *ETH Zürich* 2016.

52. Steinfeld, A., *Solar hydrogen production via a two-step water-splitting thermochemical cycle based on Zn/ZnO redox reactions.* International Journal of Hydrogen Energy, 2002. **27**(6): p. 611-619.

53. Felder, R. and A. Meier, *Well-To-Wheel Analysis of Solar Hydrogen Production and Utilization for Passenger Car Transportation,* Journal Solar Energy Engineering, 2008. **130**: p. 011017-1 – 011017-10.

54. Meier, A., *Life cycle analysis and economic assessment of solar hydrogen*, in *Handbook of Hydrogen Energy*, D.Y.G. S.A. Sherif, E.K. Stefanakos, and A. Steinfeld, CRC Press Editor 2014. p. 537-563

55. Charvin, P., et al., *Analysis of Solar Chemical Processes for Hydrogen Production From Water Splitting Thermochemical Cycles.* Energy Conversion Management, 2008. **49**: p. 1547–1556.

56. Kromer, M., et al., *Support for cost analyses on solar-driven high temperature thermochemical water-splitting cycles*, in *DE-DT0000951, Final Report to Department of Enerrgy, by TIAX, LLC*2011: Lexington, MA, U.S.A.

57. Martinek, J., et al., *Considerations for the Design of Solar-Thermal Chemical Processes.* Journal of Solar Energy Engineering, 2010. **132**: p. 031013-1 - 031013-6.

58. Haltiwanger, J., J. Davidson, and E. Winston, *Renewable Hydrogen From the Zn/ZnO Solar Thermochemical Cycle: A Cost and Policy Analysis* J. Sol. Energy Eng., 2010. **132**: p. 041011-1 - 041011-8.

59. Osinga, T., et al., *Experimental Investigation of the Solar Carbothermic Reduction of ZnO Using a Two-Cavity Solar Reactor.* Journal of Solar Energy Engineering, 2004. **126**(1): p. 633–637.

60. Kräupl, S., Frommherz, U., and Wieckert, C., *Solar Carbothermic Reduction of ZnO in a Two-Cavity Reactor: Laboratory Experiments for a Reactor Scale-Up.* Journal of Solar Energy Engineering, 2006. **128**(1): p. 8-15.

61. Wieckert, C., et al., *A 300 kW Solar Chemical Pilot Plant for the Carbothermic Production of Zinc.* Journal of Solar Energy Engineering, 2007. **129**(2): p. 190–196.

62. Wieckert, C. and A. Steinfeld, *Solar thermal reduction of ZnO using CH_4:ZnO and C:ZnO molar ratios less than 1,* Journal of Solar Energy Engineering, 2002. **124**: p. 55-62.

63. Epstein, M., Olalde, G., Santén, S., Steinfeld, A., Wieckert, C., *Towards the Industrial Solar Carbothermal Production of Zinc.* Journal of Solar Energy Engineering, 2008. **130**(February): p. 014505.

64. Kräupl, S. and C. Wieckert, *Economic evaluation of the solar carbothermic reduction of ZnO by using a single sensitivity analysis and a Monte-Carlo risk analysis.* Energy, 2007. **32**(7): p. 1134-1147.

65. Berman A., Epstein M., *The kinetics of hydrogen production in the oxidation of liquid zinc with water vapor.* Int. J. Hydrogen Energy, 2000. **25**(10): p. 957-967.

66. Venstrom, L.J. and J.H. Davidson, *Splitting Water and Carbon Dioxide via the Heterogeneous Oxidation of Zinc Vapor: Thermodynamic Considerations.* Journal of Solar Energy Engineering 2011.

67. Venstrom, L.J. and J.H. Davidson, *The Kinetics of the Heterogeneous Oxidation of Zinc Vapor by Carbon Dioxide.* Chemical Engineering Science, 2013. **93**: p. 163-172.

68. Vishnevetsky, I. and M. Epstein, *Production of hydrogen from solar zinc in steam atmosphere.* International Journal of Hydrogen Energy 2007. **32**: p. 2791 – 2802.

69. Vishnevetsky, I., A. Berman, and M. Epstein, *Features of solar thermochemical redox cycles for hydrogen production from water as a function of reactants' main characteristics.* International Journal of Hydrogen Energy, 2011. **36**: p. 2817-2830.

70. Lapp, J., et al., *Modeling of a solar receiver for superheating sulfuric acid*. in *Proceedings of the 9th International Conference on Energy Sustainability*. 2015. San Diego, California, USA.

71. Lüpfert, E., *Der Einfluß konzentrierter Solarstrahlung auf die Reaktionsgeschweindigkeit der Abfallschwefelsäure-Spaltung*, 1996, RWTH Aachen University, Germany.

72. Noglik, A., *Entwicklung eines solaren Reaktors zur Schwefelsäurespaltung für die thermochemische Wasserstofferzeugung*, in *Fortschrittberichte VDI : Reihe 3, Verfahrenstechnik* 2008, VDI-Verlag: Düsseldorf. p. 155.

73. Thomey, D., et al. *Development and Test Operation of a Demonstration Plant for Sulfuric Acid Splitting at the DLR Concentrating Solar Power Tower Facility*. in *2016 AIChE Annual Meeting*. 2016. San Francisco, USA.

74. Summers, W.A. and M.B. Gorensek. *Nuclear Hydrogen Production Based on the Hybrid Sulfur Thermochemical Process*. in *International Congress on Advances in Nuclear Power Plants (ICAPP)*. 2006. Reno, NV USA.

75. Guerra Niehoff, A., et al., *Process modelling and heat management of the solar hybrid sulfur cycle.* International Journal of Hydrogen Energy, 2015. **40**(13): p. 4461-4473.

76. Corgnale, C. and W.A. Summers, *Solar hydrogen production by the Hybrid Sulfur process.* International Journal of Hydrogen Energy, 2011. **36**(18): p. 11604-11619.

77. Liberatore, R., et al., *Integration of photovoltaic and concentrated solar thermal technologies for H_2 production by the hybrid sulfur cycle.* in AIP Conference Proceedings, 2017. **1850**: p. 1000132.

78. Möller, S., et al. *Solar Production of Syngas for Electricity Generation: SOLASYS Project Test-Phase*. in *Proceedings of the 11th SolarPACES Int. Symposium on Concentrated Solar Power and Chemical Energy Technologies*. 2002. Zürich.

79. Möller, S., Kaucic, D., Sattler, C., *Hydrogen production by solar reforming of natural gas: A comparison study of two possible process configurations.* Journal of Solar Energy Engineering, 2006. **128**: p. 16-23.

80. Möller, S., et al. *SOLREF – Development of an advanced Solar High-temperature Reformer*. in *Proceedings of ISEC2006: ASME International Solar Energy Conference*. 2006. Denver, CO, USA.

81. Liu, K., C. Song, and V. Subramani, *Hydrogen and Syngas Production and Purification Technologies* 2010: Wiley-AIChE.

82. Gioconia, A., *Multi-fuelled Solar Steam Reforming for Pure Hydrogen Production Using Solar Salts as Heat Transfer Fluid.* Energy Procedia, 2015. **69**: p. 1750-1758.

83. *European project MATS - Multipurpose Applications by Thermodynamic Solar, Contract n° 268219.*

84. *http://cordis.europa.eu/result/rcn/192700_en.html*.

85. Gahleitner, G., *Hydrogen from renewable electricity: An international review of power-to-gas pilot plants for stationary applications.* International Journal of Hydrogen Energy, 2013. **38**(5): p. 2039-2061.

86. *Water electrolysis & Renewable energy systems.* FuelCellToday, 2013.

87. Smolinka, T., *Fuels-Hydrogen production: Water electrolysis*, in *Encyclopedia of electrochemical power sources*, Elsevier, Editor 2009, G.Jürgen. p. 394-413.

88. Yu, B., et al., *Advance in highly efficient hydrogen production by high temperature steam electrolysis.* Sci. China Ser. B Chem., 2008. **51**(4): p. 289–304.

89. Schiller, G., et al., *High temperature water electrolysis using metal supported solid oxide electrolyser cells (SOEC).* Journal of Applied Electrochemistry, 2008. **39**(2): p. 293-301.

90. Erdle, E.G., J.; Meyringer, V.:, *Possibilities for Hydrogen Production by Combination of a Solar Thermal Central Receiver System and High Temperature Electrolysis of Steam.* Solar Thermal Central Receiver Systems Proc. of the 3r^d Intl. Workshop, 1986. **2**: p. 727-736.

91. Sigurvinsson, J., et al., *Can high temperature steam electrolysis function with geothermal heat?* Int. J. Hydrogen Energy, 2007. **32**(9): p. 1174–1182.

92. Harvego, E.A., et al., *Parametric evaluation of large-scale high-temperature electrolysis hydrogen production using different advanced nuclear reactor heat sources.* Nucl. Eng. Des., 2009. **239**: p. 1571–1580.

93. Sanz-Bermejo, J., et al., *Optimal integration of a solid-oxide electrolyser cell into a direct steam generation solar tower plant for zero-emission hydrogen production.* Applied Energy, 2014. **131**: p. 238-247.

94. Steinfeld, A., *Solar thermochemical production of hydrogen—a review.* Solar Energy, 2005. **78**(5): p. 603–615.

95. *http://www.sophia-project.eu/.*

96. Monnerie, N., et al., *Hydrogen production by coupling pressurized high temperature electrolyser with solar tower technology.* International Journal of Hydrogen Energy, 2017. **42**: p. 13498-13509.

97. Romero, M. and J. González-Aguilar, *Solar thermal power plants: from endangered species to bulk power production in sun-belt regions.* Energy and Power Generation Handbook, ASME, 2011. **3**.

98. Medrano, M., et al., *State of the art on high-temperature thermal energy storage for power generation. Part 2—Case studies.* Renewable and Sustainable Energy Reviews, 2010. **14**(1): p. 56-72.

99. Berger, M., et al., *Mirror fresnel process heat collectors for industrial applications and solar cooling*, in *SolarPACES* 2009: Berlin.

100. Zaetta, R. and B. Madden, *Hydrogen fuel cell bus technology state of the art review.* 2011.

101. *EbsilonProfessional* Available from: http://www.steag-systemtechnologies.com/ebsilon_professional+M52087573ab0.htm.

102. Laing, D., et al., *Solid media thermal storage for parabolic trough power plants.* Solar Energy, 2006. **80**(10): p. 1283-1289.

103. Tamme, R., D. Laing, and W.-D. Steinmann, *Advanced Thermal Energy Storage Technology for Parabolic Trough.* Journal of Solar Energy Engineering, 2004. **126**(2): p. 794-800.

104. Bo, Y., et al., *Status and research of highly efficient hydrogen production through high temperature steam electrolysis at INET.* International Journal of Hydrogen Energy, 2010. **35**(7): p. 2829–2835.

105. Licht, S. and H. Wu, *STEP iron, a chemistry of iron formation without CO2 emission: molten carbonate solubility and electrochemistry of iron ore impurities.* J. Phys. Chem. C, 2011. **115**: p. 25138-25147.

106. Yin, H., et al., *Capture and electrochemical conversion of CO2 to valued-added carbon and oxygen by molten salt electrolysis* Energy Environ. Sci., 2013. **6**: p. 1538-1545.

107. Graves, C., et al., *Sustainable hydrocarbon fuels by recycling CO2 and H2O with renewable or nuclear energy.* Renewable and Sustainable Energy Reviews, 2010. **15**(1): p. 23-1.

108. Frangini, S., C. Felici, and P. Tarquini, *A Novel Process for Solar Hydrogen Production Based on Water Electrolysis in Alkali Molten Carbonates.* ECS Transactions, 2014. **61**(22): p. 13–25.

109. Hu, L., et al., *Electrochemical performance of reversible molten carbonate fuel cells.* International Journal of Hydrogen Energy, 2014. **39**(23): p. 12323-12329.

110.   Wall, T., et al., *An overview on oxyfuel coal combustion—State of the art research and technology development.* Chemical Engineering Research and Design, 2009. **87**(8): p. 1003-1016.

111.   Antolini, E., *The stability of molten carbonate fuel cell electrodes: A review of recent improvements.* Applied Energy, 2011. **88**(12): p. 4274–4293.

112.   Petitpas, F., A. Brisse, and C. Bouallou, *Model-based behaviour of a high temperature electrolyser system operated at various loads.* Journal of Power Sources, 2013. **239**: p. 584–595.

113.   Brouwer, J., et al., *Analysis of a molten carbonate fuel cell: Numerical modeling and experimental validation.* Journal of Power Sources, 2006. **158**(1): p. 213–224.

114.   Dortmundt, D. and K. Doshi, *Recent Developments in CO_2 Removal Membrane Technology.* UOP, 1999: p. 1–32.

115.   Maccari, A., et al., *Archimede solar energy molten salt parabolic trough demo plant: Improvements and second year of operation.* in AIP Conference Proceedings, 2016. **1734**: p. 100007.

116.   Gangi, J. and S. Curtin, *Fuel cell technologies market report 2013*, 2014, DoE Technical report.

117.   Sau, S., et al., *Techno-economic comparison between csp plants presenting two different heat transfer fluids.* Applied Energy, 2016. **68**: p. 96-109.

118.   Wieckert, C., et al., *Syngas Production by Thermochemical Gasification of Carbonaceous Waste Materials in a 150 kWth Packed-Bed Solar Reactor.* Energy & Fuels, 2013. **27**(8): p. 4770-4776.

119.   Piatkowski, N., et al., *Solar-driven gasification of carbonaceous feedstock-a review.* Energy & Environmental Science, 2011. **4**(1): p. 73–82.

120.   Piatkowski, N., C. Wieckert, and A. Steinfeld, *Experimental investigation of a packed-bed solar reactor for the steam-gasification of carbonaceous feedstocks.* Fuel Processing Technology, 2009. **90**(3): p. 360-366.

121.   *https://de.statista.com/statistik/daten/studie/28697/umfrage/prognose-zur-preisentwicklung-von-braunkohle-von-2000-bis-2030/.*

122.   G. Maag, Sunbiotec AG, *private communication* July 2017.

123.   Lovegrove, K. and W.E. Stein, *Concentrating solar power technology – Principles, developments and applications.* 2012: Woodhead Publishing Ltd. .

124.   Milano, J., et al., *Microalgae biofuels as an alternative to fossil fuel for power generation.* Renewable and Sustainable Energy Reviews, 2016. **58**: p. 180–197.

125.   Saber, M., B. Nakhshiniev, and K. Yoshikawa, *A review of production and upgrading of algal bio-oil.* Renewable and Sustainable Energy Reviews, 2016. **58**: p. 918–930.

126.   Alba, L.G., et al., *Microalgae growth on the aqueous phase from Hydrothermal Liquefaction of the same microalgae* Chemical Engineering Journal 2013. **228** p. 214–223.

127.   Jazrawi, C., et al., *Pilot plant testing of continuous hydrothermal liquefaction of microalgae.* Algal Research, 2013. **2**: p. 268–277.

128.   Patel, B. and K. Hellgardt, *Hydrothermal upgrading of algae paste in a continuous flow reactor.* Bioresource Technology, 2015. **191**: p. 460–468.

129.   Suesse, A.R., G.A. Norton, and J.v. Leeuwen, *Pilot-Scale Continuous-Flow Hydrothermal Liquefaction of Filamentous Fungi.* Energy Fuels, 2016. **30**: p. 7379−7386.

130.   Reimer, J., et al., *A novel salt separator for the supercritical water gasification of biomass.* J. of Supercritical Fluids, 2016. **117**: p. 113-121.

131.   Yoo, G., et al., *Lipid content in microalgae determines the quality of biocrude and Energy Return On Investment of hydrothermal liquefaction.* Applied Energy, 2015. **156**: p. 354–361.

132.   Pearce, M., M. Shemfe, and C. Sansom, *Techno-economic analysis of solar integrated hydrothermal liquefaction of microalgae.* Appl. Energy, 2016. **166**: p. 19–26.

133.   Jena, U., K.C. Das, and J.R. Kastner, *Effect of operating conditions of thermochemical liquefaction on biocrude production from Spirulina platensis.* Bioresource Technology, 2011. **102**(10): p. 6221–6229.

134.   Guo, Y., et al., *A review of bio-oil production from hydrothermal liquefaction of algae.* Renewable and Sustainable Energy Reviews, 2015. **48**: p. 776–790.

135.   Elliott, D.C., et al., *Hydrothermal processing of macroalgal feedstocks in continuous-flow reactors.* ACS Sustainable Chemistry and Engineering, 2014. **2**(2): p. 207–215.

136.   Schiavo, B., et al., *A continuous system for hydrothermal conversion of microalgae*, in *ECCE10+ECAB+EPIC5 (10th European Congress of Chemical Engineering + 3rd European Congress of Applied Biotechnology + 5th European Process Intensification Conference)* 2015: Nice (France).

137.   Valdez, P.J., V.J. Tocco, and P.E. Savage, *A general kinetic model for the hydrothermal liquefaction of microalgae.* Bioresource Technology, 2014. **163**: p. 123–127.

138.   Turton, R., et al., *Analysis, Synthesis, and Design of Chemical Processes*2013: Pearson Education, Inc.

139.   Pearce, M., M. Shemfe, and C. Sansom, *Techno-economic analysis of solar integrated hydrothermal liquefaction of microalgae.* Applied Energy, 2016. **166**: p. 19–26.

140.   *Autorità per l'energia elettrica, il gas e il sistema idrico/Dati statistici/Elettricità/Prezzi e tariffe/ Prezzi finali dell'energia elettrica per i consumatori industriali nel 2015 - UE e area Euro*. 2017 [cited 2017 01.03.2017]; Available from: http://www.autorita.energia.it/it/dati/elenco_dati.htm.

141.   Beal, C.M., et al., *Algal biofuel production for fuels and feed in a 100-ha facility: A comprehensive techno-economic analysis and life cycle assessment.* Algal Research, 2015. **10**: p. 266-279.

142.   Giaconia, A., et al., *Biorefinery process for hydrothermal liquefaction of microalgae powered by a concentrating solar plant: a conceptual study.* Applied Energy, submitted.

143.   *FCH2JU Multi Annual Work Plan* Available from: http://www.fch.europa.eu/sites/default/files/documents/FCH2%20JU%20-%20Multi%20Annual%20Work%20Plan%20-%20MAWP_en_0.pdf.

144.   *Project HELMETH, Grant Agreement Number 621210. Supported under the Seventh Framework Programme of the EU under the Fuel Cells and Hydrogen Joint Undertaking* Available from: http://www.fch.europa.eu/project/integrated-high-temperatureelectrolysis-and-methanation-effective-power-gas-conversion.

145.   *Project SOPHIA, Grant Agreement Number 621173. Supported under the Seventh Framework Programme of the EU under the Fuel Cells and Hydrogen Joint Undertaking* Available from: http://www.fch.europa.eu/project/solar-integrated-pressurizedhigh-temperature-electrolysis.

146.   *Project SELYSOS, Grant Agreement Number 671481. Supported under the Horizon 2020 Programme of the EU under the Fuel Cells and Hydrogen Joint Undertaking* Available from: http://www.fch.europa.eu/project/development-new-electrode-materials-and-understanding-degradation-mechanisms-solid-oxide.

147.   *Project GRINHY, Grant Agreement Number 700300. Supported under the Horizon 2020 Programme of the EU under the Fuel Cells and Hydrogen Joint Undertaking* Available from: http://www.fch.europa.eu/project/green-industrial-hydrogenreversible-high-temperature-electrolysis.

148.   Jaklič, A., F. Vode, and T. Kolenko, *Online simulation model of the slab-reheating process in a pusher-type furnace.* Appl. Therm. Eng., 2007. **5**(27): p. 1105–1114.

149.   Wieckert, C., N. Tzouganatos, and A. Steinfeld, *Demonstration of a 5kWth windowless packed-bed reactor for high temperture solar thermochemical processing*, in *SolarPaces Conference* 2017, Santiago de Chile, (anticipated) publication in AIP conference series, 2018.